Targeted Delivery of Polymer Vesicles Functionalized with Fibronectin Mimetic Peptides to Cancer Cells

A DISSERTATION
SUBMITTED TO THE FACULTY OF THE GRADUATE SCHOOL
OF THE UNIVERSITY OF MINNESOTA
BY

Todd Owen Pangburn

IN PARTIAL FULFILLMENT OF THE REQUIREMENTS
FOR THE DEGREE OF
DOCTOR OF PHILOSOPHY

Efrosini Kokkoli & Frank S. Bates, Advisors

September 2012

Acknowledgements

I would be remiss if I did not acknowledge the abundance of assistance that I received from many different individuals throughout the course of my PhD research. Without them I would not be where am today. First, I must thank my advisors, Efie and Frank, for their continual support and mentorship. The many meetings, discussions, and interactions that we had have kept me on track for the ultimate completion of my PhD. They were generous with both their time and their knowledge, and were instrumental in guiding my PhD research to completion. I should also thank the funding agencies that made my PhD research possible. This research was supported in part by a National Science Foundation (NSF) Graduate Research Fellowship, the MRSEC Program of the NSF under Award Number DMR-0819885, and the Camille Dreyfus Teacher-Scholar Awards Program. The cryo-TEM was carried out in the Institute of Technology Characterization Facility, University of Minnesota, a member of the NSF-funded Materials Research Facilities Network (www.mrfn.org).

I would also like to thank all the graduate students and post doctoral researchers in both the Kokkoli group and Bates group that have helped me countless times with training, advise, and day to day tasks in the lab. In particular, I should thank Kevin Davis and Sangwoo Lee in the Bates lab for teaching me the craft of anionic living polymerization, and Kamlesh Schroff, Maroof Adil, Matt Petersen, Brett Waybrant, Rachael Levine, Tim Pearce, Nicole Atchison, Emilie Rexeisen, Ashish Garg, and Döne Demirgöz in the Kokkoli group for the many tasks they have helped me with. Many thanks also go out to the two undergraduate students that have worked with me, Kelly Carnahan and Katerina Georgiou. In particular Katerina has been instrumental in completing my research in a timely manner. I would also like to thank my parents for their support and the many pep talks they gave me through the years. Last, but certainly not least, I would like to thank my wife and son for their unwavering love and support. They kept me sane through it all. I can't thank them enough for putting up with all the crazy schedules, long hours, and late nights. My wife weathered the tempest of highs and lows that is experimental research right along with, and I couldn't have done it without her. Thank you all. This thesis is as much a product of their labors as mine.

Dedication

To my wife, my love.

Abstract

Polymersomes, polymeric vesicles that self-assemble in aqueous solutions from block copolymers, have been avidly investigated in recent years as potential drug delivery agents. In this work, the feasibility of chemical conjugation of fibronectin mimetic targeting peptides (GRGDSP and PR_b) onto the surface of polymersomes is investigated, and the efficacy of these peptide functionalized polymersomes to achieve targeted delivery to cancer cells is studied. The diblock copolymer poly(ethylene oxide)-*b*-poly(1,2-butadiene) was synthesized and self-assembled to form polymersomes, which were subsequently functionalized with peptides using a "click" conjugation reaction. Delivery efficacy of these peptide functionalized polymersomes loaded with fluorescent markers, a chemotherapeutic (doxorubicin), or siRNA was assessed and compared. Both the efficacy and the process of delivery and internalization of peptide functionalized polymersomes were investigated for colon and breast cancer cells. PR_b functionalized polymersomes were found in all cases to significantly outperform both GRGDSP and non-functionalized polymersomes, in terms of promoting cell binding, internalization, specificity, and effective delivery. This work highlights peptide functionalized polymersomes in general, and PR_b functionalized polymersomes in specific, as a highly promising targeted delivery system.

Table of Contents

List of Tables

List of Figures

1 Introduction

This thesis investigates the synthesis, characterization, and utilization of peptide functionalized block copolymers for targeted delivery of therapeutics to cancer cells. Polymer vesicles are self-assembled nanoparticles capable of encapsulating chemotherapeutic drugs and more novel therapeutics such as small interfering RNA. A central theme of this work is the evaluation of the potential advantages of functionalizing polymer vesicles with fibronectin mimetic peptides relevant to targeted delivery to cancer cells.

1.1 Targeted Delivery

It has been over a century since Paul Ehrlich, the profound Nobel laureate immunologist, proposed the concept of a "magic bullet".[1] Yet still today we are continually pursuing newer and better therapies to selectively treat diseases with minimal side-effects, and this pursuit shows no sign of slowing. Targeted delivery, the ability to target a therapeutic to a specific site of disease, is at the vanguard of this pursuit. In the early 18th century Paul Ehrlich postulated a side chain theory, that involved lock-and-key receptors on the surface of cells which specifically bound components in the "protoplasm", the historic name for the extracellular environment *in vivo*.[2] From this theory he extrapolated that highly specific therapies could be formulated that would target only the malicious agents within a patient. He thus envisioned a therapy that could cure a patient with virtually no side effects, a "magic bullet", or as he termed it "therapia sterilisans magna" (the great sterilizing therapy). Although the details of Ehrlich's theories obviously did not stand the test of time, the dream of a "magic bullet" therapy is

still alive. Today targeted delivery holds great promise of approaching the long sought after "magic bullet". Through binding specificity of chemical ligands current research is beginning to show that diseases, such as cancer, can be effectively targeted and thus the adverse side effects of therapies for these diseases minimized.

In respect to targeting cancerous tissue, the primary focus of this thesis, there are two main modes of targeted delivery, passive and active. Active targeting involves the use of targeting ligands (e.g. peptides) that specifically adhere to receptors found at the target site, and will be discussed in detail later in this chapter. Passive targeting, as opposed to active targeting, does not require the use of binding ligands and instead operates purely based on the size of the drug delivery vehicle, such as polymer vesicles. Passive targeting is achieved by way of the enhanced permeability and retention (EPR) effect, and is an established method of targeting cancerous tumors. The EPR effect was first observed over 20 years ago, and has since become generally recognized as a valuable method for the targeting of drugs to the region of a tumor.[3] Since the treatment of cancer is a seminal long range goal of the *in vitro* targeted delivery research in this thesis the *in vivo* EPR effect will be briefly discussed.

Once a tumor reaches the size of approximately 2-3 mm in diameter the cancerous cells induce angiogenesis, the formation of new blood vessels, in order to supply more oxygen and nutrients to the rapidly growing tumor.[4] The neovasculature formed around the tumor is anatomically different from the vasculature of healthy tissue.[5] The blood vessels formed around a tumor have irregular shapes, dilated diameters, and frequent fenestrations due to the endothelial cells, which form the internal surface of the blood

vessel, being poorly aligned and disorganized.[6] Also, the perivascular cells and basement membrane, or smooth-muscle layer, which typically coats the exterior of blood vessels in healthy tissue, is often not present or disordered around blood vessels in the region of a tumor.[7] These defects of the blood vessel walls around tumors result in what is commonly referred to as a "leaky" vasculature. In simple terms, the newly formed blood vessels around a tumor tend to be "leaky" and much of the blood circulating through them, including larger particles, leaks out of the vessels and into the tumor tissue. Thus, there is an enhanced permeability of molecules, especially nano-sized particles, through the tumor vasculature and into the tumor as compared to healthy tissue. In addition to enhanced permeability, the slowed lymphatic drainage exhibited by tumors also contributes to an enhanced retention effect. Tumors show slower venous return and lymphatic clearance as compared to healthy tissue, so macromolecules and nano-particles are retained within the tumor. In other words, tumors tend to retain nano-sized particles within their tissue for much longer than healthy tissue. These two abnormalities of tumor tissue, the leaky vasculature and slowed clearance, combine to give rise to the phenomena known as the EPR effect, as illustrated in Figure 1.1.

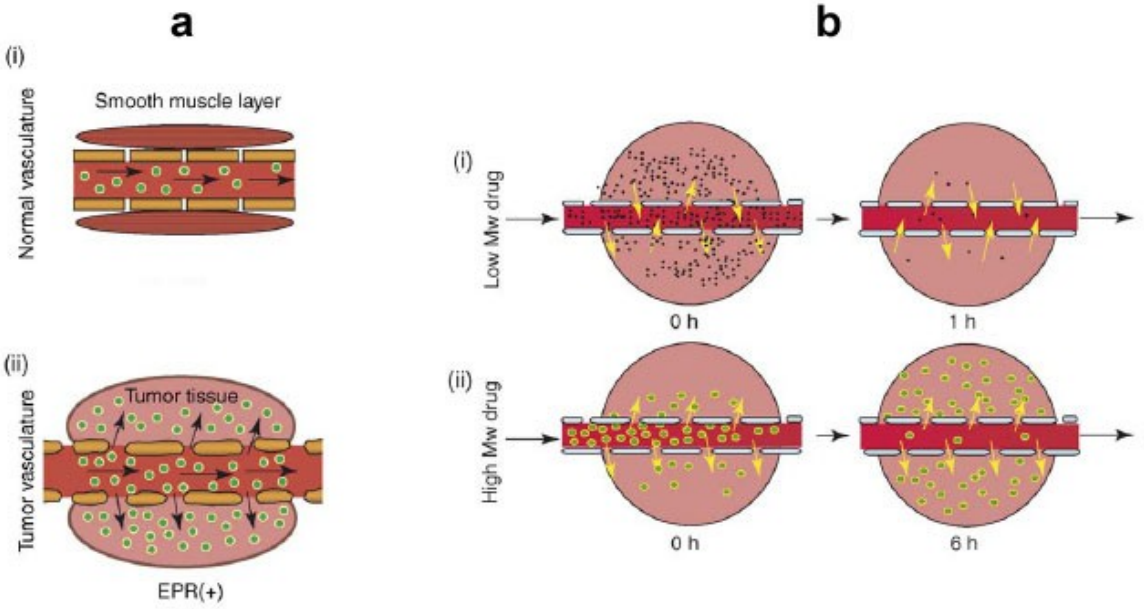

Figure 1.1 The enhanced permeability and retention (EPR) effect illustrated. Illustration of how the "leaky" vasculature in the region of tumors (a-ii) as compared to that in healthy tissue (a-i) allows for the enhanced permeability of molecules and nano-sized particles into a tumor. Illustration of how there is enhanced retention and accumulation over time of high M_w molecules and nano-sized particles in tumors due to the tumors slowed lymphatic clearance (b). Figure reproduced from Iyer et al., with permission from Elsevier.[8]

Targeted delivery systems employing targeting ligands (i.e. active targeting) are typically designed to also utilize the EPR effect, thus active and passive targeting act synergistically. Passive targeting by the EPR effect is exploited to get the nanoparticle delivery vehicles into the region of the tumor, after which active targeting via a targeting ligand promotes effective binding, internalization and delivery to the target cells in the tumor region.

The EPR effect has been found to be general for both large macromolecules (>40 kDa) and nano-sized particles on the order of a few 100 nm, such as appropriately sized polymer vesicles.[9–13] EPR effect based targeting is commonly called passive targeting

because the effect is hypothesized to depend, to a first approximation, only on the size of the particle. Another important point is that EPR effect based accumulation at the cancerous region is a slow process, potentially occurring over the course of days.[7] Because of this slow rate of accumulation in the tumor it is critical that any drug delivery vehicle that hopes to exploit the EPR effect have long circulation half-lives, $t_{1/2}$. It is believed that $t_{1/2}$ must be extended to at least a minimum of 6 h for EPR targeting to become relevant.[8] The classic example of a delivery vehicle with an extended circulation half-life is the sterically stabilized liposome which can achieve circulation half-lives on the order of ~12 h, however polymer vesicles having fully pegylated surfaces are even better exhibiting $t_{1/2}$ ~28 h.[14–18] Longer circulation half-lives have been repeatedly shown to improve passive EPR targeting, translating to increased accumulation in tumors and better efficacy (i.e. tumor shrinkage and survival times).[19–25] However, it should be noted that a handful of studies have shown counter intuitively, no increase in tumor accumulation or efficacy of sterically stabilized liposomes as compared to conventional liposomes.[26–28] In two of these studies very high drug doses were used so that the circulation half-life of conventional liposomes was increased purely due to toxicity to macrophages, but the third used more reasonable drug doses and still reported little advantage for sterically stabilized liposomes.[29] It should be made clear however that although there is some debate as to the relative efficacy of improving *in vivo* circulation half-lives, the advantages of EPR targeting are widely accepted and the majority of literature agrees that long circulation half-lives, like those demonstrated by polymer vesicles, are highly advantageous.

Encapsulation, the packaging of therapeutics within a targeted delivery vehicle and protecting and/or preventing release of these therapeutics until the delivery vehicle has reached its target, is an essential feature of any targeted delivery system. Polymer vesicles are well designed for effective encapsulation of a wide range of encapsulates, as both the internal aqueous lumen and the thick hydrophobic membrane of polymer vesicles can be loaded with both molecules and particles.[30–40] In addition, the thick hydrophobic membrane of polymer vesicles imbues them with very low permeability to any hydrophilic encapsulate, thus limiting encapsulate leakage during storage and delivery.[41–44] The encapsulated therapeutic could be any of a wide range of choices. In this thesis the encapsulation and delivery of both chemotherapeutic drugs and small interfering RNA are investigated in detail.

1.2 Self-Assembly Behavior of Block Copolymers in Aqueous Solutions

The polymer vesicles used in this thesis research self-assemble in aqueous solutions from the amphiphilic diblock copolymer, poly(1,2-butadiene)-*b*-poly(ethylene oxide) (PB-PEO or OB for short), as shown in Figure 1.2. The amphiphilic nature of the block copolymer and the strongly hydrophobic nature of PB drive the PB chains to self-associate and be shielded from the aqueous surrounding environment by the hydrophilic PEO chains. The net result is the formation of a bilayer structure consisting of a thick hydrophobic core membrane shielded on both sides by PEO brush layers. This bilayer naturally "wraps-up" to form spherical vesicle structures with large aqueous interiors, thus self-assembling polymer vesicles.

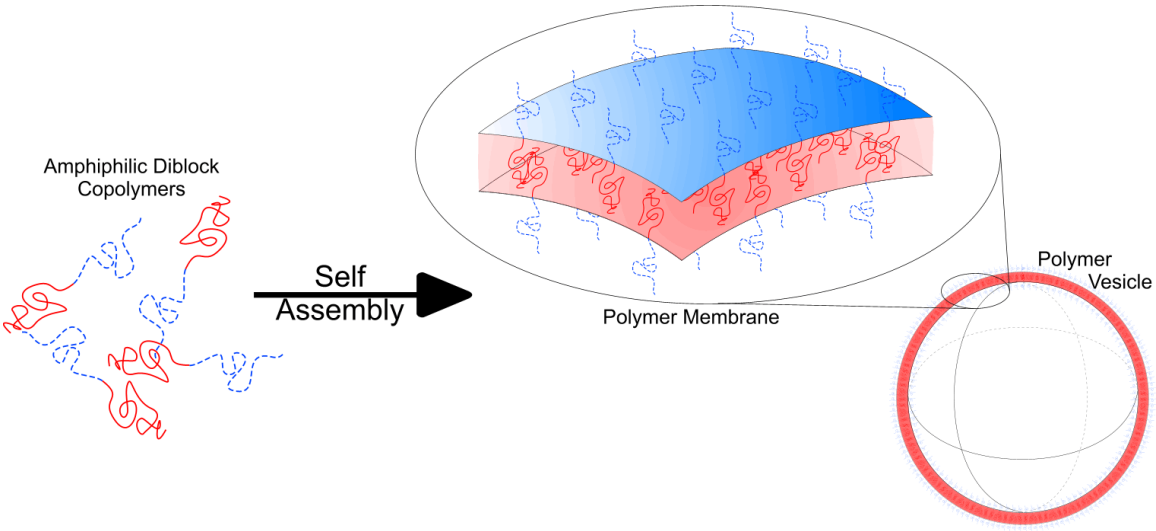

Figure 1.2 Amphiphilic block copolymers self assemble into a polymer membrane which wraps around onto itself to form a spherical polymer vesicle with a aqueous interior.

Polymer vesicles are just one possible morphology that amphiphilic block copolymers are capable of assuming in aqueous solutions. For the OB block copolymer in specific the self-assembled morphology formed depends on the fractional content of PEO and, to a lesser extent, the overall molecular weight of the polymer. In addition to the bilayer vesicle morphology, for increasing weight fraction of PEO OB diblocks form cylindrical micelles, and then spherical micelles. To a first approximation these morphology transitions follow from the simple packing argument illustrated in Figure 1.3.

In each of the morphologies the PB blocks form a compact hydrophobic domain, and the PEO blocks form a hydrated corona around this hydrophobic domain. As the fraction of PEO in the diblock increases a surface of increasing curvature is required to efficiently pack the block copolymer into this arrangement. More precisely the morphology of the amphiphilic polymer is dictated by a local minimization of free

energy, and the primary contributions to the free energy in this case are: chain stretching of the core hydrophobic block, interfacial energy, and the repulsion between coronal chains.[45] Thus, to minimize free energy the amphiphilic interface adopts a preferred curvature and this dictates the morphology. As the weight fraction of PEO increases so does the preferred curvature, and the morphology transitions from bilayers to cylinders to spheres, as illustrated in Figure 1.3.

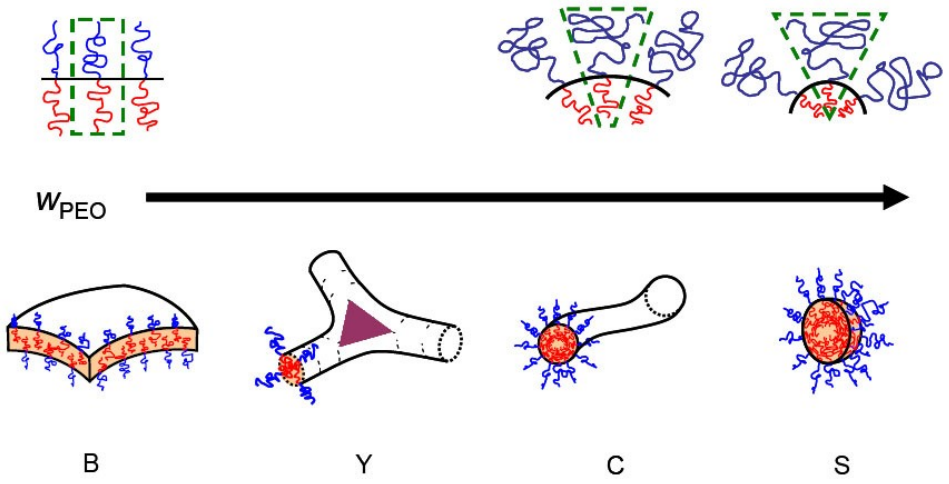

Figure 1.3 A cartoon illustration of how OB diblock copolymer morphology changes as w_{PEO}, the weight percentage of PEO in the diblock, is increased. At top the increasing curvature of the interface is illustrated, and below the morphologies are shown: bilayer (B), cylindrical micelles with Y-junction (Y), cylindrical micelle (C), and spherical micelle (S). Figure reporduced from Jain et al.[46]

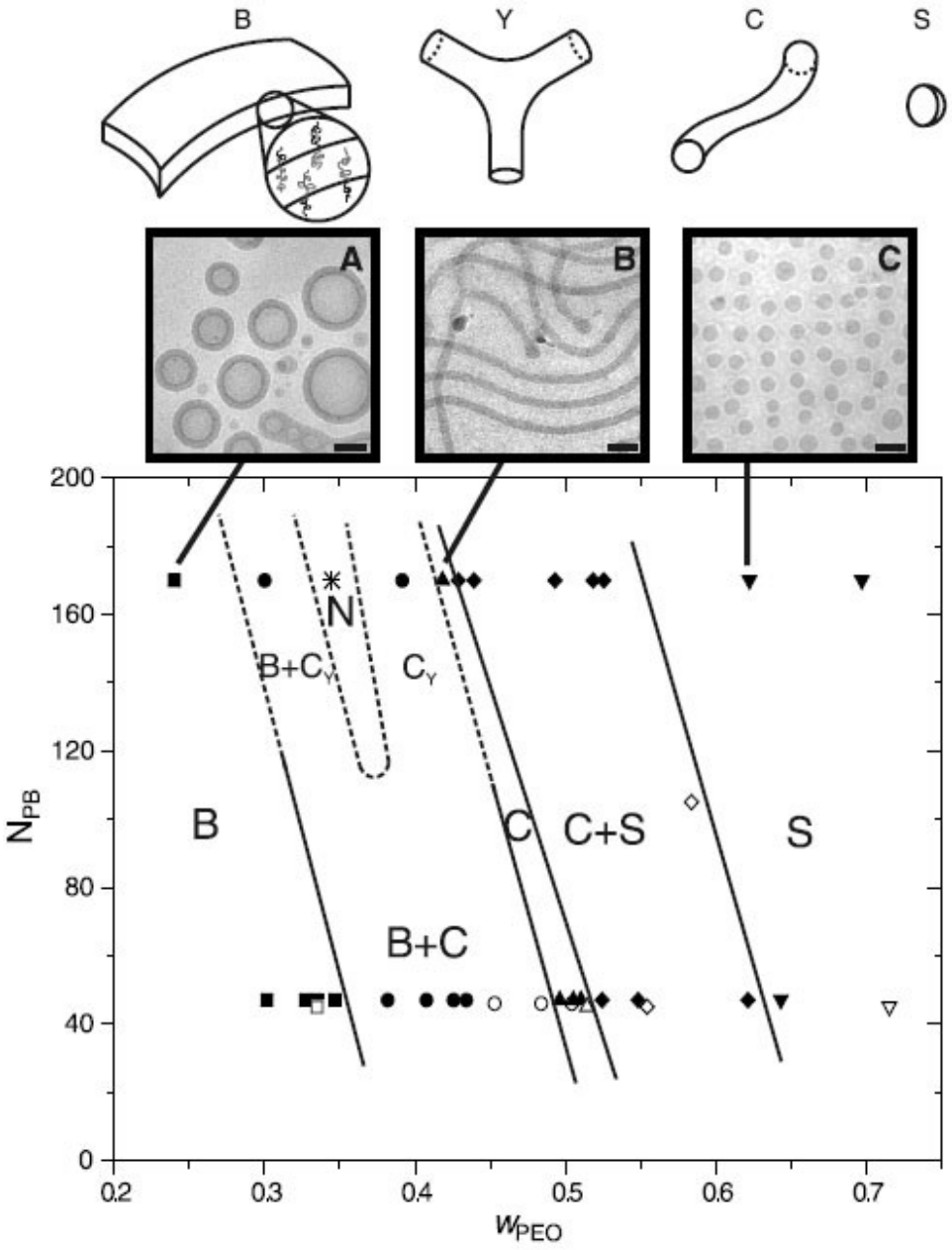

Figure 1.4 Morphological diagram for dilute (1wt%) aqueous solutions of PB-PEO (OB) diblock copolymer. Morphological regions are plotted as a function of the number average degree of polymerization of the PB block, N_{PB}, and the PEO weight fraction, w_{PEO}, in the diblock copolymer. Five morphologies are identified: bilayer membranes forming vesicles (B), cylindrical micelles (C), spherical micelles (S), cylindrical micelles with Y-junctions (C_Y), and a network of cylindrical micelles (N). Above, cartoons of these morphologies have been drawn and corresponding cryo-TEM images of bilayer vesicles (A), cylindrical micelles (B), and spherical micelles (C) are presented. Figure reproduced from Jain et al., with permission from AAAS.[45]

As shown in Figure 1.4, in addition to depending on the hydrophilic weight fraction, w_{PEO}, the morphology also has a weak dependence on the length of the PB block, N_{PB}. This is explained by the volume of the hydrated hydrophilic block growing more rapidly than that of the core hydrophobic block for a proportionate increase in chain length. By a scaling argument it was found that the core PB chain should grow in volume at a reduced rate ($V_{core} \propto N_{PB}^{1.8}$), where V_{core} is the volume of the core domain and N_{PB} is the degree of polymerization of the PB block, compared to the hydrated PEO chain volume ($V_{corona} \propto N_{PEO}^{\sim 2.3}$), where V_{corona} is the volume of the corona domain and N_{PEO} is the degree of polymerization of the PEO block.[47] Thus for a constant PEO fraction the interfacial curvature increases with increasing molecular weight.

1.2.1 Peptide Conjugated Block Copolymers

As discussed, polymer vesicles are self-assembled structures and as such the morphology adopted is critically dependent upon the fraction of a block copolymer that is hydrophilic at the time of self-assembly. As such it is not surprising to find that the conjugation of a highly hydrophilic peptide sequence onto the end of an OB block copolymer before aqueous self-assembly could drive the system to assemble unexpected morphologies, as was found by Zupancich et al.[48] OB block copolymers were first conjugated with GRGDSC peptides then self-assembled in aqueous solutions, and the morphologies formed by this methodology were found to be perturbed by the presence of the peptide during the self-assembly process, as shown in Figure 1.5. GRGDSC (Gly-Arg-Gly-Asp-Ser-Cys) is the amino acid sequence of the conjugated peptide.

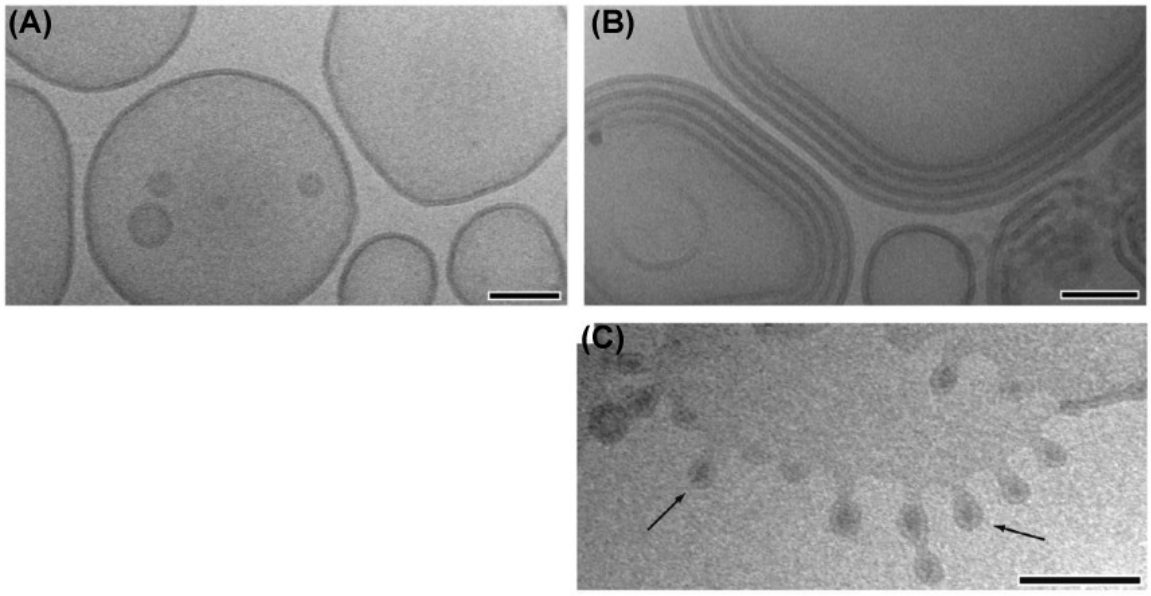

Figure 1.5 Cryo-TEM images of O_{28}-B_{46} (subscripts indicate degree of polymerization) self-assembled aqueous morphologies for OB conjugated with 0.6 molar equivalents of GRGDSC peptide (B,C) and without peptide conjugates (A). The OB polymer was conjugated with peptide moieties before hydration and self-assembly in an aqueous solution. The bulbous features pointed out by arrows in image (C) were believed to be interior aggregates of GRGDSC peptide spanning off of a large bilayer sheet. All scale bars indicate 100 nm. Figure reproduced from Zupancich et al., with permission from the ACS.[48]

This would seem to confound efforts to synthesize and form peptide functionalized polymer vesicles, however it has been shown both within this thesis work and elsewhere that if polymer vesicles are first pre-assembled in solution and then peptide ligands conjugated onto the exterior surface of the polymer vesicle the vesicle morphology can be preserved.[49–52] Amphiphilic block copolymers, including OB, behave as essentially nonergodic systems in aqueous solutions, able to achieve local equilibrium within a single morphology, but not able to achieve equilibrium between morphologies.[53] Within practical limits the high molecular weight of amphiphilic diblock copolymers, such as OB, prevent chain exchange and chain flipping between bilayers, and the dense PEO

coronas of polymer vesicles prevent fusion and fission of vesicles.[54–58] Thus, it is thought that polymer vesicles, once formed, are essentially kinetically trapped in the vesicle morphology. These features are taken advantage of in this thesis work to enable the post-assembly functionalization of the exterior of polymer vesicles with relatively high quantities of peptide ligands without disruption of the polymer vesicle morphology.

1.3 Fibronectin Mimetic Peptide Ligands

Fibronectin is a very large (~440 kDa) extracellular matrix (ECM) protein consisting of many discrete domains, as shown in Figure 1.6.[59] It is composed of a linear sequence of 29 protein modules (often called domains), each of one of three types (I, II, or III), and has a number of adhesion sites along its length. Different domains along the backbone of fibronectin are known to bind a wide variety of other proteins including collagen, fibrin, heparin, syndecan, fibronectin itself, and the $\alpha_5\beta_1$ integrin.[60,61] The adhesion domains of interest to this thesis research are contained in the III-9 and III-10 domains of fibronectin. These two adjacent domains contain the primary binding sequence, RGD (Arg-Gly-Asp), and the synergistic binding sequence, PHSRN (Pro-His-Ser-Arg-Asn), for the cell surface $\alpha_5\beta_1$ integrin complex.[62,63]

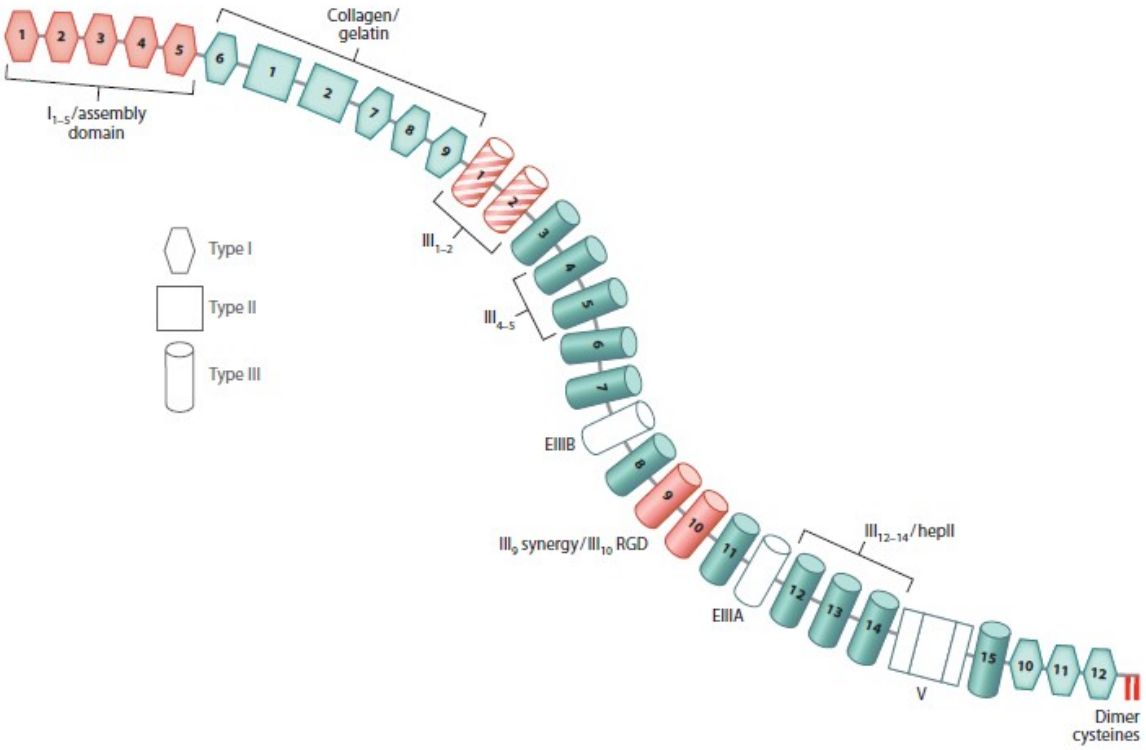

Figure 1.6 Pictographic illustration of a fibronectin subunit. Each subunit consists of a linear sequence of domains, each of either Type I, II, or III. A number of binding domains are labeled along backbone of fibronectin, in particular the III-9 synergy / III-10 RGD adhesion domains. The curvature shown in the illustration imitates that found in native fibronectin, as determined by rotary shadowing electron microscopy.[64] Figure reproduced from Singh et al., with permission from Annual Reviews.[61]

The RGD and PHSRN binding sequences are both presented on the same face of fibronectin in its folded conformation, as shown in Figure 1.7(A).[65] They each exist in conformationally mobile loops anchored between two beta sheets, and are separated by only 30-40 Å in the folded conformation of domains III-9 and III-10.[65–67] Fibronectin, through these binding sequences, selectively binds cell surface $\alpha_5\beta_1$ integrins.[68–70] It has been shown that through the synergistic activity of the PHSRN binding sequence fibronectin does not bind other RGD-adhering integrins, and instead selectively binds the

$\alpha_5\beta_1$ integrin.[71] When native fibronectin binds to cell surface integrins it promotes integrin clustering followed by recruitment of intracellular proteins to the integrin cytoplasmic domains.[61] This in turn activates actin cytoskeleton polymerization, generating contractile forces, and leads to intracellular signaling through kinase cascades.[72–74]

Short RGD containing peptide ligands are commonly used as integrin binding and cancer targeting ligands in the literature, and have been shown to perform respectably in these roles.[75–77] However these simple peptide ligands lack the synergy binding sequence, PHSRN, and therefore do not selectively bind to the $\alpha_5\beta_1$ integrin, and have less adhesion strength for cell surface integrins than native fibronectin.[62,78–80] To improve upon these deficiencies a few groups have attempted to design peptides that incorporate RGD and PHSRN and found mixed results.[78,81–86] The length of the spacer group between the two sites was found to be crucial, however simply matching the spacer length proved to be insufficient to mimic the specificity and adhesion of native fibronectin.[83,87] The Kokkoli group also sought to design a fibronectin mimetic peptide incorporating both the RGD and PHSRN binding sequences, and in addition to appropriately matching the spacing between these sequences they also mimicked the hydrophilicity of the linking region found in fibronectin.[88] This proved to be a critical insight, and after a few rounds of sequence optimization a fibronectin mimetic peptide with strong integrin adhesion and high selectivity for $\alpha_5\beta_1$ integrin was developed.[89,90] The design elements of this fibronectin mimetic peptide, named PR_b, are illustrated in Figure 1.7.

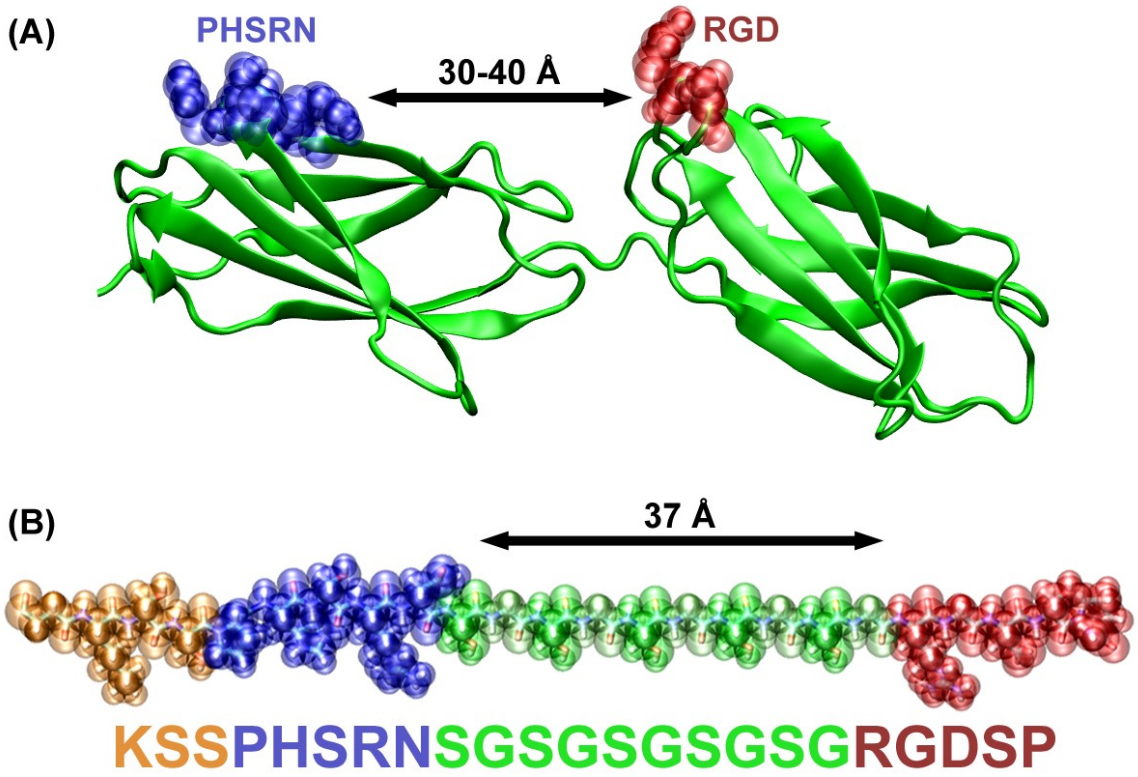

Figure 1.7 (A) Fibronectin domains III-9 and III-10 with the synergy binding sequence, PHSRN, and the primary binding sequence, RGD highlighted for clarity.[65] (B) The fibronectin mimetic peptide, PR_b, illustrated pictographically. In the design of PR_b, both the distance between the binding sequences and the hydrophilicity of the linking region, $(SG)_5$ (colored green), was matched to those of fibronectin. The short KSS spacer sequence (colored orange) is included to simply provide additional length to the PR_b peptide and allow for more degrees of freedom when adhered to a surface. (not drawn to scale)

The PR_b peptide has proven to be a highly effective fibronectin mimetic peptide, yielding comparable cell adhesion and $\alpha_5\beta_1$ integrin selectivity to that of the full fibronectin protein when surface functionalized with both were compared.[89] In addition, functionalization of liposomes with the PR_b peptide has been shown to promote cell adhesion and uptake of these liposomes, even above and beyond RGD functionalized liposomes, to cell lines expressing the $\alpha_5\beta_1$ integrin (e.g. colon and prostate cancer

cells).[91–94] Expression of $\alpha_5\beta_1$ integrin is known to be highly up-regulated in tumor vasculature and in tumor cells of breast, prostate, rectal, and colon cancers as well as being minimally expressed in normal healthy vasculature.[95–102] PR_b then, with its high selectivity for the $\alpha_5\beta_1$ integrin is a promising peptide ligand for the targeted delivery of polymer vesicles to cancerous cells. In fact, $\alpha_5\beta_1$ is prominent on embryonic cell types and is down-regulated on many cell types during development.[103] Heightened expression of $\alpha_5\beta_1$ has also been shown to be associated with increased tumorgenicity, malignancy, and invasiveness of cancer cells.[98,104–107]

2 Polymer vesicles functionalized *via* "click" chemistry with the fibronectin mimetic peptides PR_b and GRGDSP for targeted delivery to cells with different levels of $\alpha_5\beta_1$ expression[1]

2.1 Introduction

Targeted delivery holds great promise for the increased efficacy of a wide variety of currently employed and experimental therapeutic drugs. In contrast to conventional drug delivery, which distributes a drug indiscriminately, targeting strategies promote delivery only to the pathological site. This affords a number of advantages, including a reduction of side effects caused by "off-target" delivery, and increased efficacy due to greater capture of the drug by the targeted tissue.[108] In addition, targeted drug delivery strategies that can encapsulate a drug, as described in this work, have the additional advantage of protecting the drug from degradation or inactivation, along with providing potential site specific release. Most cancer treatment therapies are accompanied by deleterious side effects, which have the potential to be greatly reduced or even eliminated through the synergistic use of delivery vehicles, such as polymer vesicles endowed with targeting peptide ligands.[109,110]

Polymersomes, a term coined due to their analogous structure and similar potential applications to liposomes, are spherical vesicle nanoparticles that self-assemble from amphiphilic block copolymers.[44,55,109,111] They consist of an aqueous pocket surrounded by a polymeric bilayer membrane.[112] Hydrophilic polymer brushes on either

[1] Reproduced with permission from reference 52. Copyright 2012 The Royal Society of Chemistry.

side of this membrane shield and isolate a thick hydrophobic core layer from the surrounding aqueous environment.[113] Both the aqueous pocket and the hydrophobic membrane core can be effectively loaded with a wide range of therapeutics.[38,114–116] Polymersomes afford many advantages over liposomes, mainly deriving from the higher molecular weight block copolymers that form the polymersome membrane. Polymersomes exhibit improved mechanical properties, lower permeability, and feature a dense hydrophilic polymer brush-like corona that have been shown to result in significantly longer circulation half-lives *in vivo*.[18,44,113] Polymersomes are highly stable, exhibiting low dissociation rates and limited leakage as opposed to liposomes.[53,114,117] Moreover, the properties and surface chemistry of polymersomes can be tuned through molecular weight control and the expansive synthetic toolboxes of polymer and organic chemistry.[110] Consequently, polymersomes have already achieved preliminary research successes in drug delivery and other biomedical applications.[50,118–123]

Highly site specific targeted drug delivery requires molecules or ligands, such as peptides, capable of interacting selectively with diseased cells.[124] The PR_b peptide (amino acid sequence KSSPHSRN$(SG)_5$RGDSP) is a targeting peptide designed in our lab to mimic the cell binding site of the native fibronectin protein.[88,89] PR_b was designed to incorporate both the RGD motif, the primary binding site in fibronectin, as well as the PHSRN sequence, the synergistic binding site in fibronectin.[62,80,125] These two binding sites are connected by a linker, $(SG)_5$, chosen to match both the distance and the hydrophobicity/hydrophilicity of the linking region that exists in fibronectin.[89,90] It should be noted that fibronectin is actually a very large (~440 kDa) extracellular matrix

(ECM) protein consisting of many discrete domains.[59] Different domains along the length of fibronectin are known to bind a wide variety of other proteins including collagen, fibrin, heparin, syndecan, fibronectin itself, and the $\alpha_5\beta_1$ and $\alpha_v\beta_3$ integrins that bind to fibronectin through a separate cell-binding domain.[60,61] However, we have chosen to design PR_b to specifically mimic the primary and synergistic cell binding sites in fibronectin, found natively in the III-10 and III-9 domains of fibronectin respectively, for the cell surface integrin, $\alpha_5\beta_1$.[62,75] In past studies the PR_b peptide has been shown to significantly outperform other RGD-containing peptides both in terms of adhesion and specificity.[89,91,92] PR_b has been shown to specifically bind the $\alpha_5\beta_1$ integrin on cell surfaces, whereas other simple RGD-containing peptides bind a range of surface integrins.[89,91] Recent experiments with PR_b have demonstrated that PR_b surfaces could outperform even fibronectin coated surfaces.[89] The high selectivity of PR_b for $\alpha_5\beta_1$ integrin holds great promise for targeted drug delivery due to the fact that $\alpha_5\beta_1$ integrin is highly up-regulated in tumor vasculature and in tumor cells of breast, prostate, rectal, and colon cancers as well as being minimally expressed in normal healthy vasculature.[95–102,126] Additionally, heightened expression of $\alpha_5\beta_1$ has been shown to be associated with increased tumorgenicity, malignancy, and invasiveness of cancer cells.[98,104–107]

In this study, the targeted delivery of polymersomes to colon cancer cells (CT26.WT) has been investigated. The targeting peptides PR_b and GRGDSP were conjugated onto the exterior surface of the polymer vesicles using azide-alkyne "click" chemistry and the ability to promote targeted drug delivery was assessed and compared.

The amphiphilic block copolymer, poly(ethylene oxide)-*b*-poly(1,2-butadiene) (PEO-PB or OB for short), was synthesized and self-assembled in water to form polymer vesicles. The potential to conjugate these polymer vesicles with peptides using "click" chemistry was demonstrated and the amount of peptide conjugated onto the surface was quantified. Cell adhesion and internalization of polymer vesicles functionalized with PR_b was compared to non-functionalized and GRGDSP functionalized vesicles, and delivery of an encapsulate was studied both quantitatively and using confocal microscopy. Cytotoxicity studies were carried out to assess the ability of doxorubicin loaded polymer vesicles to effectively deliver a chemotherapeutic to colon cancer cells. More important, the specificity of the peptide functionalized polymersomes for the target of interest, $\alpha_5\beta_1$ integrin, was investigated by antibody blocking studies and assessing polymersome delivery to two cell lines with disparate levels of $\alpha_5\beta_1$ expression.

2.2 Materials and Methods

2.2.1 Materials

Unless otherwise noted all chemicals were obtained from Sigma-Aldrich (St. Louis, MO) and used as received. Peptides PR_b and GRGDSP were custom synthesized and obtained on the bead, with the side groups protected, from the Microchemical Facility at the University of Minnesota. The extruder and the 200 nm extrusion membranes were obtained from Avestin Inc. (Ottawa, Canada). The CT26.WT mouse colon cancer cell line was obtained from ATCC (Manassas, VA). Hoechst 33342 nucleic stain, Alexa Fluor® 594 wheat germ aggutin (WGA) cell membrane stain, ProLong Gold antifade reagent, and RPMI-1640 cell culture media were obtained from Invitrogen (Carlsbad,

CA). Fetal bovine serum (FBS) was obtained from Atlas Biologicals (Fort Collins, CO). Human fibronectin-coated round coverslips were purchased from BD Biosciences (San Jose, CA). Primary and secondary antibodies, anti-integrin $\alpha_5\beta_1$ (MAB2514) and anti-rat IgG, FITC conjugated (AP136F), were obtained from Millipore (Billerica, MA).

2.2.2 Polymer Synthesis

Poly(ethylene oxide)-*b*-poly(1,2-butadiene) (OB) was synthesized sequentially using previously published anionic polymerization techniques.[127] First hydroxyl terminated poly(1,2-butadiene) (PB) homopolymer was synthesized. Then in a separate reaction the poly(ethylene oxide) (PEO) block was grown off the end of the PB block to form the OB diblock.

2.2.3 Synthesis of Azide Terminated OB (OB-N3)

The hydroxyl end group of the OB polymer was replaced with an azide group via mesylation followed by reaction with sodium azide. OB diblock was dissolved in dichloromethane (DCM) (10 mM) to which a 5 times excess of triethylamine was added. The solution was cooled to 0 °C, a 2.5 fold excess of methanesulfonyl chloride was added dropwise, and the mixture was stirred overnight at room temperature (RT).[128,129] The resulting mesylated OB polymer, OB polymer with a methanesulfonyl end-group in the place of the hydroxyl end-group, was recovered by rapid washes with cold distilled water, slightly acidic water (HCl), saturated sodium bicarbonate solution, and finally brine. Dry polymer was recovered by rotary evaporation, followed by vacuum distillation from a benzene solution.

This mesylated OB polymer was then reacted with sodium azide to give azide end-capped OB diblock. Dry mesylated OB was dissolved in N,N-dimethylformamide (DMF) (8 mM) and a 3 times excess of sodium azide was added. The reactor was charged with Argon, heated to 65 °C, and stirred overnight. To sequester any unreacted sodium azide before adding DCM a 5 fold excess of 3-bromopropionic acid was added and the reactor stirred overnight. DMF was removed by vacuum distillation at 65 °C, and the resulting polymer was washed and recovered as before. Quantitative addition of the azide end group to form OB-N_3 was confirmed by ^{1}H NMR, Figure 4.9.

2.2.4 Synthesis of Alkyne Terminated Peptides

A terminal alkyne functional group was attached to the PR_b and GRGDSP peptides to enable the "click" conjugation of these peptides with OB-N_3. The peptide was synthesized using standard FMOC solid phase peptide synthesis procedures. Before cleaving and deprotecting the peptide from its solid phase support the unprotected N-terminal of the peptide was reacted with 4-pentynoic acid. To a suspension of side-group protected peptides "on-bead" in DMF was added a 4.5 fold excess of N,N-diisopropylethylamine, a 3 fold excess of HBTU (o-benzotriazole-N,N,N',N'-tetramethyl-uronium-hexafluoro-phosphate), and a 5 fold excess of 4-pentynoic acid. After shaking for 3 h the reaction suspension was washed with DMF, and the peptide was deprotected and cleaved by reaction with a solution of 95% (v/v) TFA, 2.5% water, 2.5% triisopropylsilane for 2 h. Cleavage products were separated from the beads by filtration and concentrated by rotary evaporation. The peptide was dissolved in distilled water, washed 4 times with cold ether, lyophilized, and further purified by reversed phase high

performance liquid chromatography (HPLC) using an Agilent 1100 Series system using a Waters XTerra PrepMS C_{18} column. Alkyne terminated peptides, either PR_b or GRGDSP, were analyzed by electrospray ionization mass spectrometry (ESI-MS) on a Bruker BioTOF II to confirm its identity and purity.

2.2.5 Polymer Vesicle Formation

Polymer vesicles were prepared by self-assembly of the OB diblock in aqueous solutions using film rehydration.[114] OB and OB-N_3 polymers were placed in a vial in the desired ratio, and chloroform was added to form a concentrated polymer solution (~100 mg/ml). The mixture was gently shaken at RT for 24 h. Films were formed by drying, with all traces of chloroform removed using a high vacuum. An aqueous solution was then added to the film to form a 1% (w/w) solution of polymer. For the samples used in fluorescence studies 3.0 mM carboxyfluorescein in HBS buffer (10 mM HEPES, 150 mM sodium chloride) was added, and for the samples used in cytotoxicity assays a 120 mM ammonium sulfate solution was added. After a few days of stirring, polymer vesicles were fully dispersed. Vesicles were extruded at 70 °C through polycarbonate membranes with well defined 200 nm pore sizes. After extrusion each vesicle sample was characterized by dynamic light scattering (DLS) using a 90 Plus BI-MAS instrument (Brookhaven Instrument Co.) to determine the size distribution.

2.2.6 Peptide Conjugation

The PR_b and GRGDSP peptides were conjugated onto the surface of the preformed polymer vesicles using the azide-alkyne "click" Huisgen cycloaddition reaction.[130] To a dispersion of vesicles at 4 °C was added a 2 fold excess of alkyne

terminated peptide and copper sulfate (1.1 mM), sodium ascorbate (5.5 mM), and bathophenanthrolinedisulfonic acid (2.2 mM).[131–133] The reaction was stirred for 24 h and allowed to come slowly to R.T., after which a 5 fold excess, with respect to copper, of EDTA (ethylenediaminetetraacetic acid) was added to the solution to sequester the copper. The vesicle samples were then purified by dialysis in phosphate buffered saline (PBS) with Spectra/Por 6 dialysis tubing (50 kDa MWCO). The samples were dialyzed for a total of 3 days with the dialysate being changed every 4-12 h for a total of at least 6 times. The concentration of fluorophore in the dialysate was regularly monitored by fluorescence spectroscopy to assess the progress of the purification.

2.2.7 Peptide Quantification

For each formulation, 50 µl of sample and 50 µl of 100 mM borate buffer (BB), pH 8.6, with 10% (v/v) Triton X-100 was added to a microtube. This mixture was allowed to sit at RT for 1 h to allow vesicles to fully break and dissociate.[56] Then 50 µl of fluorescamine solution, 1.0 mg/ml in acetone, was added quickly followed by rapid "up-and-down" pipetting and vortexing.[134] The mixture was allowed to incubate protected from light at RT for 30 min., allowing fluorescence to develop. Fluorescamine reacts specifically with primary amines in solution (the peptide is the only available source) to form a fluorescent complex.[135,136] The solution in the microtube was then transferred to a cuvette and diluted with 1.2 ml BB with 5% (v/v) Triton X-100. Fluorescence was measured on a Cary Eclipse fluorescence spectrophotometer (Varian) at 390/475 nm (ex/em). This measurement was correlated with a calibration curve constructed from

identical measurements of serial dilutions of free peptide in solution to determine the concentration of peptide in the sample.

Finally, to determine the mol% of polymer conjugated with peptide this measurement was combined with a measurement of the concentration of polymer in the sample. Polymer concentrations of extruded samples were found by measuring absorbance at 575 nm on a SpectraMax Plus (Molecular Devices), then correlating this measurement with a calibration curve constructed from identical measurements of serial dilutions of an extruded polymer vesicle sample of known polymer concentration.

2.2.8 Cell Culture

CT26.WT and Caco-2 cells were grown in RGM (modified RPMI-1640 medium supplemented with 10% (v/v) fetal bovine serum (FBS), 100 units/ml penicillin, and 0.1 mg/ml streptomycin) and MGM (modified Minumum Essential Medium, MEM, supplemented with 20% (v/v) FBS, 100 units/ml penicillin, and 0.1 mg/ml streptomycin) respectively, as reported previously.[91] Medias were replaced on a two day cycle and cells were passaged when they reached ~70% confluence by treatment with TrypLE™ Select (Invitrogen).

2.2.9 Fluorescence Plate Assay

A fluorescence plate assay was used to quantify the binding and internalization of polymer vesicles to cells. To each well of a cell culture treated 24 well plate was added 0.5×10^6 CT-26.WT cells in 150 µl RGM-2 (RGM with only 2% (v/v) FBS). CT26.WT cell lines were grown and maintained as reported previously.[137] Cells were allowed to adhere to the plate surface by incubating at 37 °C for 3 h. 50 µl of polymer vesicle

sample (diluted with PBS when necessary) were added to each well to make the final polymer concentration in each well 25.0 μM. That this polymer concentration also gave a consistent, within the limits of fluorescent detection, intra-well carboxyfluorescene concentration was also checked. Plates were incubated protected from light for 24 h at 37 °C. Then the plates were gently washed twice with PBS, inverting the plates to pour off the wash solutions, to remove any unbound polymer vesicles but leave the cells adhered to the plate. Plates were frozen at -80 °C to permeabilize the cells, and thawed at RT for 3 h. 500 μl of BB with 5% (v/v) Triton X-100 was added to each well and the plates were allowed to sit at RT for 3 h to completely break and dissociate the cells and the polymer vesicles.[56] Finally fluorescence was measured (SynergyMX, BioTek) at 485/516 (ex/em). Negative controls were also run where peptide conjugated polymer vesicles were delivered to wells containing no cells and nonspecific adhesion to the plate itself was determined to play no part in this measurement.

Integrin $\alpha_5\beta_1$ blocking experiments were performed in an identical fashion to the protocol detailed above, with the following slight alterations. After cells had adhered to the plate surface, they were cooled to 4 °C. The $\alpha_5\beta_1$ blocked cells were pre-incubated with an anti-integrin $\alpha_5\beta_1$ antibody at 15 μg/ml for 30 min at 4 °C. After this pre-incubation polymer vesicle samples were added and incubated with the cells for 1 h at 4 °C.

2.2.10 Confocal Microscopy

CT26.WT or Caco-2 cells were seeded onto fibronectin modified coverslips in RGM-2 or MGM-2 (MGM with only 2% (v/v) FBS) and allowed to adhere. Polymer

vesicle samples were added to the monolayer of cells at a final polymer concentration of 25.0 μM. The cells were incubated with the vesicles at 37 °C for 24 h. Afterwards the cells were prepared for confocal imaging by fixing, staining, and mounting. The coverslips were gently washed twice with 37 °C fluorescence buffer (FB), PBS supplemented with 0.02% (v/v) sodium azide and 2.5% FBS. Then they were incubated for 15 min at 37 °C in 4% (v/v) paraformaldehyde in PBS, to fix the cells. The coverslips were washed three times with 37 °C FB, followed by fluorescently staining the cells by incubating them in a mixture of nuclear and cell membrane stains in FB for 10 min at 37 °C. The cell membrane permeable blue fluorophore, Hoechst 33342 (2.0 μmol/ml), was used as a nuclear stain, and the cell impermeable red fluorophore, Alexa Fluor® 594 wheat germ agglutinin (5.0 μg/ml), was used as a cell membrane stain. After staining, the coverslips were again washed three times with FB, then mounted facedown onto glass cover slides with ProLong® Gold antifade reagent. Imaging each slide with confocal microscopy a series of "z-slices" (images of planar cross-sections at varying heights within the cell) were taken with an offset of 0.25 μm, spanning the entire height of the cells. An Olympus Fluoview 1000 Confocal Laser Scanning Microscope in the Biomedical Image Processing Laboratory (BIPL) at the University of Minnesota was used.

2.2.11 Flow Cytometry

Cells were suspended in 4 °C FB at a cell concentration of 1 x 10^6 cells/ml in 15 ml centrifuge tubes. Tubes were incubated at 4 °C for 35 min on a rotary tilter with either 10 μg/ml anti-integrin $\alpha_5\beta_1$ antibodies or 10 μg/ml rat isotype control IgG. Cells were then

pelleted by centrifugation and washed twice in 4 °C FB, and then incubated with 20 μg/ml of a secondary antibody (anti-rat IgG, FITC conjugated) on a rotary tilter for 35 min at 4 °C. Finally, cells were pelleted by centrifugation and washed twice in 4 °C FB, suspended in 4 °C FB, and analyzed by flow cytometry immediately. The FACS Caliber located at the Flow Cytometry Core facility in the Masonic Cancer Research Center of the University of Minnesota was used.

2.2.12 Doxorubicin Loading

The chemotherapeutic drug, doxorubicin (DOX), was loaded into polymer vesicles by a remote loading protocol using an ammonium sulfate gradient.[138,139] Vesicles were formed in a 120 mM solution of ammonium sulfate. Following peptide conjugation and purification by dialysis, DOX was added to each sample at a concentration of 0.25 mg/ml. The samples were shaken at RT for 72 h, and then purified by dialysis again in PBS, with regular monitoring of the doxorubicin concentration in the dialysate by fluorescence spectroscopy. The native fluorescence of DOX was also used to measure the amount of DOX encapsulated in each polymersome sample. Each sample was measured in triplicate and wells were prepared with 10 μl of sample and 190 μl of PBS with 5% (v/v) Triton X-100. The mixture was incubated at RT for 1 h, and then the DOX fluorescence 485/590 nm (ex/em) was read on a fluorescence plate reader (SynergyMX, BioTek).

2.2.13 Profiling Doxorubicin Release

Release of DOX from polymersomes was monitored fluorescently over the course of minutes or hours. On a 96-well plate polymersome samples were plated in triplicate,

with 10 µl of DOX loaded polymersomes and 190 µl of MES buffer of pH either 7.4, 6.5, 5.5, or 4.5 per well. On this same plate was run a series of serial dilutions of free-DOX in the identical buffer, such that a unique DOX concentration correlation curve could be constructed for each time point measured. The release of DOX from the self quenching environment within the polymersomes was monitored fluorescently at 37 °C over time on a fluorescent plate reader (SynergyMX, BioTek).

2.2.14 Cell Viability Assay

The MTT cytotoxicity assay was used to test the efficacy of the targeted polymer vesicle formulations to delivery DOX and kill cancer cells in vitro. Cells, either CT26.WT or Caco-2 cells, were seeded onto 96 well plates at 20,000 cells per well in 150 µl of either RGM-2 or MGM-2 respectively. Cells were allowed to adhere for 12 h at which point (t = 0 h) 50 µl of sample: polymer vesicles, free-drug in PBS, or PBS was added to each well. The plates were incubated for 24 h at 37 °C, then 15 µl of MTT reagent (5 mg/ml thiazolyl blue tetrazolium bromide in PBS) was added to each well, and the plates were incubated for 4 h more at 37 °C. A solubilizing solution of 10% (v/v) Triton X-100 and 0.1 M HCl in isopropanol was added to the plates (150 µl per well), and the plates were further incubated, protected from light, for 2 h at R.T. Finally, the absorbance and background absorbance was measured at 570 nm and 690 nm respectively using a SynergyMX spectrophotometer (Biotek).

2.2.15 Cryogenic Transmission Electron Microcopy (Cryo-TEM)

Vitreous samples were prepared within a controlled environment vitrification system (CEVS). A droplet of solution (~10 µl) was deposited on a copper TEM grid

coated with a holey polymer film (Ted Pella). A thin aqueous film (< 300 nm) was obtained by blotting with filter paper. After allowing the sample sufficient time to relax from any residual stresses imparted during blotting (~30 s), the grid was plunge cooled in liquid ethane at its freezing point, resulting in vitrification of the aqueous film. Sample grids were examined at -179 ºC in a JEOL 1210 transmission electron microscope operating at 120 kV, and images were recorded with a Gatan 724 multiscan digital camera.

2.2.16 Size Exclusion Chromotography (SEC)

Polymer polydispersity indices (PDI) were determined at RT using a Waters 717 GPC equipped with three Polymer Labs Mixed-C columns and a Waters 410 differential refractometer and THF as the mobile phase (1.0 ml/min flow rate). The instrument was calibrated with 10 monodisperse polystyrene standards with M_n ranging from 580 to 377,400 g/mol (Polymer Labs).

2.2.17 ^{1}H NMR Spectroscopy

^{1}H NMR Spectroscopy was used to determine the degree of polymerization of the OB diblock. To distinguish the end-group from the PEO backbone peaks the polymer was reacted quantitatively with trifluoroacetic anhydride 30 minutes before collecting the spectra.[140] ^{1}H NMR spectra were recorded from polymer dissolved in deuterated chloroform at ~1 wt% on a Varian Unity 300 at RT.

2.3 Results and Discussion

2.3.1 Polymer Synthesis and Characterization

An amphiphilic poly(ethylene oxide)-b-poly(1,2-butadiene) (PEO-PB or OB for short) diblock copolymer (Figure 2.1) was synthesized by living anionic polymerization yielding a product with a relatively narrow PDI (polydispersity index). PEO was chosen as the hydrophilic block because it is non-immunogenic and exhibits a well documented ability to resist opsonization and non-specific adhesion in the hydrated brush form.[141,142] The PEO blocks in the OB diblock are of sufficient length, 2 kDa Mn, and are densely packed on the surface of the polymersomes, so that good opsonization resistance can be expected.[143,144] Hydrophobic PB offers a low glass transition temperature (approximately -4 °C), and allows polymer vesicles to be formed by simple film hydration under mild conditions. The OB block copolymer was endcapped in two ways as shown in Figure 2.1 and Table 2.1: with a terminal group hydroxyl, and with an azide end-cap—used for the conjugation of targeting ligands.

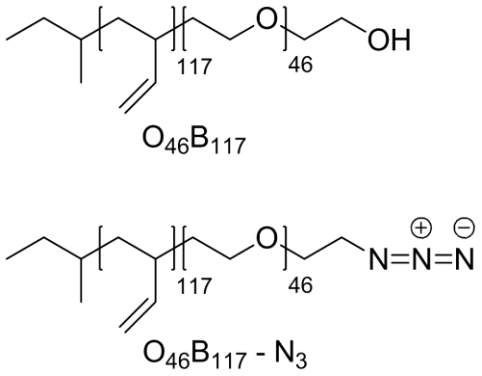

Figure 2.1 Poly(ethylene oxide)-*b*-poly(1,2-butadiene), PEO-PB (OB), block copolymers used in this research. Both azide end-capped (OB-N_3) and hydroxyl (OB) block copolymers.

Table 2.1 lists the weight fraction PEO, w_{PEO}, the number average molecular weight, M_n, as measured by NMR (Figure 4.9), and the PDI, as measured by size exclusion chromatography (SEC, Figure 2.2) for the synthesized OB block copolymers and the PB precursor homopolymer. The weight percentage PEO of 24% was targeted for the OB diblock as well as a molecular weight of 8500 Da because similarly defined OB diblocks have been found to form vesicles.[45] The SEC elution curves for these polymers are presented in Figure 2.2. SEC traces for the PB precursor homopolymer, B, and the two diblock copolymers, OB and OB-N_3 are overlaid on top of one another for comparison. All of the peaks are monomodal and relatively narrow, with PDI less than 1.05 for each polymer, Table 2.1. Adding the PEO block to the PB shifts the response to a lower elution volume. The near overlapping of the OB and OB-N_3 traces indicates that the azide end-capping reaction did not alter the polymer backbone within the detection limits of SEC.

Table 2.1 Block copolymers used in this research.

ID [a]	$\mathbf{w_{PEO}}$ [b]	$\mathbf{M_n}$ **(Da)** [c]	**PDI** [d]
B_{117}	-	6423	1.03
$O_{46}B_{117}$	0.24	8417	1.04
$O_{46}B_{117}$-N_3	0.24	8442	1.04

[a] The susbscripts following 'O' and 'B' denote the degree of polymerization of these blocks. [b] Weight fraction PEO. [c] Number average molecular weight, as measured by NMR. [d] Polydispersity index, as measured by SEC.

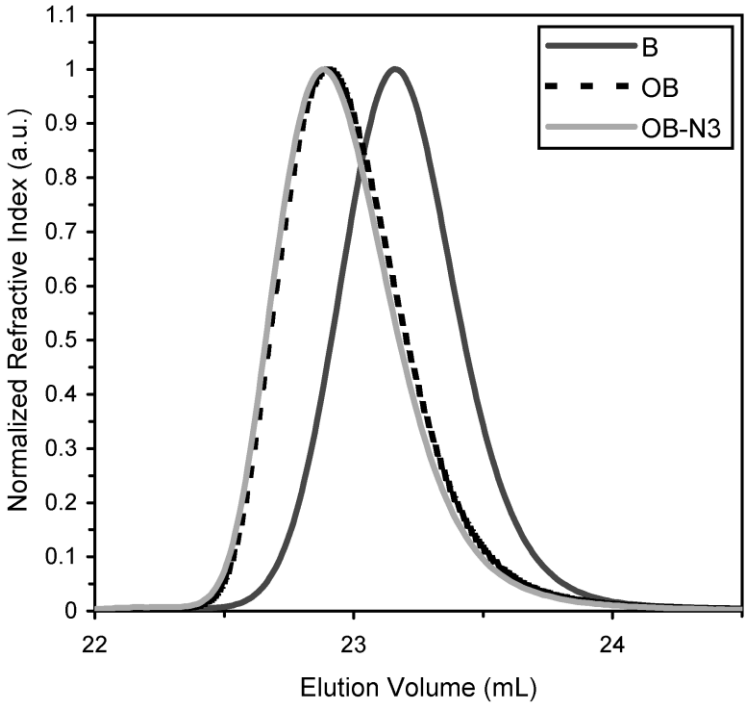

Figure 2.2 SEC traces of the precursor PB homopolymer, B, the hydroxyl end-capped PEO-PB diblock copolymer, OB, and the azide end-capped diblock copolymer, OB-N_3.

2.3.2 Polymer Vesicle Formation and Peptide Functionalization

Polymer vesicles were formed by hydration of dried diblock copolymer films and dispersed in aqueous solutions. Each sample contained a defined blend of azide and hydroxyl endcapped OB polymer so that the desired percent peptide functionalization could be achieved in the vesicle dispersions. Membrane extrusion then reduced the vesicle size to an average hydrodynamic diameter of 252 ± 77 nm as determined by DLS and confirmed empirically by cryo-TEM (Figure 2.3). This vesicle size is on the high range of sizes able to take advantage of the enhanced permeability and retention effect, however vesicles could easily be extruded down to much smaller sizes if needed for

future applications.[8] For this *in vitro* study the ~250 nm size range was simply chosen and held to consistently.

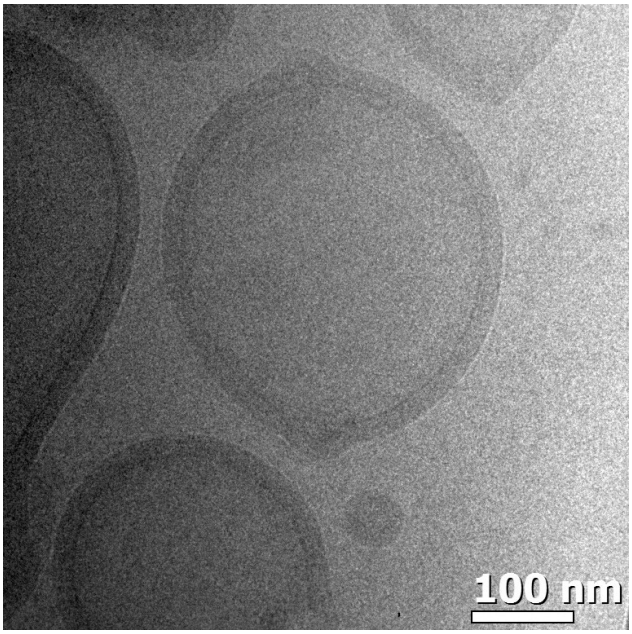

Figure 2.3 Cryogenic transmission electron microscopy (cryo-TEM) image of polymer vesicles with 22.7 mol% PR_b peptide attached.

The azide-alkyne "click" Huisgen cycloaddition reaction was used to conjugate targeting peptides onto the exterior surface of the preformed polymer vesicles. Some of the advantages of this conjugation strategy are that the "click" chemistry reaction can be performed in a mild aqueous environment, exhibits high reaction yields, and a variety of ligands have been conjugated onto the surface of the polymer vesicles with this chemistry.[130,145–151] The "click" conjugation of the peptides used in this study, GRGDSP and PR_b, onto polymer vesicles was found to be quite efficient. For all of the GRGDSP surface concentrations sampled and the PR_b samples with less than 10 mol% PR_b, quantitative conjugation to the surface azide groups was observed, within the limits of

detection. However, for the more heavily functionalized PR_b polymer vesicles, the fraction of surface azides functionalized with PR_b dropped, with for example 60% conjugation for the 17.3 mol% PR_b sample, and 54% conjugation for the 29.8 mol% PR_b sample (Table 2.2). This is presumably due to the larger and more bulky nature of the PR_b peptide. The high specificity of the "click" conjugation reaction allows the targeting peptides used in this study to be attached specifically at the N-terminus, forcing every peptide to be presented on the surface in the same orientation. Previous studies have shown that ligand orientation can have a dramatic impact on the ability of a targeting ligand to promote specific cell responses.[152] Consistent surface presentation is important for studies such as this one, where different targeting ligands are compared.

Table 2.2 Peptide conjugation yield of click chemistry reaction.

mol% Conjugation [a]	**Surface Concentration (#/nm^2)** [b]	**% OB-N_3** [c]	**% Yield** [d]
0%	0.000	0.0%	n/a
0%	0.000	0.0%	n/a
4.9% PR_b	0.048	5.0%	98%
5.6% PR_b	0.055	5.5%	102%
10.3% PR_b	0.100	12.3%	83%
17.3% PR_b	0.164	28.8%	60%
22.7% PR_b	0.221	39.8%	57%
29.8% PR_b	0.285	54.7%	54%
5.2% GRGDSP	0.051	5.3%	98%
5.2% GRGDSP	0.051	5.3%	97%
29.5% GRGDSP	0.285	30.1%	98%
33.5% GRGDSP	0.325	32.1%	104%

[a] mol% peptide with respect to OB diblock. [b] Surface concentration of peptide was estimated based on the measured mol % conjugation, the DLS measured D_h for each formulation, the cryo-TEM measured vesicle core thickness, the PB degree of polymerization (N_{PB} = 117), and the density of PB (0.902 g/cm^3). [c] Weight percent of OB-N_3 polymer loaded in the polymer vesicles. [d] Percent of OB-N_3 on the surface of the polymer vesicle that was conjugated with peptide.

In addition to these desirable features, the "click" reaction strategy permits peptide conjugation after vesicle formation, initial processing, and sizing, as well as insuring peptide conjugation solely onto the outside surface of the polymer vesicles, thereby minimizing peptide waste. Also, processing and purification of the block co-polymers is much more facile in the absence of conjugated peptide. Self-assembled block copolymer vesicles are sensitive to the composition (*i.e.*, the ratio of hydrophobic to hydrophilic block size). Attaching a large targeting pepide to the PEO terminus can disrupt the delicate balance of thermodynamic factors responsible for bilayer formation, driving self-assembly towards a morphology other than vesicles.[48] We have shown in this work that the preformed vesicles, Figure 2.4, are stable to functionalization, even at relatively high loadings of peptides, as demonstrated by the cryo-TEM image in Figure 2.3. The vesicle morphology is clearly retained even for densely functionalized vesicles with 22.7 mol% PR_b, given that the PR_b peptide has a substantial molecular weight (2144 Da) and is highly hydrophilic. Additionally, the PB bilayer core thickness can be determined from cryo-TEM micrographs and is found to be 12.6 ± 1.1 nm thick.

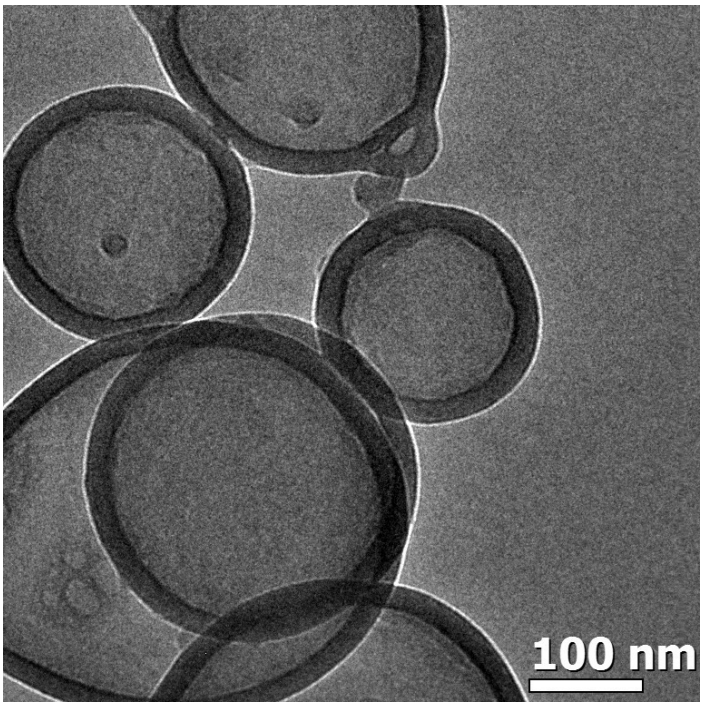

Figure 2.4 Cryogenic transmission electron microscopy (cryo-TEM) image of non-functionalized OB polymer vesicles.

Each vesicle formulation was characterized following peptide conjugation and subsequent purification by dialysis. Vesicle size distributions were analyzed by DLS (an average hydrodynamic diameter (D_h) of 252 ± 77 nm is representative of the polymersome formulations used, Table 2.3) and the concentration of OB polymer and conjugated peptide were quantified, Table 2.2. Quantification of the actual peptide conjugation level is a critical metric when testing and comparing targeting delivery systems. Table 2.2 lists calculated surface concentrations of peptides for all the formulations reported in this paper, based on the actual mol % of peptide conjugation (with respect to OB diblock) quantified for the functionalized polymersomes.

Table 2.3 Polymersome size distributions and molar loadings of encapsulates.

mol% Conjugation [a]	D_h (nm) [b]	Molar Loading ($\times 10^2$) [c]
0%	258.2 ± 68.3	141 ± 2 [d]
0%	237.4 ± 52.6	4.6 ± 0.1 [e]
4.9% PR_b	260.8 ± 38.4	211 ± 3 [d]
5.6% PR_b	273.9 ± 84.7	4.7 ± 0.2 [e]
10.3% PR_b	271.6 ± 33.8	4.6 ± 0.2 [e]
17.3% PR_b	201.9 ± 115.7	4.7 ± 0.1 [e]
22.7% PR_b	264.4 ± 57.3	4.5 ± 0.1 [e]
29.8% PR_b	222.2 ± 125.2	120 ± 3 [d]
5.2% GRGDSP	251.9 ± 60.3	4.7 ± 0.1 [e]
5.2% GRGDSP	232.6 ± 117.3	267 ± 4 [d]
29.5% GRGDSP	245.7 ± 101.8	184 ± 5 [d]
33.5% GRGDSP	263.7 ± 97.4	4.6 ± 0.1 [e]

[a] mol% peptide with respect to OB diblock. [b] Z-average hydrodynamic diameter of polymersome formulation as measured by dynamic light scattering (DLS). [c] The mole ratio of encapsulate (carboxyfluorescein or doxorubicin) to OB block copolymer in each polymersome formulation. [d] Doxorubicin encapsulated. [e] Carboxyfluorescein encapsulated.

2.3.3 Targeted Delivery to Colon Cancer Cells

To assess the ability of these "click" peptide functionalized polymer vesicles to effectively target, adhere to, and internalize into colon cancer cells, a series of *in vitro* experiments involving the targeted delivery of a fluorescent probe to CT26.WT colon cancer cells were conducted. Polymer vesicles were fluorescently tagged by loading their interior aqueous pocket with the fluorophore, carboxyfluorescein. These fluorescent polymer vesicles, with varying amounts of PR_b or GRGDSP targeting peptide on their surface, were then delivered to plated CT26.WT cells *in vitro*. The polymer vesicles were incubated with the cells for 24 h at 37 °C, after which the cells were washed to remove any unbound polymer vesicles. Then either the total fluorescence delivered was measured after the cells were lysed and the polymer vesicles broken (Figure 2.5), or the cells were fixed, stained, and imaged by confocal microscopy (Figure 2.6).

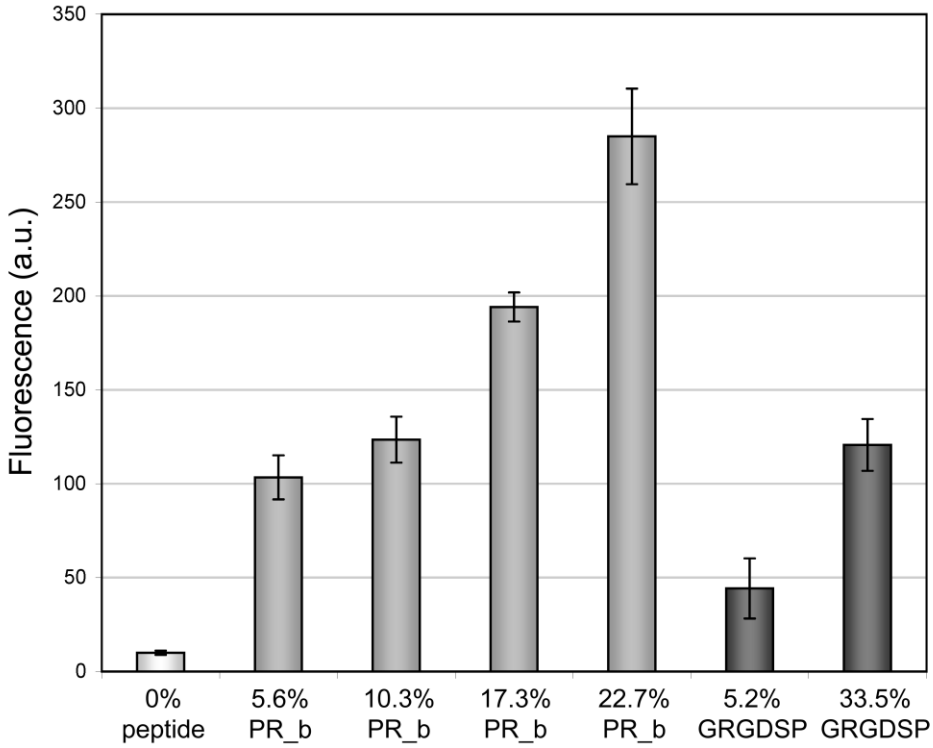

Figure 2.5 Delivery of a fluorescent dye to CT26.WT colon cancer cells by peptide functionalized polymer vesicles. CT26.WT cells were incubated with fluorophore loaded polymer vesicles functionalized with the listed mol% of targeting peptide for 24 h at 37 °C. Data is the mean ± standard deviation of two separate experiments (n=2), and each experiment was performed in triplicate. Fluorescence values have been rescaled so that 0% peptide equals 10.

In Figure 2.5, as more polymer vesicles are bound and internalized by the colon cancer cells, greater fluorescence is measured. Notably, very few of the polymer vesicles without surface peptide (0% peptide) bind or internalize. As has been reported before, these polymer vesicles strongly resist non-specific adhesion and internalization, essentially acting as stealth carriers.[18,55] However, when even small amounts of targeting peptides are installed on the surface of these vesicles they are delivered at much higher levels. When 5.6 mol% of PR_b peptide decorates the surface we observe a 10 times

increase in vesicle delivery over the formulation without peptide targeting ligands. Moreover, for a higher peptide functionalization of 22.7 mol% PR_b a 176% increase in delivery is observed over the case with 5.6 mol% peptide. Indeed, it is observed that for incremental increases in PR_b functionalization (5.6, 10.3, 17.3, 22.7 mol%) a corresponding increase in fluorescence, and therefore cellular delivery is seen. These results indicate that the PR_b targeting peptide conjugated using "click" chemistry is an effective ligand for targeted drug delivery to colon cancer cells and strongly promotes cell adhesion.

The efficacy of PR_b targeted delivery was also compared to that of its close peptide analogue, GRGDSP. Both peptides contain the widely used 'RGD' adhesion domain.[153–161] Clearly the PR_b targeting peptide strongly outperformed the GRGDSP peptide. The delivery of fluorescence to the CT26.WT colon cancer cells for the 5.2 mol% GRGDSP formulation is less than half that for the 5.6 mol% PR_b formulation. In addition, the highly functionalized 33.5 mol% GRGDSP formulation showed essentially the same fluorescence as the 5.6 mol% PR_b formulation. In contrast to PR_b, which has been shown to specifically bind $\alpha_5\beta_1$ integrin, simple RGD based peptides like GRGDSP are known to bind to a wide range of integrins.[118,124,125,162–164] The high target specificity of PR_b is hypothesized to lead to better targeted delivery.

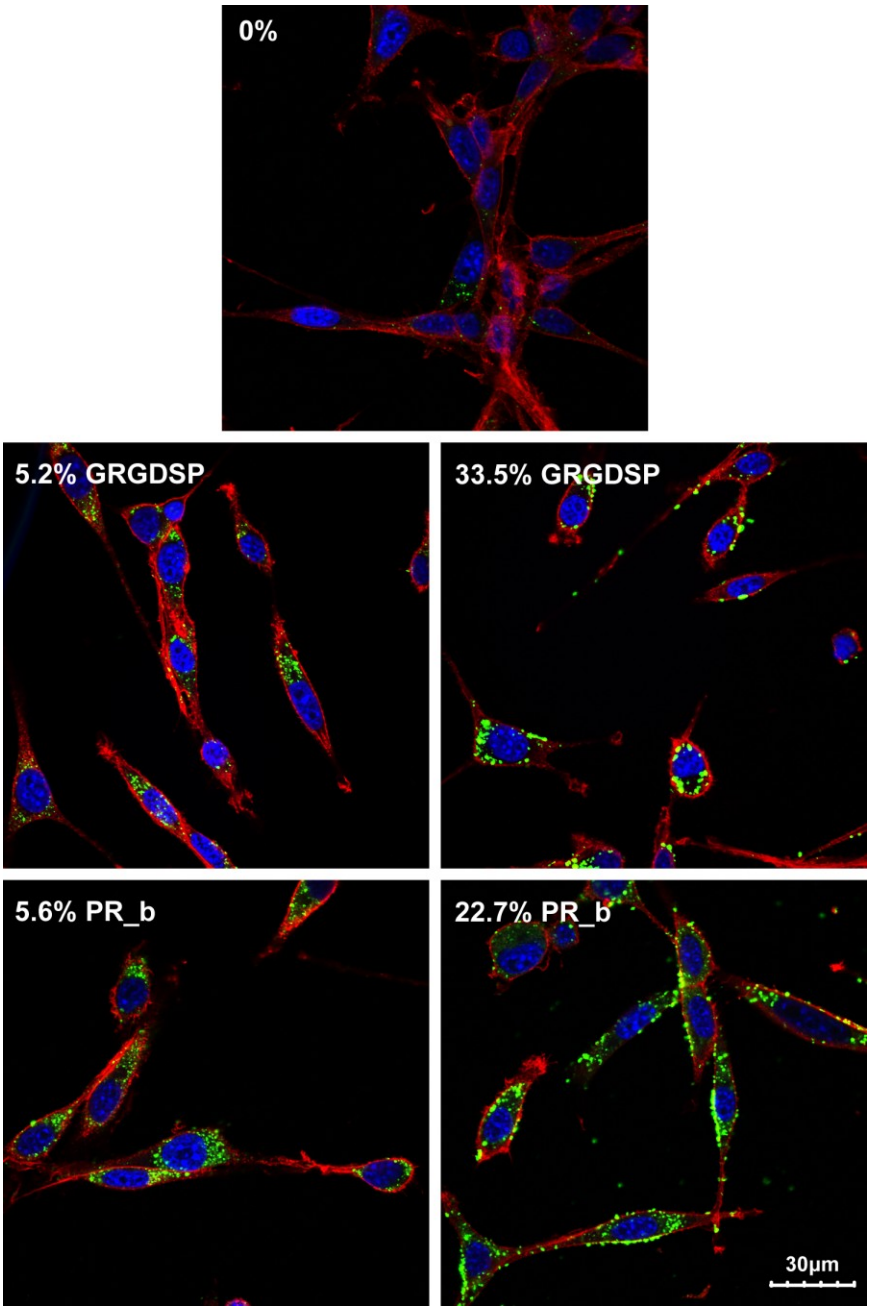

Figure 2.6 Fluorescent confocal microscopy images of CT26.WT colon cancer cells after 24 h at 37 °C incubation with polymer vesicles functionalized with the indicated mol% of targeting peptides. Polymer vesicles were fluorescently tagged green, cell nuclei were labeled blue, and cell membranes were labeled red. The images shown here all show the interior of the cell, at a "z-slice" approximately 2µm above the bottom coverslip surface and at least 2µm from top of the cell. Internalization of polymer vesicles in evidenced by the proliferation of green fluorescence within the confines of the red cell membranes.

Figure 2.6 contains fluorescent confocal microscopy images of CT26.WT cells after delivery of the polymer vesicle formulations. In these images the cell membrane is stained red, the cell nucleus is stained blue, and the polymer vesicles fluoresce green. An identical trend to that seen in Figure 2.5 can be seen here. The 0% peptide formulation leads to little or no delivery of polymer vesicles, and while the GRGDSP formulations do promote binding and internalization, the comparable PR_b formulations clearly outperform them, with greater quantities of green in each cell. These images corroborate the quantitative results presented in Figure 2.5. In addition, it should be noted that these images clearly demonstrate that peptide functionalized vesicles not only adhere to the surface of the cells, but are actively internalized by the colon cancer cells. Confocal images were taken at a height that sampled the middle of the cells, therefore the presence of the green fluorescing polymer vesicles within the confines of the red cell membrane walls indicates that the polymer vesicles were internalized and localized within the cancer cells. The fact that the green fluorescence is not evenly distributed throughout the interior of the cells and instead occurs in punctate dots indicates that the polymersomes are predominately localized within intracellular compartments and not dispersed throughout the cytosol.

2.3.4 Targeted Delivery of Doxorubicin and Cytotoxicity *in vitro*

Polymer vesicle formulations were functionalized with a low (~5 mol%) and high (~30 mol%) amount of a targeting peptide, either PR_b or GRGDSP, and were loaded with the chemotherapeutic drug doxorubicin. These doxorubicin loaded polymer vesicle formulations were delivered to CT26.WT colon cancer cells *in vitro* and the

corresponding cytotoxicity was compared to the doxorubicin drug free in solution as well as non-functionalized polymer vesicles. Plated cells were incubated for 24 h with a range of doxorubicin concentrations, either as free-drug in solution or as drug encapsulated within polymer vesicles, for each of the differing formulations, and the decrease in the cell viability was determined by the MTT assay.

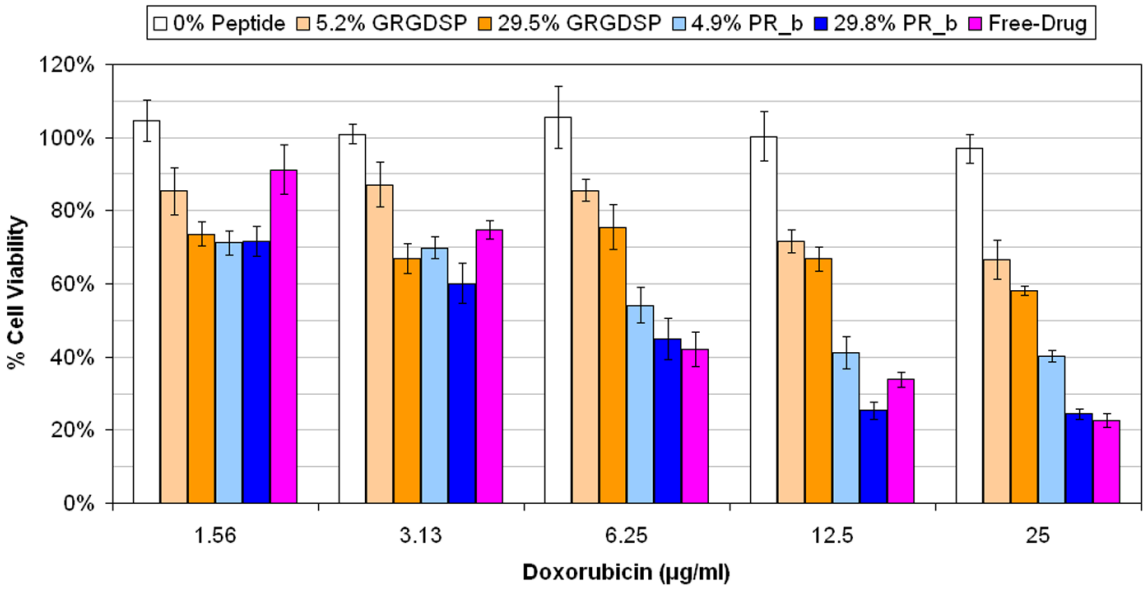

Figure 2.7 Reduction in the percent cell viability resulting from delivery of the chemotherapeutic drug, doxorubicin, to CT26.WT colon cancer cells *in vitro*. CT26.WT cells were incubated with the drug formulations noted on the figure, either encapsulated within polymer vesicles with the listed mol% of peptide functionalization or as free-drug, for 24 h at 37 °C, after which cell viability was measured using the MTT assay. The concentrations of doxorubicin that the cells were incubated with are shown along the abscissa. One-hundred percent cell viability is representative of untreated cells. Data is the mean ± standard deviation of two separate experiments (n=2), and each experiment was performed in quadruplicate.

The effect of these doxorubicin formulations on CT26.WT cell viability can be seen in Figure 2.7. Firstly, for non-functionalized polymer vesicles (0% peptide) no decrease in cell viability is seen even as increasing amounts of doxorubicin are

administered. As shown in Figure 2.5 and Figure 2.6, non-functionalized polymer vesicles exhibit little to no binding and internalization and therefore in Figure 2.7 little to none of the encapsulated doxorubicin is delivered to the cells by non-functionalized polymer vesicles. In addition, the preservation of cell viability for the non-functionalized case is indication that doxorubicin leakage out of polymer vesicles is minimal over the course of the 24 h incubation, and also further evidence of the non-toxicity of OB polymer vesicles themselves. Indeed, neither functionalized nor non-functionalized OB polymer vesicles by themselves were found to have an adverse effect on cell viability as is shown in Figure 2.8.

For all the doxorubicin concentrations administered the functionalized polymer vesicle formulations significantly outperform the non-functionalized vesicles. At lower doxorubicin concentrations there are limited differences in the resultant cell viability between the peptide functionalized vesicles, but as the amount of doxorubicin administered is increased there is increasing differentiation between the formulations, both between the PR_b and GRGDSP peptides and the lesser and greater functionalized formulations therein. Interestingly, at low doxorubicin concentrations many of the functionalized vesicle formulations slightly outperform the free-drug. We speculate that this is due to fact that doxorubicin, when it is delivered encapsulated in a vesicle, is released to the cell in a larger bolus dose, whereas for the free-drug case doxorubicin is diluted over the entire media volume. In all cases the PR_b functionalized vesicles outperform the GRGDSP functionalized vesicles and the higher functionalized vesicles for each peptide perform better than the lower functionalized vesicles. Especially at the

higher doxorubicin concentrations the PR_b functionalized vesicles outperform the GRGDSP functionalized vesicles, with the higher 29.8 mol% PR_b vesicles significantly outperforming even the 29.5 mol% GRGDSP. The only formulation that matches or exceeds the decrease in cell viability observed for the high concentration free-drug case is the 29.8 mol% PR_b formulation.

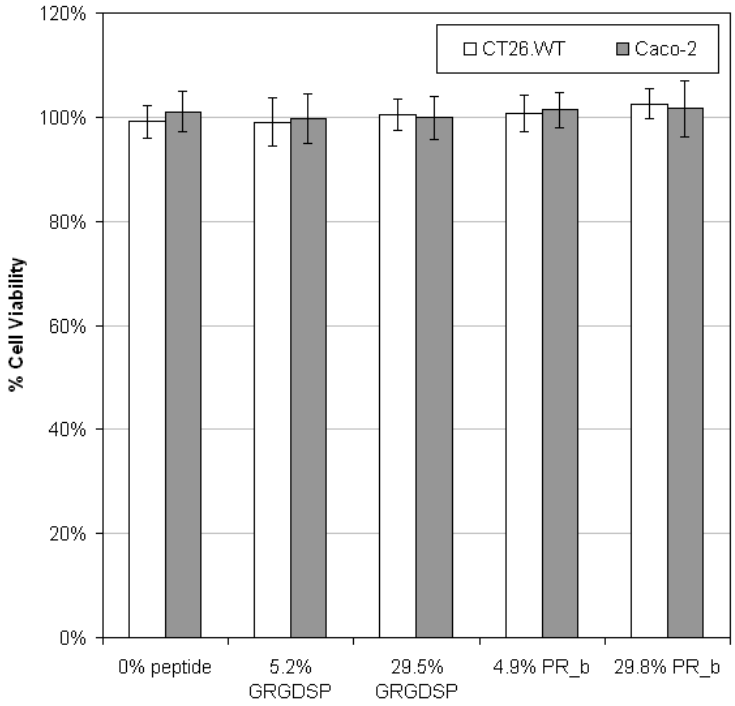

Figure 2.8 Percent cell viability resulting from delivery of "empty" polymer vesicles (vesicles not loaded with doxorubicin) to CT26.WT and Caco-2 cells *in vitro*. Cells were incubated with vesicle formulations with the indicated mol% of peptide functionalization for 24 h at 37 °C, after which cell viability was measured using the MTT assay. One-hundred percent cell viability is representative of untreated cells. Data is the mean ± standard deviation of two separate experiments (n=2), and each experiment was performed in quadruplicate.

At first pass, the level of doxorubicin release implied by the cytotoxicity results of Figure 2.7 for non-degradable OB polymersomes is perplexing. Because of this,

doxorubicin release from the polymer vesicle formulations shown in Figure 2.7 was investigated further. Doxorubicin loaded polymer vesicles were incubated in buffers of varying pH at 37 °C and doxorubicin release from these vesicles was monitored by way of the native fluorescence of doxorubicin. The measured doxorubicin release profiles are shown in Figure 2.9. Although little to no doxorubicin is released from the vesicles at pH 7.4 over the course of 24 h, doxorubicin release accelerated significantly as the external pH was decreased. Because no change in hydrodynamic diameter was observed for up to even 48 h incubation at the lowest pH tested it is believed that the release observed is simply due to passive diffusion driven leakage of doxorubicin out of the vesicles. This is conceivable, given that doxorubicin is a weak amphipathic base.[138] The accelerated release of doxorubicin at low pH explains the release implied by Figure 2.7, because polymer vesicles are likely trafficked to the low pH intracellular organelles (endosomes and lysosomes) after they are internalized within a cell.

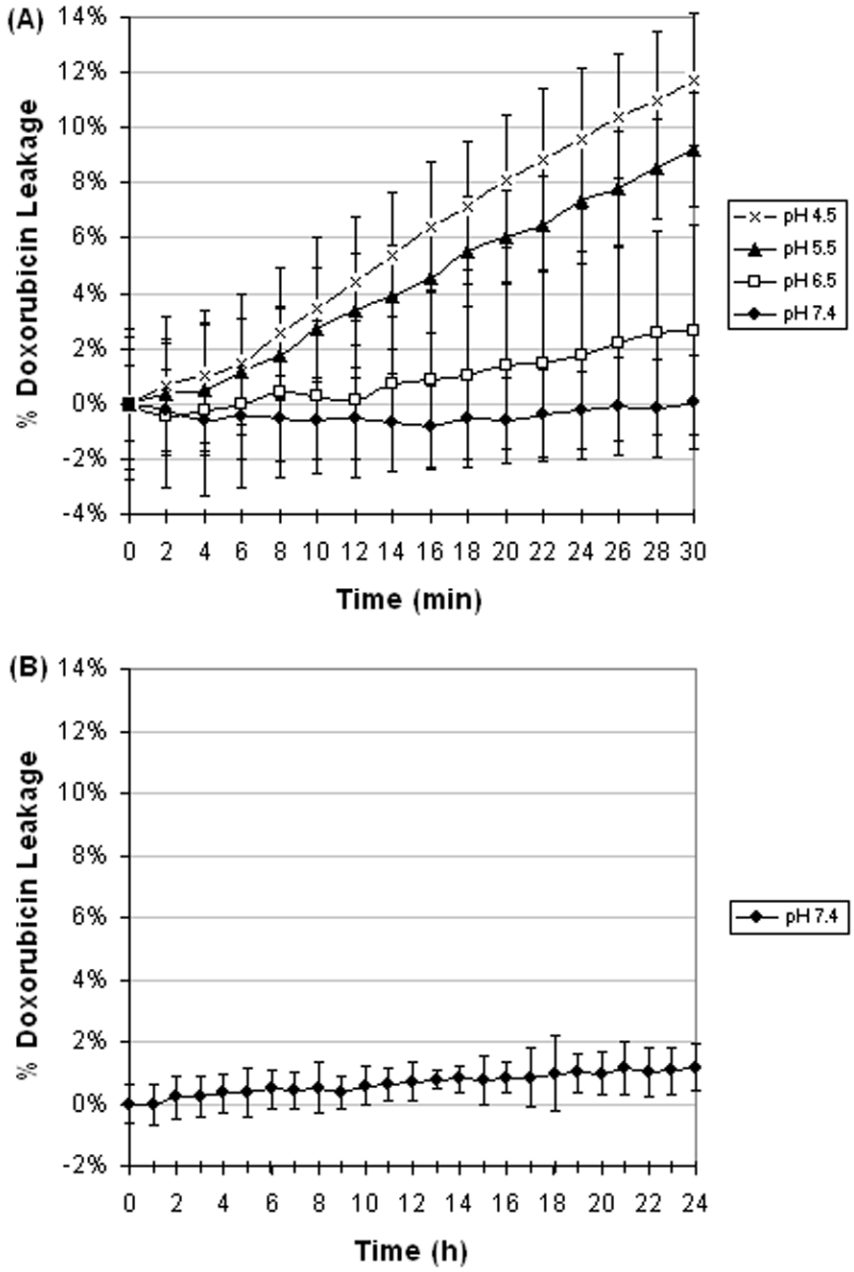

Figure 2.9 Release profiles of doxorubicin from within polymersomes in buffers of the indicated pH at 37 °C over the course of (A) 30 minutes and (B) 24 hours. Doxorubicin release is expressed as a percentage of complete release of encapsulated doxorubicin. Data is the mean ± standard deviation of two separate experiments (n=2), and each experiment was performed in triplicate. These release profiles were found to be representative of both non-functionalized and peptide functionalized polymersomes. Under storage conditions (4 °C, pH 7.4) no detectable leakage was observed over the time span of vesicle storage.

Given the pH dependent release shown in Figure 2.9, a brief discussion of the potential for drug release in the microenvironment of a tumor is pertinent. It is well established that the extracellular microenvironment within a tumor is slightly acidic (pH ~6.7), so that based on the release profile shown in Figure 2.9 some doxorubicin release may occur locally within the tumor microenvironment.[165] However given that the rate of doxorubicin release at this pH is still quite slow and that many polymer vesicles are internalized before the 24 h time mark assessed in this study, it is likely that at least a significant fraction of doxorubicin will be released after internalization inside the cancer cells. Either way the majority of the doxorubicin released within the tumor microenvironment would likely remain in the tumor.

2.3.5 Specificity of PR_b Targeted Delivery

The PR_b peptide has been previously shown to bind specifically to the $\alpha_5\beta_1$ integrin on the surface of cells.[89] To determine whether this specificity of binding translated, as might be expected, to target specific delivery of PR_b functionalized polymer vesicles, two experiments were performed. First, a blocking study was conducted, where polymer vesicle delivery was quantified for CT26.WT cells with their $\alpha_5\beta_1$ integrins blocked with an antibody. Second, polymer vesicle internalization was imaged for two cell lines with orders of magnitude differing $\alpha_5\beta_1$ integrin expression levels. These results agree with the assessment that the PR_b peptide is a highly specific ligand for the $\alpha_5\beta_1$ integrin, and indicate that this ligand specificity translates effectually to target specific delivery of PR_b functionalized polymer vesicles.

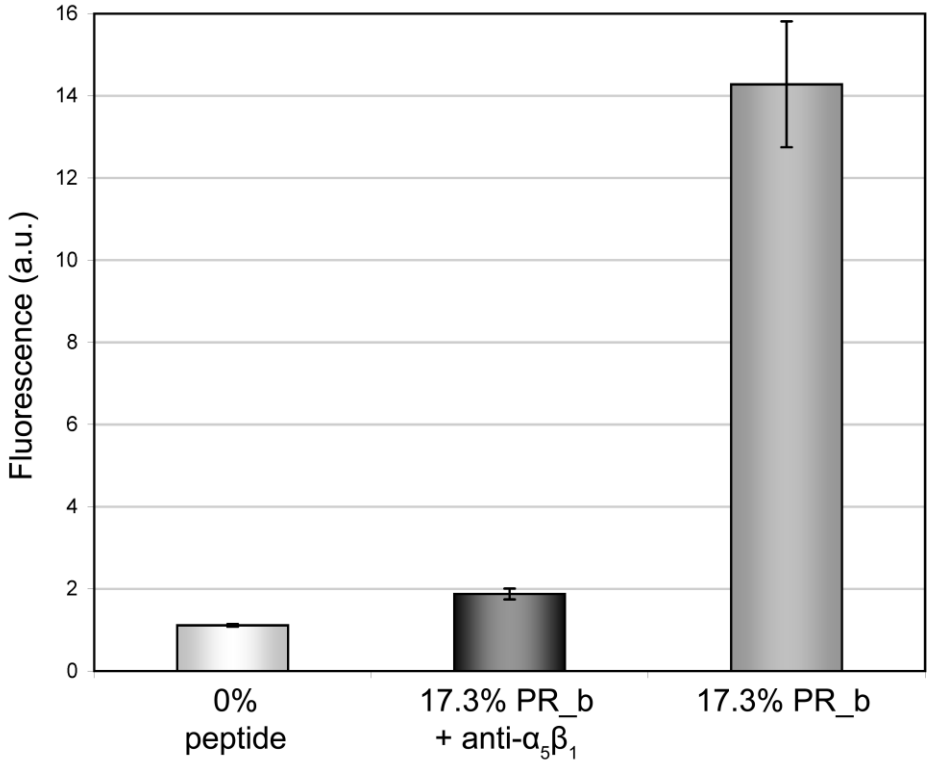

Figure 2.10 Delivery of a fluorescent dye to CT26.WT colon cancer cells by PR_b functionalized polymer vesicles. Delivery is shown for both unblocked CT26.WT cells and cells with their $\alpha_5\beta_1$ integrins blocked by anti-$\alpha_5\beta_1$ antibodies. CT26.WT cells were incubated with fluorophore loaded polymer vesicles functionalized with the listed mol% of PR_b for 1 h at 4 °C. Data is the mean ± standard deviation of two separate experiments (n=2), and each experiment was performed in triplicate.

Figure 2.10 displays the effect of blocking $\alpha_5\beta_1$ cell surface integrins using an anti-$\alpha_5\beta_1$ antibody on the level of PR_b functionalized polymer vesicle binding and internalization. CT26.WT cells were either pre-treated with anti-$\alpha_5\beta_1$ antibody for 30 minutes or not, and then incubated with identical formulations of PR_b functionalized polymer vesicles for 1 h. The anti-$\alpha_5\beta_1$ antibody binds to the free $\alpha_5\beta_1$ integrins on the surface of the cells and blocks them from binding other ligands (e.g. PR_b) at least until the integrin is recycled by the cell.[166] Thus for the anti-$\alpha_5\beta_1$ blocked cells a decrease in

binding and internalization of polymer vesicles could be expected in accordance with the specificity of the PR_b peptide for $\alpha_5\beta_1$ integrin. Indeed, an order of magnitude decrease in binding and internalization is witnessed for the case of anti-$\alpha_5\beta_1$ blocked cells as compared to unblocked cells. Only slightly more fluorescence, and hence binding and internalization, is measured in the anti-$\alpha_5\beta_1$ blocked case with 17.3 mol% PR_b functionalized vesicles than for non-functionalized vesicles. The small amount of fluorescence observed in the anti-$\alpha_5\beta_1$ blocked case is not necessarily due to off-target binding of the PR_b functionalized vesicles. This relatively minimal increase in binding over the 0% peptide case could equally well be due to competitive binding between PR_b functionalized vesicles and any free anti-$\alpha_5\beta_1$ antibodies left in solution. Especially considering that the time scale of integrin recycling is on the order of tens of minutes, $\alpha_5\beta_1$ integrins would likely be recycled over the course of the 1 h experiment.[166] Regardless, the results of Figure 2.10 clearly demonstrate that PR_b functionalized vesicles bind with high specificity to their target, the $\alpha_5\beta_1$ integrin.

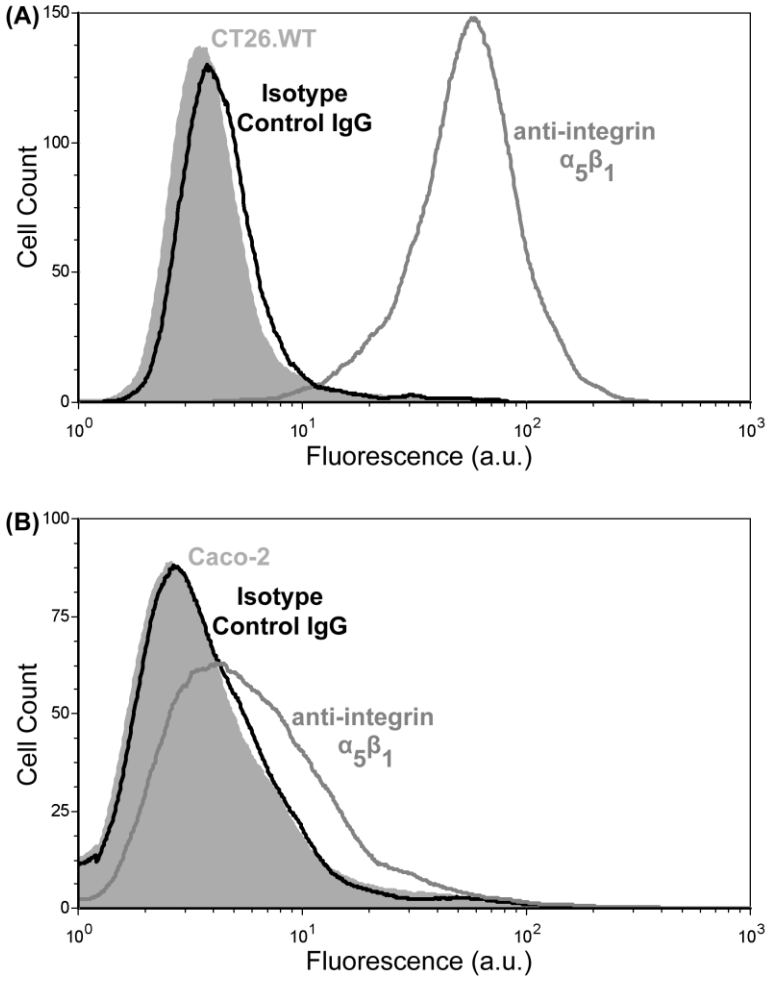

Figure 2.11 Expression of $\alpha_5\beta_1$ integrin on (A) CT26.WT and (B) Caco-2 cells as determined by flow cytometry. Cells were incubated with antibodies to $\alpha_5\beta_1$ integrin and this antibody was fluorescently tagged with a secondary antibody. Histograms of cell fluorescences were constructed through flow cytometry analysis and are shown for the native cells (grey filled area), the appropriate isotype control (black line), and the anti-$\alpha_5\beta_1$ treated cells (grey line).

To further strengthen the evidence for target specific delivery of PR_b functionalized polymer vesicles, binding and internalization was compared between two cell lines: one highly expressing $\alpha_5\beta_1$ integrin, CT26.WT, and the other minimally expressing $\alpha_5\beta_1$ integrin, Caco-2. Caco-2 is a model intestinal epithelial cell line that is known to express little to no $\alpha_5\beta_1$ integrin, while still expressing other integrins.[167–170]

The expression levels of the target of interest, $\alpha_5\beta_1$ integrin, for each cell line were measured by immunostaining for cell surface expression of $\alpha_5\beta_1$ integrin, then measuring the expression level as fluorescence of the tagged cells using flow cytometry. Figure 2.11 displays flow cytometry fluorescence histograms for these two cell lines. CT26.WT cells exhibit high $\alpha_5\beta_1$ expression as shown by the histogram in Figure 2.11 corresponding to cells with fluorescently tagged $\alpha_5\beta_1$ integrins being shifted up to higher fluorescent intensities, i.e. shifted to the right of the histogram for the native fluorescence of the cells. In contrast, Caco-2 cells show very minimal expression of $\alpha_5\beta_1$ integrin.[167] The anti-integrin $\alpha_5\beta_1$ tagged Caco-2 cells exhibit only a modest shift to higher fluorescent intensities, with the majority of cells overlapping with the histogram for the native background fluorescence of Caco-2 cells. For both cell lines a negative control involving the use of an isotype control IgG in the place of the primary antibody, anti-$\alpha_5\beta_1$, was conducted and in both cases this histogram very closely overlapped with the native cell histogram, as should be expected.

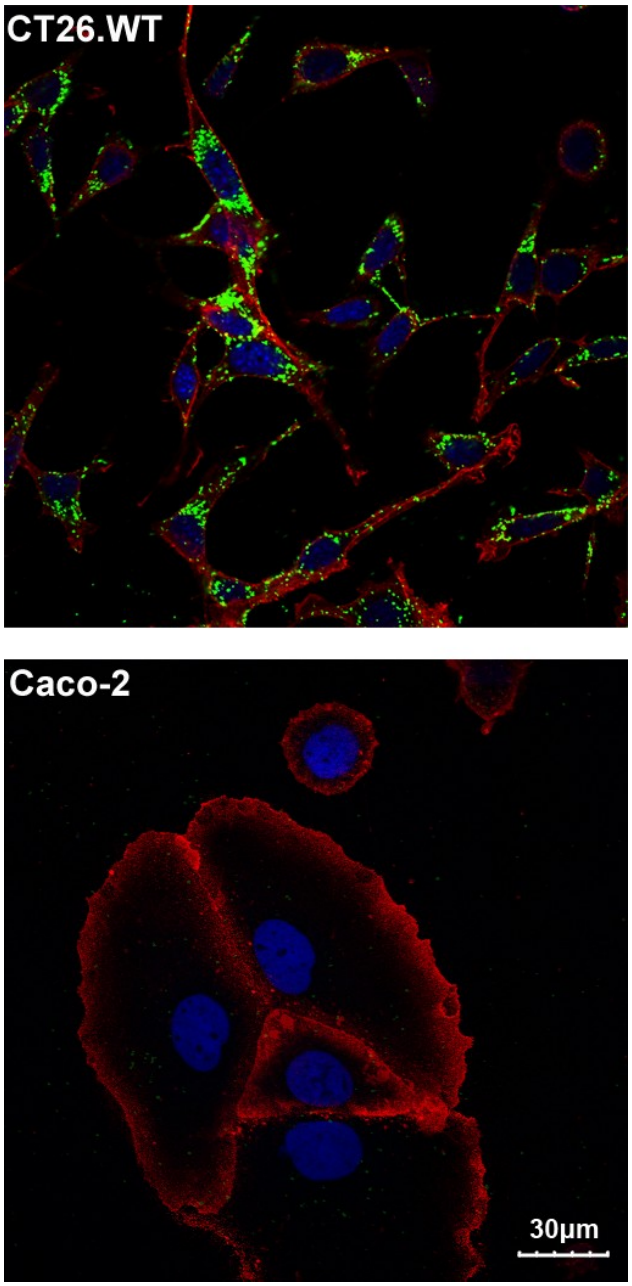

Figure 2.12 Fluorescent confocal microscopy images of CT26.WT and Caco-2 cells after 24 h at 37 °C incubation with 17.3 mol% PR_b functionalized polymer vesicles. Polymer vesicles were fluorescently tagged green, cell nuclei were labeled blue, and cell membranes were labeled red. The images shown here all show the interior of the cell, at a "z-slice" approximately 2µm above the bottom coverslip surface and at least 2µm from top of the cell. Internalization of polymer vesicles is evidenced by the presence of green fluorescence within the confines of the red cell membranes.

The confocal microscopy images in Figure 2.12 compare the internalization levels of PR_b functionalized polymer vesicles into both CT26.WT cells and Caco-2 cells. As shown in Figure 2.11 CT26.WT cells highly express the target of interest, $\alpha_5\beta_1$ integrin, while Caco-2 cells very minimally express $\alpha_5\beta_1$ integrin. As might be expected based on the cell lines disparate $\alpha_5\beta_1$ integrin expression levels, and the PR_b peptide's high specificity for $\alpha_5\beta_1$ (Figure 2.10), PR_b functionalized polymer vesicles are internalized at dramatically higher amounts in CT26.WT cells as opposed to Caco-2 cells. Cell lines were incubates with identical concentrations of the same polymer vesicle formulation, carboxyfluorescein loaded vesicles with 17.3 mol% PR_b functionalization, each for 24 h at 37 °C. The vastly different amounts of green fluorescent polymer vesicle internalization is thought to be the result of both the disparate $\alpha_5\beta_1$ integrin expression levels of the two cell lines and the high target specificity of PR_b functionalized vesicles. These confocal images reinforce the evidence that PR_b is a highly specific targeting ligand, and that PR_b functionalized polymer vesicles can be highly target specific drug delivery carriers. Interestingly, although Caco-2 cells have very minimal $\alpha_5\beta_1$ integrin expression, they do in fact express a small amount, as shown in Figure 2.11, yet they still exhibit very little binding and uptake of PR_b functionalized vesicles. Indeed, the near complete absence of any polymer vesicle internalization witnessed for the $\alpha_5\beta_1$ integrin minimally expressing Caco-2 cells, (Figure 2.12) bodes well for the target specific delivery of PR_b functionalized vesicles.

2.3.6 Specificity of Doxorubicin Delivery *in vitro*

In identical fashion to the doxorubicin delivery experiments and cell viability assay shown in Figure 2.7, doxorubicin loaded polymersomes were incubated with Caco-2 cells for 24 h at 37 °C and cell viability was assayed. Figure 2.13 shows the results of this *in vitro* cytotoxicity experiment, for the same doxorubicin formulations used in Figure 2.7: free doxorubicin drug and doxorubicin encapsulated within variously functionalized polymer vesicles. While Figure 2.7 shows cell viability results for CT26.WT cells, a highly $\alpha_5\beta_1$ integrin expressing cell line, Figure 2.13 shows cell viability results for the Caco-2 cell line, which exhibits little to no $\alpha_5\beta_1$ expression.

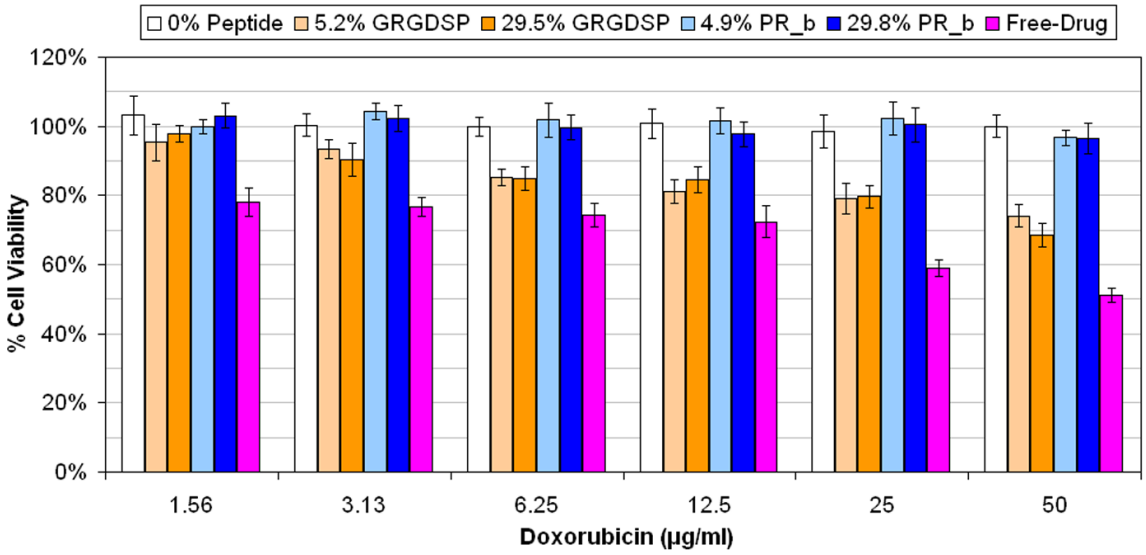

Figure 2.13 Reduction in the percent cell viability resulting from delivery of the chemotherapeutic drug, doxorubicin, to Caco-2 cells *in vitro*. Caco-2 cells were incubated with the drug formulations noted on the figure, either encapsulated within polymer vesicles with the listed mol% of peptide functionalization or as free-drug, for 24 h at 37 °C, after which cell viability was measured using the MTT assay. The concentrations of doxorubicin that the cells were incubated with are shown along the abscissa. One-hundred percent cell viability is representative of untreated cells. Data is the mean ± standard deviation of two separate experiments (n=2), and each experiment was performed in quadruplicate.

For both cell lines the non-functionalized polymer vesicles (0% peptide) result in essentially no cell death, even though they are loaded with the chemotherapeutic doxorubicin. Based on results shown in Figure 2.5 and Figure 2.6 this is likely because the non-functionalized polymer vesicles are essentially not bound and internalized by the cells. When comparing Figure 2.7 and Figure 2.13, it should be noted that Caco-2 cells are known to be more highly drug resistant to doxorubicin, and this is why less cell death is observed for comparable doxorubicin concentrations for the two cell lines.[171] This is also why higher doxorubicin concentrations were sampled for Caco-2 cells as opposed to CT26.WT cells. GRGDSP functionalized doxorubicin loaded polymer vesicles (5.2 and 29.5 mol% GRGDSP) give a decrease in cell viability that follows the same trend for both CT26.WT cell and Caco-2 cells. The cytotoxicity of these vesicles lags behind that of the free-drug for the case of either cell line, with the more highly conjugated polymer vesicles, 29.5 mol% GRGDSP, giving slightly lower cell viability than the less conjugated vesicles, 5.2 mol% GRGDSP. However, the high specificity of the PR_b functionalized polymer vesicles for the target of interest, $\alpha_5\beta_1$ integrin, yields dramatically different behavior for the cytotoxicity of these vesicles to CT26.WT cells (Figure 2.7) and Caco-2 cells (Figure 2.13).

For Caco-2 cells, which very minimally express $\alpha_5\beta_1$ integrin, little to no decrease in cell viability is observed for PR_b functionalized polymer vesicles across the spectrum of doxorubicin concentrations assayed, even for the highly functionalized vesicle formulation with 29.8 mol% PR_b. This is striking considering that PR_b functionalized polymer vesicles exhibit much greater binding, internalization, and cytotoxicity than

GRGDSP functionalized vesicles with the $\alpha_5\beta_1$ integrin expressing CT26.WT colon cancer cells. Based on the visualization of the disparate levels of PR_b functionalized polymer vesicle internalization for the two cell lines shown in Figure 2.10, the PR_b functionalized vesicles aren't cytotoxic to Caco-2 cells most likely because they cannot bind and internalize into the cells without the $\alpha_5\beta_1$ integrin on the cell surface and therefore never release the encapsulated doxorubicin. This is a clear proof of concept that the high specificity of the PR_b peptide can yield effective target specific delivery and even target specific drug delivery in the *in vitro* studies conducted here. The lack of target specificity for the GRGDSP functionalized vesicles is not surprising, considering that simple RGD peptides are known to bind to a wide variety of integrins, many of which have been shown to be highly expressed by Caco-2 cells.[168–170,172]

Target specific drug delivery, such as that demonstrated here for PR_b functionalized polymer vesicles, is expected to be advantageous. As noted previously, $\alpha_5\beta_1$ integrin has been shown to be highly expressed by a myriad of different cancers, and is comparatively expressed at lower levels in normal healthy tissue.[95–97,99–102,126] Heightened expression of $\alpha_5\beta_1$ expression has also been shown to be associated with increased tumorgenicity, malignancy, and invasiveness of cancer cells.[98,104–107] In light of this evidence the results of this research are promising. We have demonstrated that PR_b functionalized vesicles can differentially deliver to highly $\alpha_5\beta_1$ expressing cells, CT26.WT, as opposed to minimally expressing cells, Caco-2, the very conditions that are likely prescient for systemic delivery.

2.3.7 Conclusion

Polymer vesicles functionalized with PR_b targeting peptides via "click" chemistry are effective targeted drug delivery vectors. The azide-alkyne "click" Huisgen cycloaddition reaction was demonstrated to be a robust and versatile conjugation reaction for the functionalization of polymer vesicles with targeting ligands. Polymersomes functionalized with the PR_b targeting peptide were shown to bind and internalize into CT26.WT colon cancer cells at much higher levels than non-functionalized polymer vesicles and GRGDSP functionalized polymer vesicles. We have demonstrated that PR_b functionalized polymer vesicles can effectively deliver encapsulated doxorubicin, a chemotherapeutic, to colon cancer cells, and outperform comparable GRGDSP functionalized vesicles. Furthermore, evidence of the target specificity of PR_b functionalized polymer vesicles was presented. Binding and internalization of PR_b functionalized polymer vesicles into CT26.WT cells was blocked with an anti-$\alpha_5\beta_1$ antibody. Moreover, internalization of PR_b functionalized polymer vesicles was found to be dependent on the surface expression of the target of interest, $\alpha_5\beta_1$ integrin, when internalization was compared for two cell lines, one highly $\alpha_5\beta_1$ expressing (CT26.WT) and the other minimally $\alpha_5\beta_1$ expressing (Caco-2). Finally, cell viability and therefore encapsulated drug delivery was found to be dependent upon cell line $\alpha_5\beta_1$ integrin expression for PR_b functionalized polymer vesicles, but not for GRGDSP functionalized vesicles. This proven target specific delivery for PR_b functionalized polymer vesicles is expected to be advantageous for *in vivo* applications. However, the mechanism of clearance and metabolism *in vivo* of the non-biodegradable OB polymers used in this study is unclear, so that utilization of PR_b functionalized vesicles in an *in*

vivo setting may require extending the findings for this model OB polymer system to a biodegradable system.

3 Targeted Polymer Vesicle Delivery of siRNA Induces Cell Death of Breast Cancer Cells Dependent upon Orai3 Protein Expression[1]

3.1 Introduction

Small interfering RNA (siRNA), discovered only briefly over a decade ago has rapidly been applied as both a tool for profiling protein function and as a potential therapeutic for a wide array of diseases.[173–175] siRNA molecules, double stranded RNA typically 20-25 nucleotides in length, act to down-regulate expression of a specific target gene. This down-regulation is accomplished with help from the cells own RNA interference machinery. A single strand of the siRNA molecule is selected by the cell, typically the antisense strand, and incorporated into an endogenous RISC (RNA-induced silencing complexes) assembly in the cytosol which then acts to catalytically degrade complementary messenger RNA (mRNA).[176] Of interest to this work, a number of gene targets have been identified with potential relevance for the treatment of cancer.[177] In particular, the calcium channel protein, Orai3, has been recently identified as a potential therapeutic target for breast cancer.[178]

Down-regulation of Orai3 in breast cancer cells was found to reduce cell viability of T47D human breast cancer cells and arrest cell-cycle progression in the G1 phase eventually leading to apoptosis, while for MCF-10A normal breast epithelial cells down-regulation of Orai3 resulted in no measurable decrease in cell viability.[178] Thus Orai3 was identified as a potential breast cancer specific therapeutic target for siRNA down-

[1] Reproduced with permission from reference 194. Copyright 2012 American Chemical Society.

regulation. Orai3 is one of a class of calcium channel proteins located on the plasma membrane (along with Orai1 and 2) that operates along with the stromal interacting molecule (STIM) proteins to replenish calcium levels within the cell via what is termed the store operated calcium (Ca^{2+}) entry (SOCE) pathway.[179,180] The SOCE pathway is ubiquitous and has been shown to be important for a number of cell functions including cell-cycle progression, cell proliferation, and migration.[181–183] In addition, there is evidence that SOCE is mediated by Orai3 in many breast cancer cells, as opposed to being dominated by the canonical Orai1 mediated pathway observed in normal cells.[184–186] It has been proposed that the dominance of either Orai1 or Orai3 in the SOCE pathway is dependent upon which is rate limiting under the particular conditions of the cell.[187] Moreover, Orai3 was found to be over-expressed in the majority of breast cancer tumors tested as compared to normal tissue in the same patient.[178] Considering this current body of evidence Orai3 was chosen as a potential cancer specific target for siRNA delivery to breast cancer cells.

Effective delivery of siRNA molecules to tumors and cancer cells present a number of unique challenges.[188,189] Firstly, RNA is rapidly degraded in the presence of serum or really any ribonuclease (RNase), so that for effective delivery the siRNA molecules must be protected from degredation.[190,191] Secondly, because siRNA is a highly negatively charged and relatively large molecule (~13 kDa) it cannot effectively gain entry into a cell alone, intracellular delivery must typically be assisted. Finally, siRNA has to get specifically to the cytosol of the cell to assemble with the RISC protein complex, which in most cases means that the siRNA must escape endolysosomal intracellular

compartments. All these barriers to delivery exist for both *in vitro* and *in vivo* siRNA delivery, however additional challenges present themselves for the case of *in vivo* delivery, including finding and delivery to the appropriate tissue in the body, evading host immune response and phagocytosis, colloidal stability, toxicity, and avoiding simple filtration in the kidneys.[189] We expected that cancer targeting peptide functionalized polymersomes could be a facile delivery agent of siRNA, well poised to confront the challenges of siRNA delivery, and tested that expectation in this work with model polymersomes. It should be noted that although the current work tests strictly the *in vitro* efficacy of our model siRNA delivery system, the findings presented here could be extended to biodegradable polymersome systems, which have been shown to be well suited to overcome the challenges of *in vivo* delivery.[109]

Polymersomes are essentially polymeric nano-capsules similar in construction and function to their low molecular weight analogues, liposomes.[55,111] They are self-assembled structures formed from amphiphilic block copolymers in aqueous solution. For example, the diblock copolymer, poly(1,2-butadiene)-*b*-poly(ethylene oxide) (PB-PEO or OB), used in this research self assembles to form thick polymer membranes composed of a PB membrane core with PEO brush layers shielding this hydrophobic membrane core from the aqueous surroundings on either side. This membrane inherently forms into a closed spherical vesicle in order to minimize free energy, thus self-assembling into a nano-capsule structure containing an aqueous lumen space protected and isolated from the surrounding aqueous environment by a thick (~10-20 nm) polymeric membrane.[112] We chose to encapsulate siRNA molecules within this aqueous

lumen in this study, with the expectation that they would be effectively shielded from interaction with the external environment when encapsulated. The vast majority of non-viral gene delivery agents reported in the literature employ ionic complexation of negatively charged nucleotides to a positively charged delivery agent, thus the encapsulation of siRNA within a vesicle represents an alternative modality for siRNA packaging and protection.[189,192] In addition, because of the thickness and hydrophobicity of a polymer vesicle membrane, permeability, and therefore leakage, is very low, even trending toward zero for large charged molecules such as siRNA and carboxyfluorescein.[193] Furthermore, polymer vesicle coronas, composed of a dense PEO brush layer, have been shown to effectively resist opsonization and therefore host immune response and clearance from the body.[18,142]

The polymer vesicles used in this study were further functionalized with peptide targeting ligands, to enhance cellular uptake and confer an active targeting modality to the vesicles, as shown schematically in Figure 3.1. Azide-alkyne "click" chemistry was utilized to covalently decorate the exterior surface of polymer vesicles with either the integrin binding GRGDSP peptide or an $\alpha_5\beta_1$ integrin binding peptide, named PR_b (with amino acid sequence KSSPHSRN$(SG)_5$RGDSP).[52,89,90] The PR_b peptide was designed to mimic the cell binding site of native fibronectin protein recognized by integrin $\alpha_5\beta_1$.[88] It incorporates both the primary $\alpha_5\beta_1$ binding sequence, RGD, and the synergistic binding sequence, PHSRN, connected by an $(SG)_5$ linker, which was chosen to accurately mimic both the separation distance and the hydrophobicity/hydrophilicity of the linker region in the native fibronectin protein.[62,80,125] The design of PR_b has been shown repeatedly to

result in greatly improved adhesion and $\alpha_5\beta_1$ specificity over other RGD containing peptide ligands.[52,89,91,92,118]

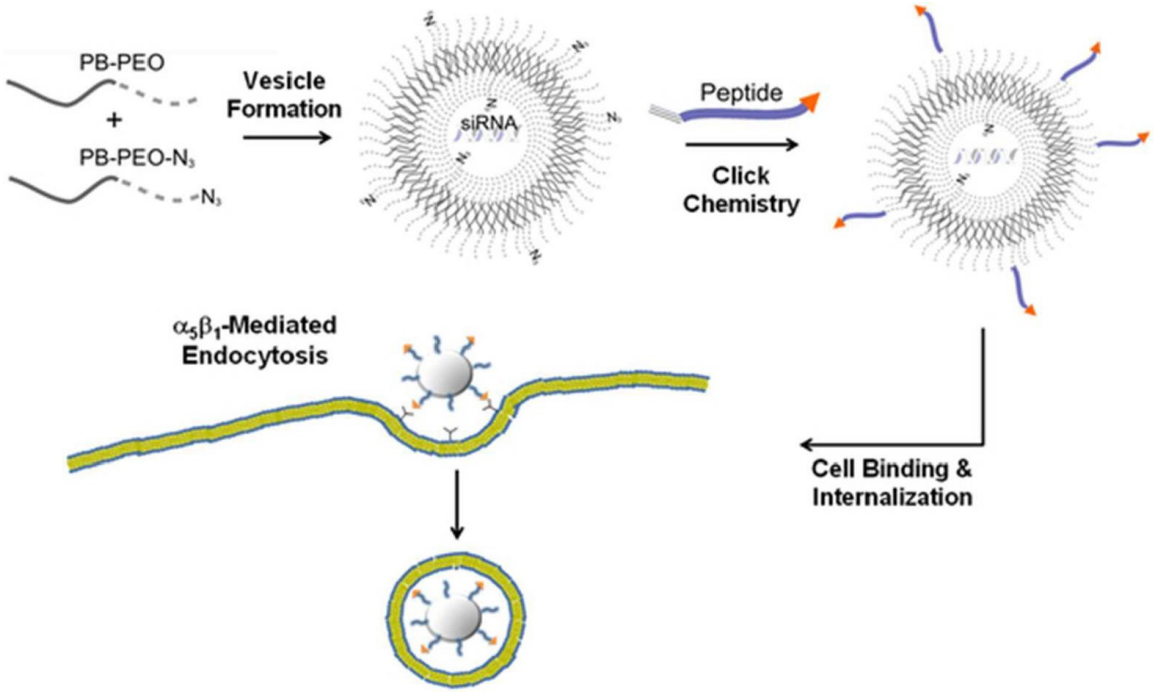

Figure 3.1 Schematic representation of vesicle formation, peptide conjugation of PB-PEO (OB) polymer vesicles and interaction with cells.

In this research, the ability of peptide functionalized OB polymer vesicles to effectively deliver siRNA to breast cancer cells *in vitro* was studied.[194] Delivery to two different cell lines, the MCF10A (immortalized but noncancer fibrocystic MCF10A breast cells) and the T47D breast cancer cell line, was investigated and compared. Both cell lines have been previously shown to express $\alpha_5\beta_1$ and adhere readily to fibronectin.[101,195–197] Both GRGDSP and PR_b peptide functionalized polymer vesicles were evaluated for effective delivery to these cell lines, and binding specificity to cell surface integrins was examined for PR_b functionalized vesicles using blocking peptides. Delivery of PR_b functionalized polymer vesicles to MCF10A and T47D cells was

visualized by fluorescent confocal microscopy, and colocalization with cellular endosomes and lysosomes was assessed by organelle staining. Finally, the ability of PR_b functionalized polymer vesicles to effectively encapsulate and deliver siRNA to breast cancer cells was studied, and the effect of siRNA delivery on cell viability for both the cancerous T47D cells and the MCF10A cells was assessed. siRNA delivery by polymer vesicles was also compared to that by a commercial siRNA transfection agent.

3.2 Materials and Methods

3.2.1 Materials

Unless otherwise noted all chemicals were obtained from Sigma-Aldrich (St. Louis, MO) and used as received. Peptides PR_b and GRGDSP were custom synthesized and obtained on the bead, with the side groups protected, from the Microchemical Facility at the University of Minnesota. The extruder and the 200 nm extrusion membranes were obtained from Avestin Inc. (Ottawa, Canada). The MCF10A and T47D epithelial human breast cells were obtained from ATCC (Manassas, VA). Cellular stains used in confocal imaging, the RiboGreen® assay kit, Lipofectamine™ RNAiMAX, and cell culture media and supplements were obtained from Invitrogen (Carlsbad, CA). Fetal bovine serum (FBS) was obtained from Atlas Biologicals (Fort Collins, CO). Human fibronectin-coated round coverslips were purchased from BD Biosciences (San Jose, CA). Small interfering RNA, siOrai3 (siGENOME siRNA Orai3, catalog number: D-015896-04) and siControl (siGENOME Non-Targeting siRNA #2, catalog number: D-001210-02, anti-sense sequence: 5'-UAAGGCUAUGAAGAGAUAC-3') were obtained from Dharmacon Inc. (Chicago, IL).

3.2.2 Polymer Synthesis

Poly(ethylene oxide)-b-poly(1,2-butadiene) (OB) was synthesized sequentially using previously published anionic polymerization techniques.[127] First hydroxyl terminated poly(1,2-butadiene) (PB) homopolymer was synthesized. Then in a separate reaction the poly(ethylene oxide) (PEO) block was grown off the end of the PB block to form the OB diblock.

3.2.3 Synthesis of Azide Terminated OB (OB-N_3)

The hydroxyl end group of the OB polymer was replaced with an azide group via mesylation followed by reaction with sodium azide. The details of this synthesis have been previously reported.[52]

3.2.4 Synthesis of Alkyne Terminated Peptides

A terminal alkyne functional group was attached to the PR_b and GRGDSP peptides to enable the "click" conjugation of these peptides with OB-N_3. The details of this synthesis have been previously reported.[52]

3.2.5 Polymer Vesicle Formation

Polymer vesicles were prepared by self-assembly of the OB diblock in aqueous solutions using film rehydration.[114] OB and OB-N_3 polymers were placed in a vial in the desired ratio, and chloroform was added to form a concentrated polymer solution (~100 mg/ml). The mixture was gently shaken at room temperature (RT) for 24 h. Films were formed by drying, with all traces of chloroform removed using a high vacuum. An aqueous solution was then added to the film to form either a 1% (w/w) (or 5% for siRNA encapsulation) solution of polymer. For the samples encapsulating carboxyfluorescein (CbF) either 3.0 mM or 80.0 mM CbF in phosphate buffered saline (PBS) was added, and

for samples encapsulating siRNA a solution of 6 μM siRNA and 5 μM RNAsecure™ (Ambion, Grand Island, NY) was added. To remove any traces of RNase, samples incorporating siRNA were heated while stirring to 60°C for the first 15 min after adding the aqueous solution to the polymer film, then stirred at 45 °C for 2 days before being allowed to cool to RT. After a few days of stirring, polymer vesicles were fully dispersed. Vesicles were extruded at 60 °C through polycarbonate membranes with well defined 200 nm pore sizes. After extrusion each vesicle sample was characterized by dynamic light scattering (DLS) using a 90 Plus BI-MAS instrument (Brookhaven Instrument Co.) to determine the size distribution.

3.2.6 Peptide Conjugation

The PR_b and GRGDSP peptides were conjugated onto the surface of the preformed polymer vesicles using the azide-alkyne "click" Huisgen cycloaddition reaction.[130] To a dispersion of vesicles at 4 °C was added a 2 fold excess of alkyne terminated peptide and copper sulfate (1.1 mM), sodium ascorbate (5.5 mM), and bathophenanthrolinedisulfonic acid (2.2 mM).[131,132,198] The reaction was allowed to come to room temperature and stirred for 24 h after which a 5 fold excess, with respect to copper, of EDTA (ethylenediaminetetraacetic acid) was added to the solution to sequester the copper. The vesicle samples were then purified by dialysis in PBS with Spectra/Por 6 dialysis tubing (50 kDa MWCO, Spectrum Labs, Rancho Dominiguez, CA). The samples were dialyzed for a total of 3 days with the dialysate being changed every 4-12 h for a total of 6 times. Samples used in colocalization studies were alternatively purified by passing through a Sepharose CL-4B gel filtration column, and then used in

experiments immediately after purification. This was done primarily so that the vesicles encapsulating self-quenching concentrations of CbF could be more quickly purified.

3.2.7 Peptide Quantification

Quantification of the mol% of surface bound peptide on polymer vesicles was carried out as previously described, using a fluorescamine based fluorescent assay.[52]

3.2.8 Encapsulate Quantification

The amount of either CbF or siRNA encapsulated in polymer vesicles was assessed as follows. For CbF quantification a small volume of polymer vesicle sample was diluted into PBS + 10% Triton X-100 to give a final volume of 200 μl within a well of a black 96 well plate. Two concentrations of polymer vesicles were assayed for each formulation with 6 repeats of each: one expected to give approximately 0.01 μM CbF in the well and the other half this. After incubating for 1 h in the Triton solution at RT, fluorescence (485/528 ex/em) was measured on a SynergyMX fluorometer (BioTek, Winooski, VT). The fluorescence obtained from the vesicle samples was correlated with a standard curve constructed for free CbF dissolved in the identical buffer to enable calculation of the CbF concentration in the polymer vesicle sample.

The fluorescent Quant-iT™ RiboGreen® RNA Assay Kit (Invitrogen, Grand Island, NY) was used to quantify the amount of siRNA encapsulated within polymer vesicles. First a standard curve was constructed for both the siOrai3 and siControl siRNAs as per the manufacturer's published protocol, with the concentration of siRNA in each stock solution measured on a NanoDrop 2000c spectrophotometer (Thermo Scientific, Waltham, MA). For the analysis of the siRNA content of vesicle samples, the

polymer was first extracted out of solution then the liberated siRNA was quantified with the RiboGreen reagent. To 140 µl of RNase-free Tris-EDTA (TE) buffer 10 µl of polymer vesicle sample was added in an RNase-free microtube. Then 1 ml of HPLC grade chloroform was added to the microtube and the mixture was shaken vigorously. The microtube was centrifuged at 16,000 g for 5 min, then 10 µl of the top aqueous phase containing the siRNA was added to 90 µl of TE buffer in a new microtube. To this was added 100 µl of a 200-fold dilution of RiboGreen reagent in TE buffer, and the total volume was mixed by pipetting up and down. The contents of the microtube were added directly into a well on a black 96 well plate and fluorescence was measured (485/528 ex/em) on a SynergyMX fluorometer (BioTek, Winooski, VT) 3 min after adding the RiboGreen reagent. It should be noted that for each point on the standard curves an identical extraction procedure was carried out, and each measurement was performed in triplicate.

3.2.9 Cell Culture

T47D and MCF10A cells were grown in RGM (modified RPMI-1640 medium supplemented with 10% (v/v) FBS, 100 units/ml penicillin, 0.1 mg/ml streptomycin, 10 mM HEPES, and 10 µg/ml insulin) and DFGM (modified Dulbecco's Modified Eagle Medium: Nutrient Mixture F-12, DMEM/F12, supplemented with 5% (v/v) FBS, 100 units/ml penicillin, 0.1 mg/ml streptomycin, 15 mM HEPES, 10 µg/ml insulin, 20 ng/ml epidermal growth factor, 0.5 µg/ml hydrocortisone, and 100 ng/ml cholera toxin) respectively at 37 °C, 5% CO_2. Growth media was replaced every two days and cells were passaged when they reached ~70% confluence by treating with TrypLE™ Express

(Invitrogen, Grand Island, NY), and reseeding in new flasks at lower cell densities. Only cells of passage number 1-5 were used in experiments.

3.2.10 Cellular Delivery Quantification

A fluorescence plate assay was used to quantify the binding and internalization of polymer vesicles to cells. To each well of a cell culture 24 well plate was added 0.5 x 10^6 cells in 150 µl FBS restricted growth media (growth media with only 2% (v/v) FBS) without phenol red. Cells were allowed to adhere to the plate surface by incubating at 37 °C, 5% CO_2. Up to 50 µl of polymer vesicle sample (diluted with PBS when necessary) with encapsulated CbF was added to each well to make the overall CbF concentration in each well 1.0 µM. Plates were incubated protected from light for 24 h at 37 °C, 5% CO_2. Then the plates were gently washed twice with PBS to remove any unbound polymer vesicles but leave the cells adhered to the plate. Plates were frozen at -80 °C to permeabilize the cells, and thawed at RT for 3 h. To completely break and dissociate the cells and the polymer vesicles, 500 µl of Borate Buffer (100 mM borate, pH 8.6) with 5% (v/v) Triton X-100 was added to each well and the plates were allowed to sit at RT for 3 h.[56] Finally fluorescence was measured using a SynergyMX fluorometer (BioTek, Winooski, VT) at 485/516 (ex/em). Negative controls were also run where peptide conjugated polymer vesicles were delivered to wells containing no cells.

Blocking experiments were performed in an identical fashion to the protocol detailed above, with the following slight alterations. The blocked cells were pre-incubated with the integrin binding free peptide, GRGDSP, at 0.5 mg/ml for 1h at 37 °C,

5% CO_2. After this pre-incubation polymer vesicle samples were added and incubated with the cells for 4 h at 37 °C, 5% CO_2.

3.2.11 Confocal Microscopy

Cells were seeded onto fibronectin modified coverslips in FBS restricted growth media without phenol red and allowed to adhere. Polymer vesicle samples were added to the monolayer of cells to yield an overall CbF concentration of 1.0 μM for all cases, except when polymer vesicles containing a self-quenching concentration of CbF were added, for which an overall CbF concentration of 5.0 μM was used. For the organelle staining images, the CellLight™ Early Endosomes-RFP *BacMam 2.0* (Invitrogen, Grand Island, NY) early endosomal stain was added at this time at a concentration of 40 particles/cell as per the manufacturers procedure. The cells were incubated with the vesicles at 37 °C, 5% CO_2 for 24 h. The LysoTracker® Blue DND-22 was added directly to the media at the 22h time point to give a final concentration of 100 nM. After the full 24 h incubation the cells were prepared for confocal imaging by washing, fixing, staining, and mounting. The coverslips were gently washed twice with 37 °C fluorescence buffer (FB), PBS supplemented with 2.5% FBS. Then they were incubated for 15 min at 37 °C in 4% (v/v) paraformaldehyde in PBS, to fix the cells. The coverslips were washed three times with 37 °C FB, followed by fluorescently staining the cells by incubating them with either a mixture of nuclear and cell membrane stains in FB for 10 min at 37 °C or a far-red cell membrane stain in FB for 10 min at RT. The cell membrane permeable blue fluorophore, Hoechst 33342 (2.0 μmol/ml), was used as a nuclear stain, and the cell impermeable red fluorophore, Alexa Fluor® 594 wheat germ agglutinin (5.0 μg/ml), was

used as a cell membrane stain for the confocal images in Figure 2. The far-red cell membrane stain Alexa Fluor® 647 wheat germ agglutinin (5.0 μg/ml) was employed for the organelle stained confocal images in Figure 3.5 - Figure 3.7. After staining, the coverslips were again washed three times with FB, then mounted facedown onto glass cover slides with ProLong® Gold antifade reagent (Invitrogen, Grand Island, NY). The slides were imaged immediately after preparation on an Olympus Fluoview 1000 Confocal Laser Scanning Microscope in the Biomedical Image Processing Laboratory (BIPL) at the University of Minnesota. Colocalization analysis was performed using the software ImageJ and the quantification procedure developed by Costes et. al.[199,200]

3.2.12 Cell Viability Assay

The MTT cytotoxicity assay was used to test the effect of siRNA delivery on the viability of each cell line. Cells, either T47D or MCF10A, were seeded onto 96 well plates at 5,000 or 2,000 cells per well, respectively, in 150 μl of the appropriate FBS restricted growth media without phenol red. Cells were allowed to adhere, then 50 μl of sample: polymer vesicles diluted in PBS, free siRNA in PBS, Lipofectamine™ RNAiMAX (Invitrogen, Grand Island, NY) complexed siRNA, or just PBS was added to each well. For samples containing siRNA a concentration of 50 nM was added to the wells, while for empty polymer vesicle samples an identical concentration of polymer to the analogous siRNA containing vesicle sample was added. The delivery of siRNA to cells by Lipofectamine™ RNAiMAX (Invitrogen, Grand Island, NY) was carried out as per the manufacturer's published procedure. After adding the samples the plates were incubated for 24 h at 37 °C, 5% CO_2, then 100 μl of the supernatant media was carefully

removed from each well, as to not disturb the adhered cells, and replaced with 100 µl full growth media without phenol red. After an additional 48h of incubation at 37 °C, 5% CO_2, 15 µl of MTT reagent (4.75 mg/ml thiazolyl blue tetrazolium bromide in PBS) was added to each well, and the plates were incubated for 4 h more at 37 °C, 5% CO_2. A solubilizing solution of 75% dimethyl sulfoxide (DMSO):25% H_2O (v/v) plus 5% sodium dodecyl sulfate (SDS) (w/v) was added to the plates (150 µl per well), and the plates were further incubated, protected from light, for 24 h at RT. Finally, the absorbance and background absorbance were measured at 570 nm and 690 nm respectively using a SpectraMax Plus spectrophotometer (Molecular Devices, Sunnyvale, CA).

3.2.13 qRT-PCR Expression Quantification

The level of Orai3 mRNA expression was assessed using quantitative real time reverse transcription polymerase chain reaction (qRT-PCR). First an assay was designed and validated at the BioMedical Genomics Center (BMGC) at the University of Minnesota to reliably quantify Orai3 mRNA expression. The assay design was prepared using the Roche Universal Probe Library (UPL) technology. Each assay design generated a sequence for the forward primer, reverse primer, amplicon and provided the UPL probe number (Orai3: forward 5'- CAGGCAGAGTTCAGATTCCTG-3', reverse 5'-CAGACTGATGGGGAAAATCC-3', UPL probe no. 24; ACTB: forward 5'-AAGTCCCTTGCCATCCTAAAA-3', reverse 5'-ATGCTATCACCTCCCCTGTG-3', UPL probe no. 55; GAPDH: forward 5'-CTCTGCTCCTCCTGTTCGAC-3', reverse 5'-ACGACCAAATCCGTTGACTC-3', UPL probe no. 60). Each primer was ordered

through the BMGC Oligonucleotide and Peptide Synthesis service using Integrated DNA Technologies (IDT, Coralville, IA).

To validate the primer probe sets, qPCR was carried out on a dilution series of complementary DNA (cDNA) using an ABI 7900 HT real-time PCR system (Applied Biosystems, Grand Island, NY) (2 min activation at 60 °C and 5 min denaturation at 95 °C, followed by 45 cycles of 10 sec at 95 °C and 1 min at 60 °C). The primer probe set with the highest validated efficiency (97%) was selected for future use.

For expression quantification, cells were seeded at 1 million cells per well on a 6 well plate in 1.4 ml of FBS restricted growth media. Cells were allowed to adhere then 100 µl of sample was added to each well (diluted as needed in PBS). The samples added were identical to those used in the MTT cell viability studies (50 nM of siRNA, etc.). The plates were incubated for 24 h at 37 °C, 5% CO_2, at which point 3 ml of full growth media was added to each well, and the plates were further incubated for another 24 h at 37 °C, 5% CO_2. After the full 48 h incubation, growth media was poured off the plate and 1 ml of RNAzol® RT reagent (Molecular Research Center, Cincinnati, OH) was added immediately to each well. Total RNA from the cells in each well was isolated following the manufacturer's procedures. The final RNA isolate was dissolved in RNase-free water and the concentration yielded was assessed with a NanoDrop 2000c spectrophotometer (Thermo Scientific, Waltham, MA). Then qRT-PCR was carried out using the RNA isolated from cells at BMGC to assess the mRNA expression levels for each sample of the gene of interest, Orai3, and two housekeeping genes, ACTB and GAPDH.

Total RNA samples were synthesized to first-strand cDNA using SuperScript II RT (Invitrogen, Grand Island, NY). Then qPCR was carried out on these cDNA samples as previously detailed using an ABI 7900 HT. For each qPCR sample 48 ng of cDNA was used along with forward primer, reverse primer, and probes each at a concentration of 10μM. Reverse transcriptase negative controls were run for each RNA isolation, and no DNA contamination of the total RNA isolate could be detected. The percentage knockdown of Orai3 was calculated relative to the geometric mean of the cycle thresholds, C_t, of both housekeeping genes (ACTB and GAPDH) using the $\Delta\Delta C_t$ method.[201,202]

3.3 Results and Discussion

3.3.1 Polymer Vesicle Formation

Polymer vesicles were formed by simple film hydration of poly(1,2-butadiene)-*b*-poly(ethylene oxide), PB-PEO or OB for short, block copolymer in aqueous solutions. The OB block copolymer was chosen because it has been extensively studied, and shown to form a wide variety of self-assembled morphologies in aqueous solution, including vesicles, and because our previous work has shown that OB polymer vesicles could allow for some release of encapsulates after cellular internalization.[44,45,53,54,203] Thus, the OB polymer system represented a good model system with potential for biological efficacy. The full specifications for the OB block copolymers used to form vesicles in this study have been previously reported.[52] Briefly, OB block copolymers were synthesized by living anionic polymerization, to give polymers with narrow PDI (polydispersity index), 1.04, and number averaged molecular weight (M_n) of 8.4 kDa. A weight percentage of

PEO of 24% in the final block copolymer was targeted, because this weight percentage has previously been shown to form vesicles in solution for OB polymers of similar molecular weight.[53] Both PB and PEO are considered bio-compatible and OB vesicles have shown promising early results both *in vitro* and *in vivo*.[18,52,114]

Vesicles encapsulating molecules of interest were formed by film hydration without the aid of any organic co-solvent, by simply introducing aqueous solutions of the molecule of interest to a dried film of OB polymer. After extrusion the vesicle size was evaluated using Dynamic Light Scattering (DLS) and was found to be 249 nm ± 117 nm (representative average hydrodynamic diameter for all vesicle samples used in this study). This vesicle size is on the high range of sizes able to take advantage of the enhanced permeability and retention effect, however vesicles could easily be extruded down to much smaller sizes if needed for future applications.[8] For this *in vitro* study the ~250 nm size range was simply chosen and held to consistently. To functionalize these vesicles with peptide targeting ligands, azide-alkyne "click" conjugation chemistry was utilized. The details of this conjugation strategy have been previously reported in the literature.[52,151,204] For illustrative and comparative purposes, a single surface concentration of peptide ligand was used throughout this study, with an average mol percentage peptide conjugation for all vesicle samples of 21 ± 1 mol% peptide, which corresponds to an estimated surface concentration of peptide for these vesicles of 0.20 ± 0.01 peptides/nm^2. This degree of surface functionalization was chosen based on our previous experience with peptide functionalized polymer vesicles and their delivery to cancer cells, as it could be readily achieved using "click" chemistry surface conjugation

and it has elicited significant polymer vesicle internalization into cancer cells.[52] A strength of this "click" conjugation strategy is that every peptide ligand is conjugated to the exterior surface with identical orientation, specifically at the N-terminus of the peptide. Previous studies have demonstrated that ligand surface orientation can be critical for proper adhesion and interaction with cell surface adhesion molecules.[152]

For the experiments in this study two encapsulates were used, siRNA and carboxyfluorescein (CbF). CbF is a highly anionic fluorescent dye molecule, which is membrane impermeable due to its negative charge, like siRNA, and is used as a vesicle encapsulate to allow effective experimental quantification and tracking of vesicles.[44,205] In addition, encapsulating CbF at self-quenching concentrations (80 mM) enables visualization of encapsulate release. Two siRNA molecules were encapsulated: siOrai3, a siRNA specifically designed to target the Orai3 gene, and siControl, a non-targeting negative control siRNA designed to not target any gene present in the cells in this study. The average siRNA encapsulation efficiency across all the vesicle samples tested was 50.2 ± 9.5% with no discernable difference in the encapsulation efficiency between the two siRNA molecules, as might be expected given their similar molecular weights. This encapsulation efficiency is nearly twice that previously reported in the literature for alternate methods of encapsulation in polymersomes and liposomes.[206,207] For comparison, we also attempted the encapsulation of a fluorescein tagged double stranded (dsDNA) analogue to siOrai3, having the same sequence except with thymine (T) replacing uracil (U), and an encapsulation efficiency of 73.1% was achieved, as determined by vesicle purification followed by fluorescence measurment. This small

discrepancy in encapsulation efficiencies between the siRNA and the dsDNA analogue may likely be due to some siRNA degradation in the initial film hydration and vesicle formation process. The relatively high siRNA encapsulation efficiency indicates that very little siRNA degradation is observed. Moreover, after siRNA has been encapsulated within polymersomes it remains protected from degradation, and within the limits of measurement no siRNA degradation was observed over weeks of vesicle storage at 4 °C (encapsulated siRNA was quantified initially and after a couple weeks of storage and no decrease in siRNA was observed).

3.3.2 Delivery of Peptide Functionalized Vesicles to MCF10A and T47D Cells

Delivery of peptide functionalized polymer vesicles to two different cell lines, MCF10A and T47D, was investigated in this study. MCF10A is a human cell line that originated from spontaneous immortalization of breast epithelial cells obtained from a patient with fibrocystic disease, and are frequently used as a model cell line for non-cancerous human breast cells.[208] T47D cells are human epithelial cancerous breast cells, that have been previously shown to highly over-express Orai3 over both normal human mammary epithelial cells obtained directly from patients and MCF10A cells.[178] These two cell lines allowed us to contrast delivery of siRNA to cancerous breast cells, T47D, and non-cancerous MCF10A cells.

Previous reports by our group have found peptide functionalized vesicles (both polymersomes and liposomes), especially PR_b functionalized vesicles, to effectively deliver to a variety of cancer cell lines, however delivery to the MCF10A and T47D cell lines remained untested.[52,91–93,118] CbF encapsulated fluorescent polymer vesicles were

utilized to investigate delivery of peptide functionalized vesicles to the cancerous T47D breast cell line and the MCF10A breast cell line. Polymer vesicles encapsulating the fluorescent dye, CbF, were functionalized with either the simple GRGDSP peptide or the PR_b peptide. These vesicles were introduced, at a total overall concentration of 1 μM CbF, to the media surrounding a growing monolayers of cells, then allowed to incubate with the cells at 37 °C for 24 h. After which the cell monolayer was extensively washed to remove any vesicles that were not bound to or internalized within cells, and subsequently either lysed and the total CbF delivered quantified (Figure 3.2) or were imaged by confocal microscopy (Figure 3.3).

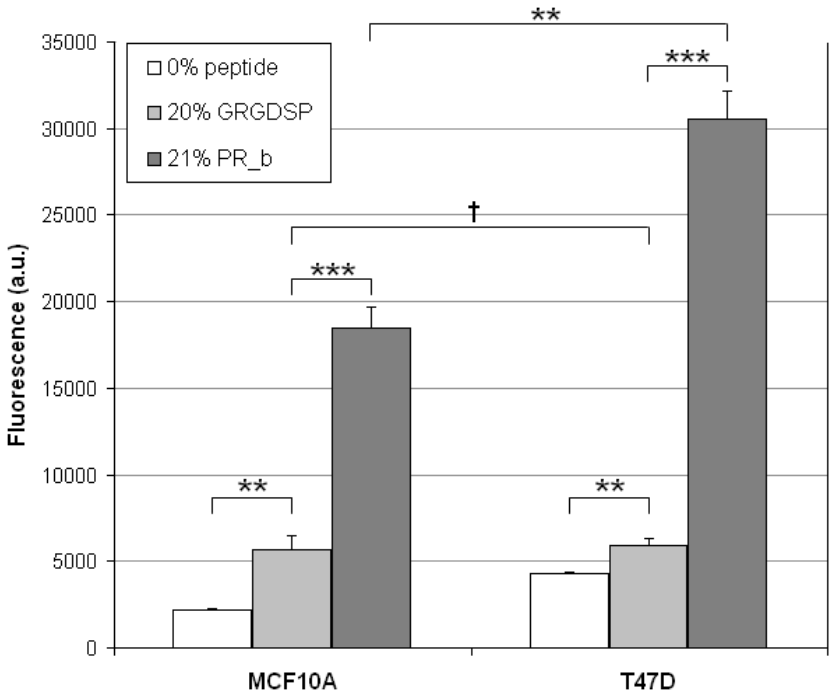

Figure 3.2 Delivery of the CbF fluorophore encapsulated within peptide functionalized polymer vesicles to either MCF10A breast cells, or T47D cancerous breast cells. Cells were incubated with CbF loaded polymer vesicles functionalized with the mol% of peptide noted in the figure for 24 h at 37 °C, after which the amount of delivery for each case was quantified. Data is the mean ± standard error of 3 separate experiments (n=3), with each experiment performed in triplicate. Students t-test statistical analyses were performed and the statistical significances notated for the bracketed data († $p > 0.05$ indicating no statistically significant difference) (* $p < 0.05$, ** $p < 0.01$, *** $p < 0.001$).

Figure 3.2 shows quantification of the level of binding and internalization (termed delivery when considered together) of peptide functionalized vesicles to the two contrasted cell lines. Very minimal delivery of non-functionalized vesicles, the 0% peptide case, is observed for both cell lines. This is as expected, considering the fully PEGylated surface of these non-functionalized vesicles is known to resist non-specific adhesion and protein interactions.[142] Akin to "stealth" liposomes the PEG chains coating the surface of the vesicles create a steric barrier to adhesion, and therefore active

internalization by the cells.[114,141] The limited amount of delivery that is observed for the non-functionalized vesicles is likely due to non-specific pinocytosis of the surrounding media by the cells.[120,206] Polymer vesicles functionalized with the targeting peptides, GRGDSP and PR_b, are thought to internalize by a more active route involving cell-surface integrin binding followed by active cellular internalization.[91] Vesicles functionalized with the peptide ligand, GRGDSP, performed better than non-functionalized vesicles for both cell lines. However, the increase in delivery observed for GRGDSP functionalized vesicles is minimal in comparison to PR_b functionalized vesicles, and additionally no statistically significant difference in delivery was seen for GRGDSP functionalized vesicles between the two cell lines. In contrast, polymer vesicles functionalized with the PR_b peptide delivered much more effectively to both cell lines than either non-functionalized vesicles or GRGDSP functionalized vesicles, giving seven times the delivery of non-functionalized vesicles and five times the delivery of GRGDSP functionalized vesicles for T47D cells. The PR_b functionalized vesicles yielded significantly greater levels of delivery in the cancerous T47D cells as compared to the non-cancerous MCF10A cells, a distinction that GRGDSP functionalized vesicles were not able to achieve. It is unclear at this time what causes PR_b functionalized polymer vesicles to deliver more effectively to T47D cells as opposed to MCF10A cells. However, one likely explanation lies in the relative expression level of $\alpha_5\beta_1$ integrin on the surface of each cell line, as there is evidence in the literature that T47D cells may have more $\alpha_5\beta_1$ integrin surface expression than MCF10A cells.[196,209]

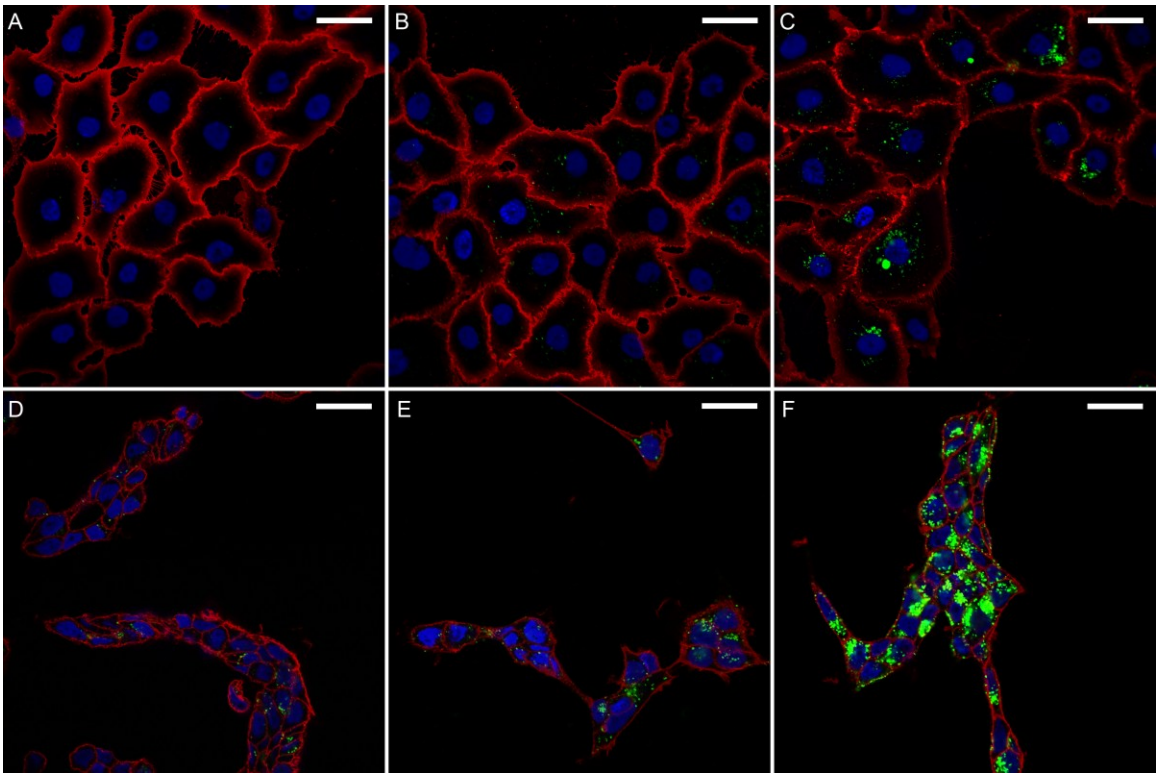

Figure 3.3 Confocal microscopy images of polymer vesicle delivery to MCF10A breast cells (A, B, C) and breast cancer T47D (D, E, F) cells. Cells were incubated with CbF loaded polymer vesicles functionalized with 0 mol% peptide (A, D), 20 mol% GRGDSP (B, E), and 21 mol% PR_b peptide (C, F) for 24 h at 37 °C, after which cells were fixed stained and imaged. Polymer vesicles encapsulating 3 mM of CbF were delivered to cells at a concentration of 1 μM CbF. Nuclei are stained blue, cell membranes red, and polymer vesicles encapsulating CbF are shown as green. Internalization of polymer vesicles is shown by the presence of green within the confines of the red cell membranes. All scale bars are 30 μm. The images show a slice from the interior of the cells, at a "z-height" approximately 2 μm above the bottom coverslip surface that cells are adhered to.

Confocal microscopy of polymer vesicles delivered to cells (Figure 3.3) was performed to corroborate the results shown in Figure 3.2 and to gain a better understanding of polymer vesicle delivery. Fluorescent polymer vesicles were delivered to cells identically to the procedure used to quantify delivery (Figure 3.2), only after the 24 h incubation period cells were fixed and stained for imaging rather than being lysed for fluorescence quantification. For the images shown in Figure 2, the cell plasma

membranes were stained red, the cell nuclei were stained blue, and CbF, the fluorescent encapsulate delivered by the polymer vesicles, appears green. Each cell monolayer was imaged ~2 μm above the surface of coverslip on which they were grown, so that the confocal images shown are a slice from within the cell. Thus, in these images simple surface binding can be differentiated from actual internalization within the cell. Whenever the green of the CbF fluorophore appears within the confines of a red cell wall, this indicates internalization of the polymer vesicles, and it is clear in all the images in Figure 3.3 that the vast majority of delivery is by internalized vesicles and not simply surface bound vesicles. As in Figure 3.2, either non-functionalized, GRGDSP functionalized, or PR_b functionalized polymer vesicles were delivered to both cell lines, MCF10A and T47D. Although it is always dubious to extrapolate the delivery observed in the relatively small sample population contained within a confocal image to more quantitative measures of delivery, the levels of delivery observed in Figure 3.3 do agree, at least on a qualitative basis, with the levels of delivery measured in Figure 3.2. The non-functionalized polymer vesicles (0% peptide) give very minimal delivery; green dots are very occasionally observed within a cell. Also, slightly higher delivery of non-functionalized vesicles is observed for T47D cells as compared to MCF10A cells. Slightly more delivery is observed for GRGDSP (20 mol% GRGDSP) functionalized vesicles for both cell lines. However, dramatically more internalization is seen for PR_b (21 mol% PR_b) functionalized vesicles, especially for T47D cells. A common feature of all the confocal images presented in Figure 2 is that the green CbF vesicle encapsulate is for a large part localized within punctate dots within the cells. These green fluorescing

bodies within the cells are clearly much larger than the size of the polymer vesicles (~250 nm), so it is inferred that these bodies are in fact intracellular organelles (likely endosomes and lysosomes). It is difficult to determine from Figure 2 whether the encapsulate is effectively released from the polymer vesicles or moreover whether the encapsulate can escape the intracellular organelles that they are likely contained within, but these questions will be dealt with later in the paper.

Taken together, the results of Figure 3.2 and Figure 3.3, clearly demonstrated that PR_b functionalized vesicles were highly effective at delivering to both cell lines, but especially the cancerous T47D cells. Moreover, PR_b functionalized vesicles were delivered at levels many times greater than those observed for GRGDSP functionalized vesicles, and exhibited enhanced delivery to cancerous T47D cells not seen for GRGDSP functionalized vesicles. Considering these results, the decision was made to focus the rest of our investigations solely on PR_b functionalized vesicles, as they were clearly delivering much more effectively, and were thus the best prospect for successful siRNA delivery.

To better characterize the nature of binding and internalization for PR_b functionalized vesicles, integrin blocking studies were conducted (Figure 3.4). Cell surface integrins were blocked by adding a high concentration of free (i.e., not conjugated to a polymer chain) GRGDSP peptide to the media that the cell monolayers were growing in. Then PR_b functionalized polymer vesicles were added to the cell media and allowed to deliver over the course of a 4 h incubation period at 37 °C. Delivery was then quantified in an identical fashion to that employed in the quantification experiments

shown in Figure 3.2. Figure 3.4 compares the level of delivery for PR_b functionalized polymer vesicles to integrin blocked T47D cells, to the levels of un-blocked delivery for both non-functionalized vesicles and PR_b functionalized vesicles. All of the data shown in Figure 3.4 is for the same 4h incubation, and this shorter incubation time is the reason for the lower fluorescence values shown in Figure 3.4 as compared to those in Figure 3.2. For the un-blocked case, PR_b functionalized vesicles are again shown to give higher levels of delivery than non-functionalized vesicles, as would be expected. However, when cell surface integrin binding sites are blocked by GRGDSP peptides, the level of delivery for PR_b functionalized vesicles drops to approximately that observed for non-functionalized vesicles. Short RGD containing peptides, such as GRGDSP, have been shown to bind to a wide variety of cell surface integrins, so they are a convenient molecule to use for blocking integrin adhesion.[172] Then because delivery of PR_b functionalized vesicles is nearly completely reduced to the levels seen for non-functionalized vesicles by GRGDSP blocking, it can be inferred that PR_b functionalized vesicles are primarily internalized by specific adhesion to cell surface integrins followed by uptake, and not by non-specific adhesion or non-specific uptake routes. This result is corroborated by previous results from our group, including results demonstrating that delivery of PR_b functionalized polymer vesicles is mitigated by $\alpha_5\beta_1$-receptor mediated endocytosis as demonstrated by blocking experiments with anti-$\alpha_5\beta_1$ antibody and by delivering to cell lines with minimal $\alpha_5\beta_1$ expression.[52,89,91] This body of evidence along with the results of Figure 3 suggest that delivery of PR_b functionalized polymer vesicles may be $\alpha_5\beta_1$-mediated.

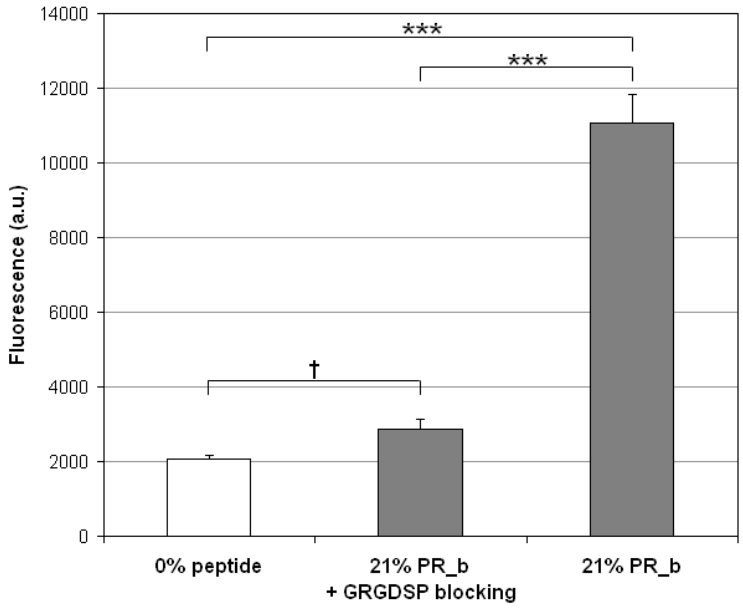

Figure 3.4 Delivery of CbF encapsulated within PR_b functionalized polymer vesicles to either unblocked T47D cells or T47D cells with their surface integrins blocked by GRGDSP peptides free in solution. Cells were incubated with CbF loaded polymer vesicles functionalized with 21 mol% PR_b for 4 h at 37 °C, after which the amount of delivery for each case was quantified. Data is the mean ± standard error of 3 separate experiments (n=3), with each experiment performed in triplicate. Students t-test statistical analyses were performed and the statistical significances notated for the bracketed data († $p > 0.05$, * $p < 0.05$, ** $p < 0.01$, *** $p < 0.001$).

3.3.3 Visualization of Intracellular Encapsulate Release with Organelle Colocalization

To better understand the intracellular fate of polymer vesicles and any encapsulates they hold, fluorescence co-localization studies were performed. Prior to these studies, relatively little was known about the pathway of internalization of PR_b functionalized polymer vesicles and the degree of intracellular release upon internalization within cells.

PR_b functionalized polymer vesicles encapsulating CbF were introduced to MCF10A (Figure 3.5) and T47D (Figure 3.6 and Figure 3.7) cells, and after a 24 h

incubation at 37 °C any polymer vesicles that were not delivered were washed away and the cells were imaged by confocal microscopy. Intracellular organelles were fluorescently stained, so that fluorescence from the CbF vesicle encapsulate (shown as green in Figure 3.5, Figure 3.6, and Figure 3.7) could be colocalized with the organelles of interest. Based on the punctuate nature of the CbF fluorescence shown in Figure 3.3 we speculated that polymer vesicles were likely primarily contained within intracellular organelles, and the most likely candidates for those organelles would be endosomes and lysosomes. Thus we stained these organelles for colocalization. Early endosomes were stained with the CellLight™ Early Endosomes-RFP transfection based fluorescent tag (shown as red in Figure 3.5, Figure 3.6, and Figure 3.7). This fluorescent tag is highly specific for early endosomal organelles as it operates by transfecting the cell with the red fluorescent protein (RFP) tagged to the Rab5a protein, an early endosomal marker. For late endosomal and lysosomal staining the LysoTracker® Blue stain was utilized (shown as blue in Figure 3.5, Figure 3.6, and Figure 3.7). This stain consists of a weakly basic fluorophore that preferentially accumulates in acidic intracellular compartments and is thus staining all acidic compartments within the cell including both lysosomes and endosomes (early and late). This can be clearly seen by colocalization of blue with red in Figure 3.5, Figure 3.6, and Figure 3.7. Thus in these figures, early endosomes are stained red, lysosomes, early and late endosomes are all stained blue, and the polymer vesicles encapsulating CbF fluoresce green. In addition, a far-red cell membrane stain has been applied to the cells to clarify the boundaries of each cell, and this is shown as yellow in the images.

Two different PR_b functionalized polymer vesicle formulations were delivered to each cell line. One containing 3 mM CbF delivered at 1 μM within 20 mol% PR_b functionalized polymer vesicles (Figure 3.5A and Figure 3.6A), and the other containing a self-quenching concentration of CbF (80 mM), delivered at 5 μM (so that CbF fluorescence could be seen clearly), within 21 mol% PR_b functionalized vesicles (Figure 3.5B and Figure 3.6B). While the vesicles with the 3 mM CbF concentration allow us to visualize the encapsulate within the cell, the self-quenching vesicles allow us to clearly visualize encapsulate release. For the vesicles with the 80 mM CbF concentration, the CbF is at a high enough concentration that it is effectively self-quenching and therefore non-fluorescent, so that only after the encapsulate has been released and diluted does it appear in the confocal images. Therefore, delivery of polymer vesicles containing self-quenching concentrations of CbF allows us to address the question of whether an encapsulate delivered by PR_b functionalized OB polymer vesicles can be effectively released.

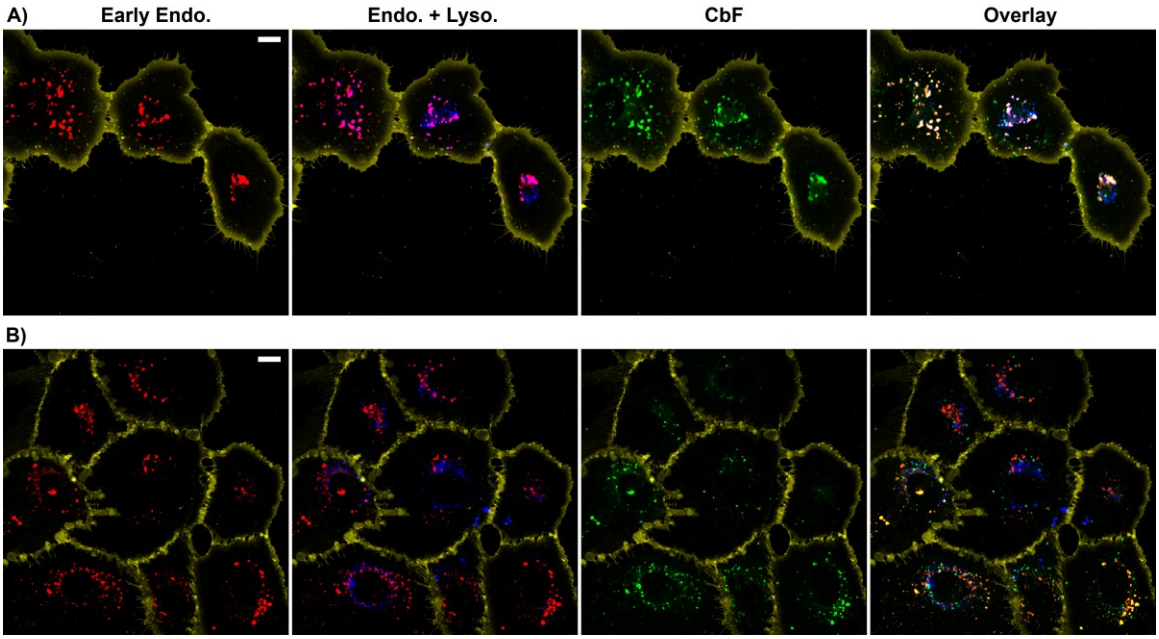

Figure 3.5 Confocal microscopy images showing colocalization of CbF delivered by PR_b functionalized polymer vesicles with stained endosomes and lysosomes in MCF10A cells. Cells were incubated with PR_b functionalized polymer vesicles for 24 h at 37 °C, after which cells were imaged. (A) 20 mol% PR_b functionalized polymer vesicles encapsulating 3 mM CbF, delivered to cells at a concentration of 1 μM CbF. (B) 21 mol% PR_b functionalized polymer vesicles encapsulating 80 mM CbF, a self-quenching concentration, delivered to cells at a concentration of 5 μM CbF. Cells membranes were stained yellow, early endosomes were stained red, all acidic organelles (endosomes and lysosomes) were stained blue, and polymer vesicle delivered CbF appears green. All scale bars are 10 μm. The images show a slice from the interior of the cells, at a "z-height" approximately 2 μm above the bottom coverslip surface that cells are adhered to.

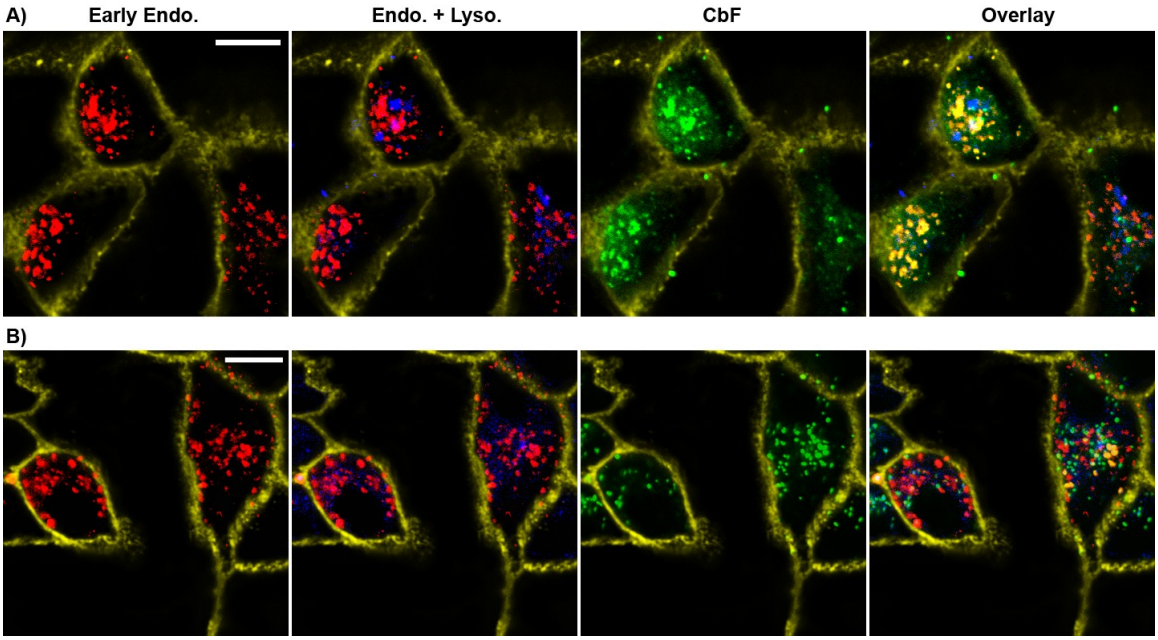

Figure 3.6 Confocal microscopy images showing colocalization of CbF delivered by PR_b functionalized polymer vesicles with stained endosomes and lysosomes in T47D cells. Cells were incubated with PR_b functionalized polymer vesicles for 24 h at 37 °C, after which cells were imaged. (A) 20 mol% PR_b functionalized polymer vesicles encapsulating 3 mM CbF, delivered to cells at a concentration of 1 μM CbF. (B) 21 mol% PR_b functionalized polymer vesicles encapsulating 80 mM CbF, a self-quenching concentration, delivered to cells at a concentration of 5 μM CbF. Cells membranes were stained yellow, early endosomes were stained red, all acidic organelles (endosomes and lysosomes) were stained blue, and polymer vesicle delivered CbF appears green. All scale bars are 10 μm. The images show a slice from the interior of the cells, at a "z-height" approximately 2 μm above the bottom coverslip surface that cells are adhered to.

Confocal images showing organelle colocalization for the delivery of PR_b functionalized polymer vesicles are presented in Figure 3.5 for MCF10A cells and Figure 3.6 for T47D cells. Delivery of polymer vesicles containing a lower concentration of CbF are shown on top (Figure 3.5A and Figure 3.6A), and delivery of polymer vesicles containing a self-quenching concentration of encapsulate are shown on the bottom (Figure 3.5B and Figure 3.6B). First, from Figure 3.5A and Figure 3.6A it is clear that for both cell lines the polymer vesicle encapsulate is highly colocalized with the early

endosomes, as well as, to some degree, the late endosomal and lysosomal compartments. Looking at the self-quenching series of images (Figure 3.5B and Figure 3.6B), where encapsulate release is selectively visualized, it can be seen that the vesicle encapsulate is being released in the early endosomes as well as the late endosomes and lysosomes, with more release apparent in the early endosomes. It is interesting that we observe release from these not explicitly degradable OB polymer vesicles, and the mechanism of this release is currently not fully understood. It is well established that the enzymatic low pH slurry that exists within cellular lysosomes is significantly more degradative than a simple acidic solution.[210] Additionally, one potential hypothesis is that the double bonds in the polybutadiene block of the OB polymer could be oxidized within the cell, thus leading to a reduction in hydrophobicity and polymer vesicle destabilization, however this hypothesis needs detailed investigation.

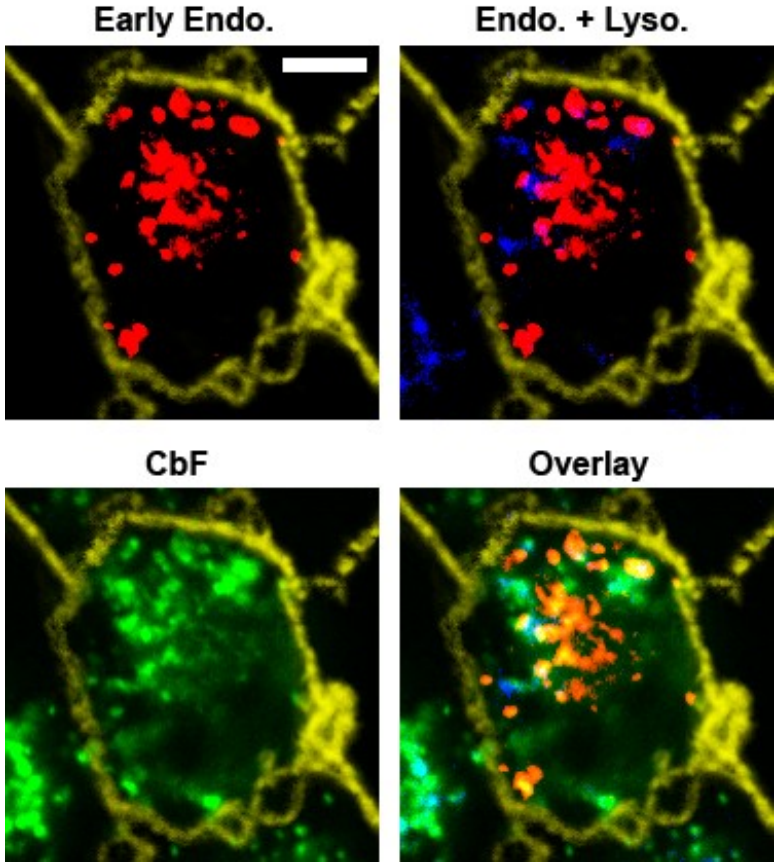

Figure 3.7 Confocal microscopy images showing colocalization of CbF delivered by PR_b functionalized polymer vesicles with stained endosomes and lysosomes in T47D cells. Cells were incubated with 20 mol% PR_b functionalized polymer vesicles for 24 h at 37 °C, after which cells were imaged. The polymer vesicles were encapsulating 3 mM CbF and were delivered to cells at a concentration of 1 μM CbF. Cells membranes were stained yellow, early endosomes were stained red, all acidic organelles (endosomes and lysosomes) were stained blue, and polymer vesicle delivered CbF appears green. Evidence of CbF escape from the cellular organelles is clearly illustrated in this magnification of a single cell. The scale bar is 5 μm. The images show a slice from the interior of the cells, at a "z-height" approximately 2 μm above the bottom coverslip surface that cells are adhered to.

A general feature of these images is that although the polymer vesicle encapsulate colocalizes well with the endosomes and lysosomes there is also a distinct amount of hazy, diffuse green surrounding many of the more punctate spots of fluorescence. This feature is most distinct in the T47D cell images (Figure 3.6 and Figure 3.7), although it is

also present in the MCF10A images (Figure 3.5). Figure 3.7 shows a blown up image of a single T47D cell, that is not shown in Figure 3.6, which clearly shows this diffuse encapsulate fluorescence. In these images, background fluorescence was rigorously subtracted, and we are quite confidant that the diffuse green fluorescence seen in these images is not auto-fluorescence of the cells, but is visualization of CbF escape from the organelles into the cytosol. This escape is highly relevant for delivery of siRNA, because siRNA must be able to escape the endosome or lysosome and reach the cytosol of the cell for it to be effective. This ability of polymer vesicles to facilitate some escape of encapsulates from endosomes and lysosomes could be instrumental to successful delivery of siRNA. Previous studies for biodegradable polymer vesicles have demonstrated that escape from acidic organelles can be facilitated by polymer vesicles through a route thought to involve pore formation in the walls of the endosomes and lysosomes.[109,120,206] However it is dubious whether a similar mechanism could be at play with the OB polymer vesicles studied here, as the membrane lytic properties observed were thought to derive from partially degraded block copolymer chains behaving similar to small molecule surfactants.

Table 3.1 Colocalization Quantification of Delivered Fluorophore with Intracellular Organelles

Cells	Colocalization with Early Endo.[a)]	Colocalization with Endo. + Lyso.[b)]
	polymersomes encapsulating 3 mM CbF[c)]	
MCF10A	58%	67%
T47D	56%	62%
	polymersomes encapsulating 80 mM CbF[d)]	
MCF10A	57%	61%
T47D	47%	54%

a) Colocalization of carboxyfluorescein (CbF) with stained early endosomes, reported as the percentage of overall CbF intensity that colocalizes.
b) Colocalization of CbF with all acidic organelles (endosomes and lysosomes), reported as the percentage of overall CbF intensity that colocalizes.
c) Colocalization quantified for images shown in Figure 3.5A and Figure 3.6A, where polymer vesicles encapsulating 3mM carboxyfluorescein (CbF) were delivered to cells.
d) Colocalization quantified for images shown in Figure 3.5B and Figure 3.6B, where polymer vesicles encapsulating 80mM carboxyfluorescein (CbF), a self-quenching concentration, were delivered to cells.

The levels of colocalization of the polymer vesicle encapsulate delivered with the early endosomes and with both the endosomes and lysososomes were quantified for the images shown in Figure 3.5 and Figure 3.6. The percentage of the total green fluorescence intensity that colocalizes with the intracellular organelles of interest is tabulated for each case in Table 3.1. From the colocalization values reported in Table 3.1 a couple of points hold true for all the cases tested. First, although the CbF encapsulate colocalizes with both endosomes and lysosomes, a large majority of the encapsulate localized within the early endosomes. This is likely an important point for the effective delivery of siRNA, as the environment within early endosomal compartments is milder, and therefore less likely to rapidly degrade any released siRNA, as opposed to the harsh environment within a lysosome. Along these lines, for the self-quenching polymer vesicles (Figures 4B and 5B) it is clear that a majority of the colocalized encapsulate is

not only localized within the early endosomes, but is in fact released within the early endosomes. Second, there is a notable percentage of encapsulate that is not accounted for in the percentages and is therefore not colocalized with either the endosomes or the lysosomes. This is likely the diffuse green that is seen in the cytosol of the images in Figure 3.5, Figure 3.6, and Figure 3.7, and represents escape of encapsulate from the cellular organelles into the cell cytosol. As discussed previously, achieving endosomal and lysosomal escape is critical to attaining effective siRNA delivery.

3.3.4 siRNA Delivery by PR_b Functionalized Vesicles to T47D and MCF10A Cells

To the knowledge of the author, only a few previous studies has dealt with delivery of siRNA by polymer vesicles, and these works investigated significantly different systems, in terms of siRNA, cells, and polymer.[206,211] Furthermore, these previous reports dealt with non-targeted delivery, thus the effect of functionalizing the polymer vesicles with a targeting ligand, such as the PR_b peptide, was not studied. We sought to investigate the proficiency with which PR_b functionalized polymer vesicles could be utilized to deliver a novel siRNA therapeutic, siOrai3, to the breast cancer cell line, T47D. Additionally, the effect of siOrai3 delivery to cancerous T47D cells was contrasted to the effect of delivery to non-cancerous MCF10A cells.

Although it is clear from the results presented thus far that PR_b functionalized OB polymer vesicles themselves deliver with high efficacy to both T47D and MCF10A cells, effective delivery of siRNA is a further level of complexity. The siRNA must first be protected from degradation before it is internalized within the cell, then it must be effectively released from the polymer vesicles and make its way to the cytosol, where it

can assemble with the endogenous RISC protein complex to effect the desired mRNA knockdown. As discussed previously, two siRNA molecules, siOrai3 and siControl, were encapsulated inside of polymer vesicles and their effect on cells was compared. siOrai3 is a siRNA that specifically targets the Orai3 gene for RNAi knockdown. It has previously been shown in the literature that knockdown of Orai3 expression can specifically arrest cell cycle progression for T47D breast cancer cells eventually leading to apoptosis and a reduction in cell viability, but has minimal effect on the cell viability of non-cancerous breast cells.[178] So it was expected that siOrai3 could behave as a cancer cell specific therapeutic in our experiments. The siControl sequence chosen in this study targets firefly luciferase mRNA and therefore is used as a non-targeting siRNA as it does not target any of the genes present in either T47D cells or MCF10A cells. Thus, siControl gives a baseline cellular siRNA response for comparison with that of siOrai3.

The two siRNA molecules, siOrai3 and siControl, were delivered to MCF10A and T47D cells in a variety of forms, and the resultant effect on cell viability and Orai3 knockdown were measured (Figure 3.8 - Figure 3.11). Figure 3.8 and Figure 3.9 show the effect of siOrai3 delivery for each of the varying formulations on cell viabilities and Orai3 knockdown respectively normalized to the appropriate siControl case, and Figure 3.10 and Figure 3.11 show all the control cases (delivery of siControl and delivery of "empty" polymer vesicles) with values normalized to untreated cells. Delivery of siOrai3 encapsulated within polymer vesicles was compared to delivery of free siOrai3 in solution, and to siOria3 complexed with a commercial transfection agent, Lipofectamine™ RNAiMAX. A consistent siRNA delivery concentration of 50 nM was

used for all siRNA formulations. Cell viability was assessed at 72 h using the MTT assay, and Orai3 mRNA expression levels were assessed at 48 h using qRT-PCR.

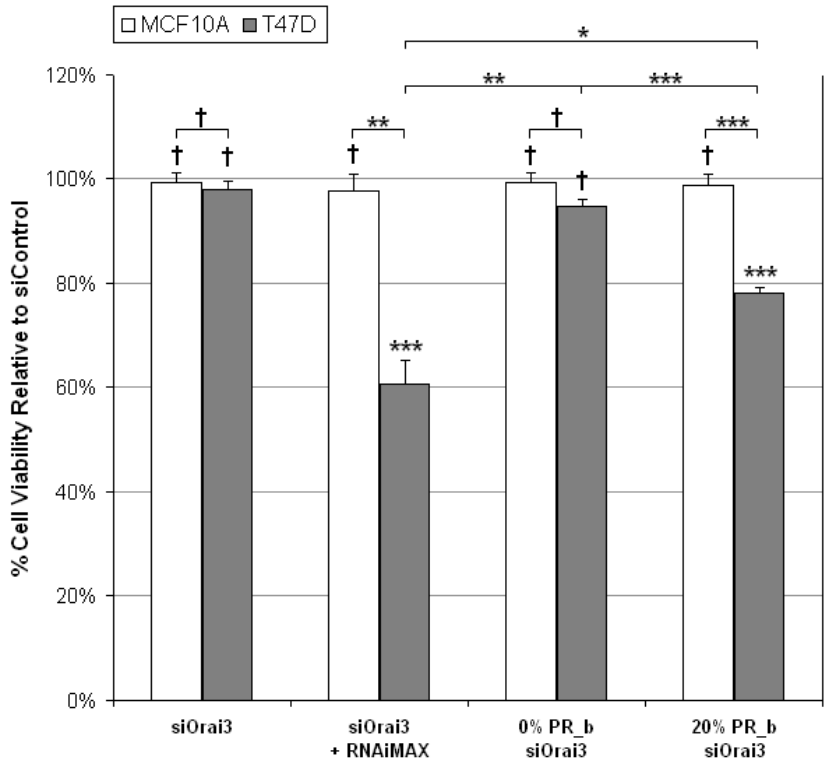

Figure 3.8 Percent cell viabilities in MCF10A breast cells and T47D breast cancer cells after treatment with the indicated siOrai3 formulations. Cells were incubated with 50 nM of siOrai3 delivered as a formulation with the indicated delivery agents for 24 h at 37 °C, after which the cell media was refreshed and incubation continued. Cell viability was quantified using the MTT assay at 72 h after siOrai3 delivery. Data is the mean ± standard error of 3 separate experiments (n=3), with each experiment performed in quadruplicate. Cell viabilities are normalized with respect to the appropriate siControl case for each formulation (shown in Figure 3.10). The formulations of delivery agents tested were: siRNA free in solution without the aid of any delivery agent (siOrai3), siRNA complexed with the RNAiMAX commercial transfection agent (siOrai3 + RNAiMAX), siRNA encapsulated within non-functionalized polymer vesicles (0% PR_b siOrai3), and PR_b functionalized vesicles encapsulating siRNA (20% PR_b siOrai3). The percentages of PR_b functionalization shown are mol%. Students t-test statistical analyses were performed and the statistical significances notated († $p > 0.05$, * $p < 0.05$, ** $p < 0.01$, *** $p < 0.001$). *P*-value markers directly above each column indicate the statistical significance between that column and the corresponding siControl case (shown in Figure 3.10), while markers over brackets indicate the statistical significance between the two bracketed columns.

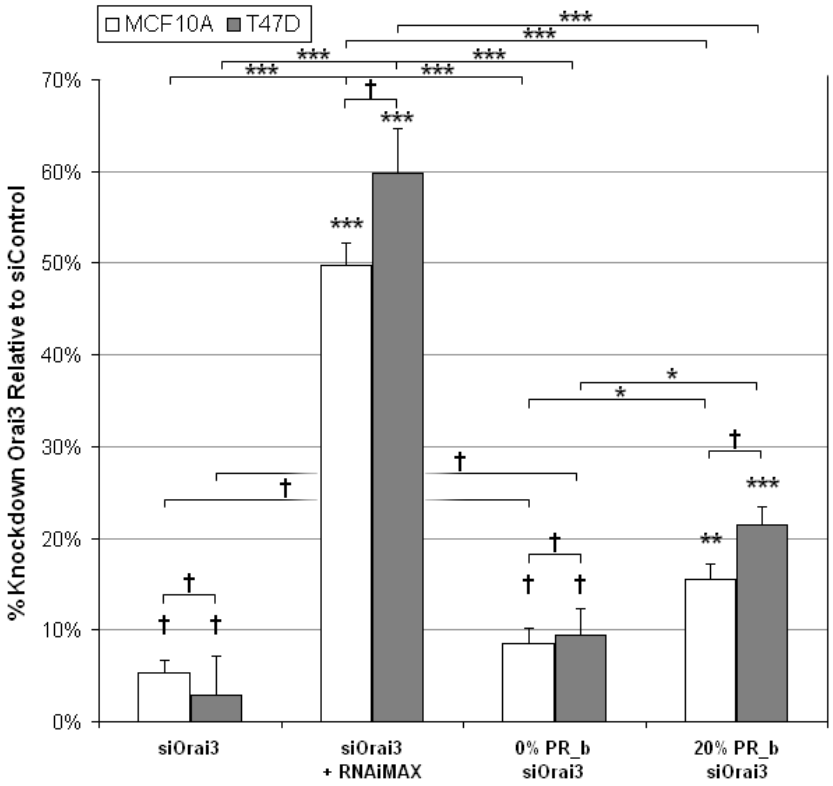

Figure 3.9 Percent knockdown of Orai3 in MCF10A breast cells and T47D breast cancer cells after treatment with the indicated siOrai3 formulations. Cells were incubated with 50 nM of siOrai3 delivered as a formulation with the indicated delivery agents for 24 h at 37 °C, after which the cell media was refreshed and incubation continued. Orai3 knockdown was quantified using qRT-PCR at 48 h after siOrai3 delviery. Data is the mean ± standard error of 4 separate experiments (n=4), with each experiment performed in duplicate. Percent Orai3 knockdowns are normalized with respect to the appropriate siControl case for each formulation (shown in Figure 3.11). The formulations of delivery agents tested were: siRNA free in solution without the aid of any delivery agent (siOrai3), siRNA complexed with the RNAiMAX commercial transfection agent (siOrai3 + RNAiMAX), siRNA encapsulated within non-functionalized polymer vesicles (0% PR_b siOrai3), and PR_b functionalized vesicles encapsulating siRNA (20% PR_b siOrai3). The percentages of PR_b functionalization shown are mol%. Students t-test statistical analyses were performed and the statistical significances notated († $p > 0.05$, * $p < 0.05$, ** $p < 0.01$, *** $p < 0.001$). *P*-value markers directly above each column indicate the statistical significance between that column and the corresponding siControl case (shown in Figure 3.11), while markers over brackets indicate the statistical significance between the two bracketed columns.

As seen in Figure 3.8and Figure 3.9, siOrai3 either as free siRNA in solution (siOrai3) or encapsulated in non-functionalized polymer vesicles (0% PR_b siOrai3) gave no statistically significant change in cell viability or Orai3 expression for either cell line with respect to cells treated with siControl. Without the aid of some delivery agent, free siRNA has very little chance of internalizing within a cell, due to its anionic nature, and because siRNA is rapidly degraded in serum without some form of encapsulation or protection. Thus, it is unsurprising that no significant decrease in cell viability or Orai3 knockdown are observed for the case where free siOrai3 in solution was introduced to the cells (siOrai3). Without PR_b functionalization polymer vesicle delivery is minimal so that it could be expected that siOrai3 delivery by non-functionalized vesicles (0% PR_b siOrai3) would be ineffective, as is seen in Figure 3.9.

In contrast, delivery of RNAiMAX complexed siOrai3 (siOrai3 + RNAiMAX) was found to be considerably more effective, and gave relatively high amounts of Orai3 knockdown in both cell lines. The RNAiMAX commercial siRNA transfection agent yielded in general a 50-60% knockdown of Orai3 relative to the siControl case for both MCF10A cells and T47D cells, with no statistically significant difference between the knockdown levels of the two cell lines (Figure 3.9). However, a striking difference is seen in the resultant cell viability of the two cell lines for the siOrai3 + RNAiMAX case (Figure 3.8). A 37% decrease in cell viability of the T47D cancerous breast cell line as compared to the MCF10A breast cell line is observed. Just as importantly, for MCF10A cells no statistically significant decrease in cell viability from the baseline siControl + RNAiMAX case is observed for delivery of siOrai3 by RNAiMAX. As was expected, it

appears that siOrai3 is able to act as a cancer cell specific therapeutic. It was proposed in the literature that knockdown of Orai3 could have a cancer cell specific effect on cell viability, decreasing T47D cell viability while preserving MCF10A breast cell viability, and our results have confirmed this effect.[178] Considering that Orai3 was knocked down similarly for both cell lines, yet only T47D cells saw a decrease in cell viability it is reasonable to conclude that Orai3 is critical for T47D cell proliferation and survival, while it is not for MCF10A cells.

Lipofectamine™ RNAiMAX is a well established, highly effective *in vitro* siRNA transfection agent. Repeated investigations have identified RNAiMAX as one of the most effective commercial siRNA transfection agents currently available.[212–216] Taken together, delivery of siOrai3, either complexed with RNAiMAX or as free siRNA in solution, represents an approximate window of current siRNA delivery *in vitro*, with RNAiMAX representing a highly effective current commercial siRNA transfection agent and free siRNA representing the least effective siRNA delivery system imaginable.

Delivery of siRNA by PR_b functionalized polymer vesicles lies within this window of delivery effectiveness. As was seen for the RNAiMAX formulation, delivery of siOrai3 encapsulated within PR_b functionalized polymer vesicles (20% PR_b siOrai3) resulted in Orai3 knockdown in both cell lines, concomitant with T47D specific decreases in cell viability (Figure 3.9 and Figure 3.8 respectively). However, both the amount of Orai3 knockdown and the level of T47D cell viability decrease are more moderate for the case of siOrai3 delivery by PR_b functionalized polymer vesicles compared to the delivery by RNAiMAX. Still, siOrai3 delivery by PR_b functionalized

polymer vesicles effect on average 22% knockdown of Orai3 expression and a 22% decrease in T47D cell viability, relative to siControl baselines. Just as with the RNAiMAX case no measurable drop in cell viability is elicited in the breast cell line, MCF10A. Although these results are not overwhelmingly positive for siRNA delivery by polymer vesicles, one must keep in mind that these are for a model OB block (non-degradable) copolymer system and they can represent a first step toward future improvements and advancements in polymersome design tailored for the task of siRNA delivery.

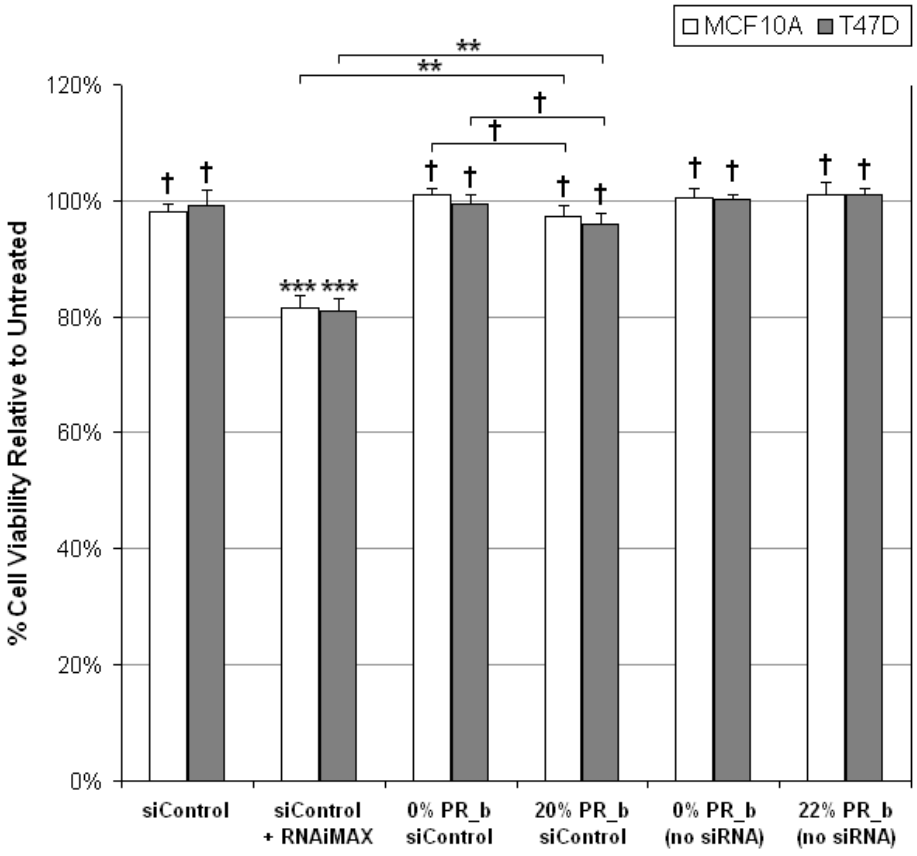

Figure 3.10 Percent cell viabilities in MCF10A breast cells and T47D breast cancer cells after treatment with the indicated siControl formulations. Cells were incubated with 50 nM of siControl delivered as a formulation with the indicated delivery agents for 24 h at 37 °C, after which the cell media was refreshed and incubation continued. Cell viability was quantified using the MTT assay at 72 h after siControl delivery. Data is the mean ± standard error of 3 separate experiments (n=3), with each experiment performed in quadruplicate. Cell viabilities are normalized with respect to untreated cells. The formulations of delivery agents tested were: siRNA free in solution without the aid of any delivery agent (siControl), siRNA complexed with the RNAiMAX commercial transfection agent (siControl + RNAiMAX), siRNA encapsulated within non-functionalized polymer vesicles (0% PR_b siControl), PR_b functionalized vesicles encapsulating siRNA (20% PR_b siControl), and non-functionalized and PR_b functionalized "empty" vesicles (0% PR_b and 22% PR_b (no siRNA)). The percentages of PR_b functionalization shown are mol%. Students t-test statistical analyses were performed and the statistical significances notated († $p > 0.05$, * $p < 0.05$, ** $p < 0.01$, *** $p < 0.001$). *P*-value markers directly above each column indicate the statistical significance between that column and untreated cells, while markers over brackets indicate the statistical significance between the two bracketed columns.

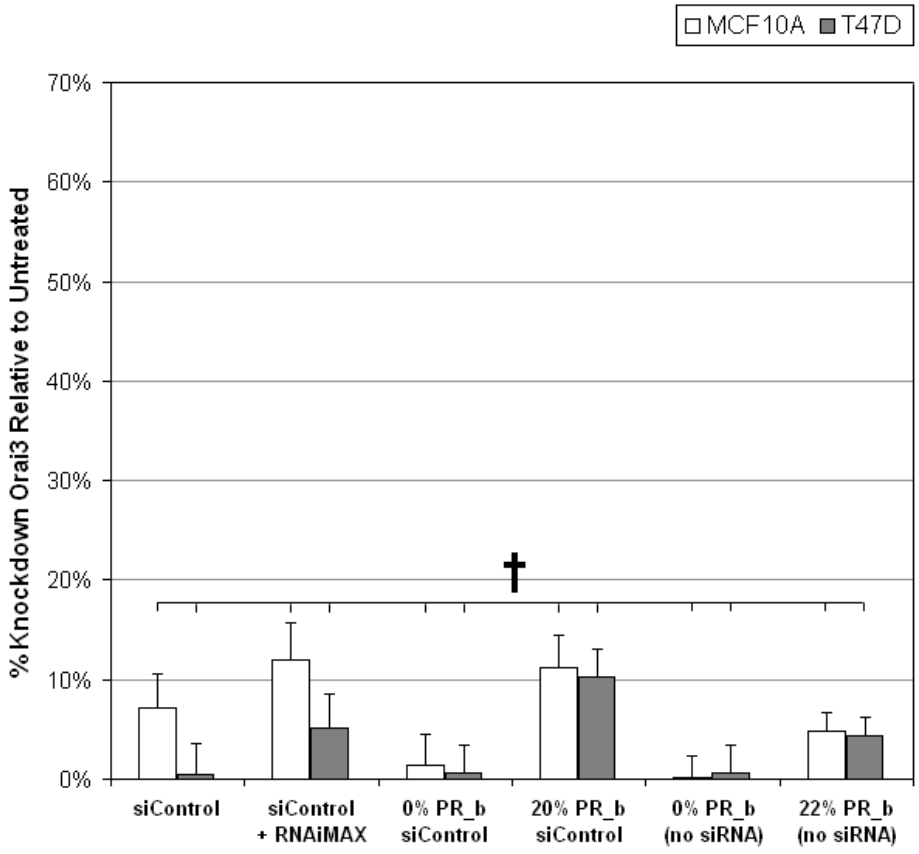

Figure 3.11 Percent knockdown of Orai3 in MCF10A breast cells and T47D breast cancer cells after treatment with the indicated siControl formulations. Cells were incubated with 50 nM of siControl delivered as a formulation with the indicated delivery agents for 24 h at 37 °C, after which the cell media was refreshed and incubation continued. Orai3 knockdown was quantified using qRT-PCR at 48 h after siControl delviery. Data is the mean ± standard error of 4 separate experiments (n=4), with each experiment performed in duplicate. Percent Orai3 knockdowns are normalized with respect to untreated cells. The formulations of delivery agents tested were: siRNA free in solution without the aid of any delivery agent (siControl), siRNA complexed with the RNAiMAX commercial transfection agent (siControl + RNAiMAX), siRNA encapsulated within non-functionalized polymer vesicles (0% PR_b siControl), PR_b functionalized vesicles encapsulating siRNA (20% PR_b siControl), and non-functionalized and PR_b functionalized "empty" vesicles (0% PR_b and 22% PR_b (no siRNA)). The percentages of PR_b functionalization shown are mol%. Students t-test statistical analyses were performed and the statistical significances notated († $p > 0.05$). None of the control formulations produced a statistically significantly difference ($p > 0.05$ for all) in siOrai3 expression compared to the untreated cells, as indicated by the overarching all-inclusive bracket.

Figure 3.10 and Figure 3.11 show the percent cell viabilities and Orai3 knockdowns respectively, relative to untreated cells for each of the control cases, both siControl formulated with varying delivery agents and "empty" polymer vesicles containing no siRNA. First, it must be pointed out than none of the control cases produced a statistically significant knockdown in Orai3 expression (Figure 3.11) compared to the untreated cells as indicated by the overarching all-inclusive bracket in this figure. This is unsurprising given that siControl is designed to give minimal off-target knockdown of gene expression, and certainly no Orai3 knockdown could be expected for "empty" polymer vesicles, since no siRNA is delivered. Likewise, for all the control formulations except the RNAiMAX transfection agent (siControl + RNAiMAX) no statistically significant decrease in cell viability is observed compared to the untreated cells (Figure 3.10). Corroborating previous reports in the literature concerning the biocompatibility and non-toxic nature of OB polymer vesicles, "empty" polymer vesicles, both non-functionalized (0% PR_b (no siRNA)) and PR_b functionalized (22% PR_b (no siRNA)), were found to have no effect on the cell viability of either cell line.[18,52,114] In addition, encapsulation and deliver of control siRNA by polymer vesicles (0% PR_b siControl and 20% PR_b siControl) also were found to have no statistically significant effect on cell viability compared to the untreated cells. In Figure 7B it was seen that PR_b functionalized polymer vesicles are capable of delivering siRNA at moderate levels so that it is likely that siControl is being delivered to the cells for this case in Figure 8 as well. The levels of siControl delivered to cells by

PR_b functionalized polymer vesicles appear then to have no significant effect on the viability of either cell line.

In contrast to all the other control cases shown in Figure 3.10, the RNAiMAX transfection agent complexed with siControl (siControl + RNAiMAX) produced an approximately 19% drop in cell viability for both MCF10A non-cancerous breast cells and T47D breast cancer cells. It is unclear from this data whether this decrease in cell viability derives from the RNAiMAX transfection agent itself or from the delivery of siControl, or as is more likely a combination of the two. It should be noted that others have observed similar levels of toxicity for the RNAiMAX transfection agent, and in fact among the variety of commercial siRNA transfection agents currently available, RNAiMAX is recognized as one of the least toxic and most effective.[212–218] Figure 3.10 clearly shows that RNAiMAX complexed with siControl (siControl + RNAiMAX) gives some moderate toxicity in both cell lines as compared to both untreated cells and delivery of siControl by PR_b functionalized polymersomes (20% PR_b siControl), but it is uncertain to what extent this difference in toxicity derives from the differing levels of siRNA delivery for these two formulations. Ideally one would like to measure the cell viabilities resulting from RNAiMAX delivered alone without siRNA to assess the inherent toxicity of the delivery agent itself, similar to what was done with "empty" polymer vesicles. This experiment was attempted, however an accurate measure of the toxicity of RNAiMAX alone could not be obtained. Since the RNAiMAX transfection agent forms a complex with siRNA in solution, and it is this tightly bound complex that delivers to the cells, delivery of the RNAiMAX reagent alone (i.e. un-complexed, without

any siRNA) is inherently different and does not interact with cells in a similar manner, and thus does represent a valid measure of RNAiMAX toxicity.

3.4 Conclusion

The ability of peptide functionalized OB polymer vesicles to deliver siRNA to T47D breast cancer cells was investigated, and compared to that with MCF10A breast cells. Both GRGDSP and PR_b peptide functionalized polymer vesicles were found to effectively deliver to both cell lines, however PR_b functionalized vesicles gave significantly higher levels of delivery. In addition, PR_b functionalization of polymer vesicles resulted in significantly more delivery of encapsulates to cancerous T47D cells as compared to MCF10A cells. Confocal microscopy with endosomal and lysosomal intracellular organelles stained for visualization of colocalization revealed that PR_b polymer vesicles, upon internalization, are passaged through the endosomes and lysosomes. The polymer vesicle encapsulate was most colocalized with early endosomes, and it was also found that the majority of encapsulate release from polymer vesicles occurs in the early endosomes. Also some evidence of organelle escape was observed. siRNA molecules were then effectively encapsulated within polymer vesicles, and delivered to these cell lines. The Orai3 gene was targeted for siRNA knockdown, because a recent report in the literature indicated that knockdown of Orai3 could have a differential effect on cell viability for breast cancer cells, as opposed to non-cancerous breast cells.[178] Delivery of siRNA targeting the Orai3 gene, siOrai3, by PR_b functionalized polymer vesicles gave Orai3 knockdown in both cell lines, but decreased T47D, breast cancer cell viability while having no measurable negative effect on the

viability of MCF10A, breast cells. Compared to the highly effective commercial transfection agent, Lipofectamine™ RNAiMAX, Orai3 knockdown by PR_b functionalized polymer vesicles is admittedly moderate, however lower toxicity was observed for the delivery of siRNA by polymer vesicles as opposed to by RNAiMAX. Although both encapsulate release from polymer vesicles and encapsulate escape from acidic organelles was observed, neither was highly prevalent. These factors likely contribute to the only moderate levels of Orai3 knockdown observed for PR_b functionalized vesicles, even though these vesicles were found to be very effectively internalized by the cells. However the results shown here are promising, considering that these OB polymer vesicles are a first generation model non-degradable polymer vesicle system. Future improvements could likely be achieved for siRNA delivery by polymer vesicles by designing block copolymers that would more effectively release encapsulates and facilitate endosomal escape.

4 Experimental Details

4.1 Poly(1,2-butadiene)-*b*-Poly(ethylene oxide) Block Copolymer Synthesis

The synthesis of poly(1,2-butadiene)-*b*-poly(ethylene oxide) (OB) block copolymers was achieved through two sequential syntheses.[127] First a poly(butadiene) (PB) homopolymer was synthesized by living anionic polymerization; then, after purification and workup of the PB polymer, a poly(ethylene oxide) (PEO) block was grown off the end of the PB chain. This resulted in a linear amphiphilic block copolymer with low poly dispersity index (PDI).

4.1.1 Poly(1,2-butadiene) Synthesis

Poly(butadiene), PB, is formed from the monomer 1,3-butadiene, the simplest conceivable conjugated diene. Butadiene is efficiently polymerized by a variety of different mechanisms: radical, anionic, cationic, or with Ziegler-Natta like catalysts. Anionic polymerization of butadiene was chosen in this case because it can produce PB with low PDI and controlled structural isomerism, as well as providing a simple means of quantitatively end functionalizing the PB.

The polymerization scheme for poly(1,2-butadiene) is shown in Figure 4.1. Polymerization of 1,3-butadiene was carried out in tetrahydrofuran (THF) under an inert Argon atmosphere with sec-butyl lithium as an initiator. All reaction vessels, reactants, and solvents were rigorously purged of air and moisture because both water and O_2 can terminate the growing chain. THF was obtained dry and degassed after passing through a home built solvent purification system consisting of activated alumina columns.[219] Approximately 20 ml of THF were used for each gram of butadiene used. The initiator,

sec-butyl lithium in hexane was stored in a dry box and transferred to the reactor with a gas tight syringe. The monomer, 1,3-butadiene was purified twice over n-butyl lithium to remove all terminating agents and then transferred to the reactor. The polymerization was allowed to proceed for 5 h at -50 °C with constant stirring.

The amount of initiator used was chosen to target a specific degree of polymerization and was determined by assuming quantitative initiation and living propagation. The concentration of initiator was analytically determined by NMR referenced to a known amount of 1,5-cyclooctidiene immediately prior to initiation.

The polymerization asymptotically approaches complete conversion without measurable termination of the reactive chain end, at which point a large excess of purified ethylene oxide (EO) monomer was added to the reaction mixture. Because lithium counter ions rapidly and strongly bind to any activated EO chain ends, essentially only a single ethylene oxide monomer adds to the PB chain end.[220,221] The reaction was left at room temperature for 20 h to ensure complete and quantitative addition of EO to the end of the PB chain. To terminate the chain an excess of methanol with 1% (v/v) hydrochloric acid was added to the reaction mixture and allowed to react for 30 minutes.

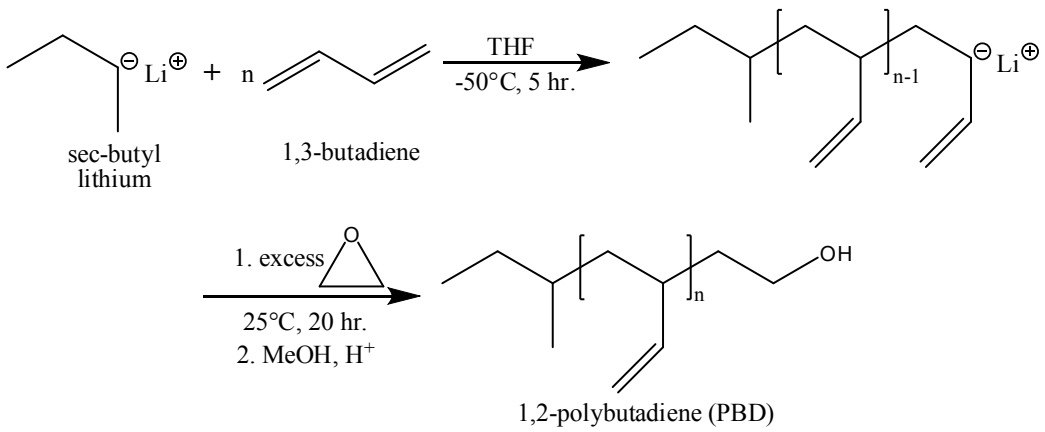

Figure 4.1 Reaction scheme for the synthesis of poly(1,2-butadiene).

Like most dienes butadiene can polymerize to yield varying structural isomers. Neglecting the possibility of head-to-head, as opposed to head-to-tail addition, which is thermodynamically and kinetically favored, there remain three distinct forms of repeat units that are possible, as shown in Figure 4.2. Two forms of monomer addition exist; 1,2 addition is where the growing chain attacks the first carbon in butadiene and the second carbon goes on to react with another monomer, and 1,4 addition is where the first carbon is attacked and the fourth becomes activated through rearrangement and goes on to react with another monomer. In 1,4 addition the repeat unit can be in either the cis or trans configuration.

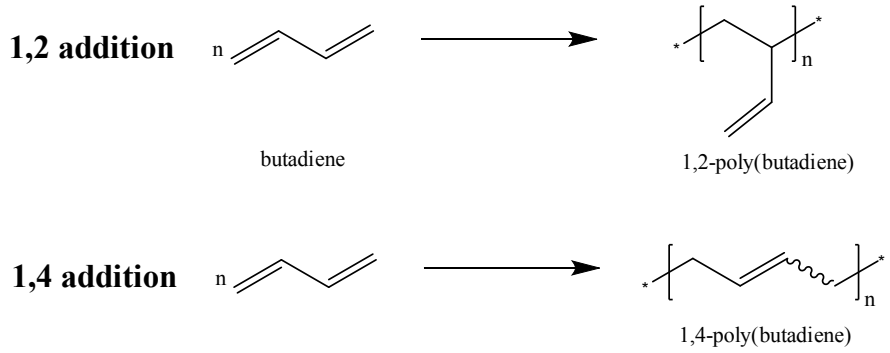

Figure 4.2 1,2 vs. 1,4 addition of butadiene.

Typical industrial PBD, like that used in tires, consists of mainly 1,4 additions. The long linear sections in 1,4-poly(butadiene) favor chain packing and therefore crystallization. Therefore 1,2 addition is desirable for formation of polymer vesicles because it exhibits a low glass transition and crystallization temperature. The short side chains of poly(1,2-butadiene) break symmetry and prevent close packing of the chains, thus disfavoring crystallization and the glass transition.

The structural isomerism of the poly(butadiene) chain is controlled mainly by the choice of solvent.[222,223] In general a more polar solvent favors 1,2-addition. Tetrahydrofuran was used because it is reasonably polar, but lacks strongly electrophilic groups which would terminate the polymerization. The low temperatures used were to ensure that the polymerization proceeds in a controlled manner. More polar solvents, such as THF, accelerate the polymerization kinetics by increasing the concentration of free anions and preventing anion aggregation by solvating them more effectively.[224] The polymerization scheme shown in Figure 4.1 for example gave approximately 92% 1,2-addition.

After the polymerization was terminated with acidic methanol, the PB homopolymer was recovered by rotovapping the THF solvent off and drying under high vacuum (on the order of 100 mTorr). The polymer was dissolved in dichloromethane and impurities were removed by extraction against aqueous solutions. Extraction was performed twice against a saturated sodium bicarbonate solution and at least three times against distilled water. The recovered polymer rich dichloromethane phase was then

rotovaped and dried under vacuum. To remove any traces of water the polymer was dissolved in benzene and freeze-dried azeotropically under high vacuum. The recovered dry polymer was stored under Argon at -25 °C. The quality of purification is evident by the clarity of the final PB polymer. When salts remain in the sample the polymer will have a yellowish hue, however these salts appear to have little effect on future syntheses so rigorous purification may not be essential. PB number average molecular weight (M_n) and fraction of 1,2 addition was determined by NMR spectroscopy and end-group analysis, as indicated by the NMR peak assignment shown in Figure 4.3. Size exclusion chromatography (SEC) was used to determine the PDI and the weight average molecular weight (M_w) of the polymers.

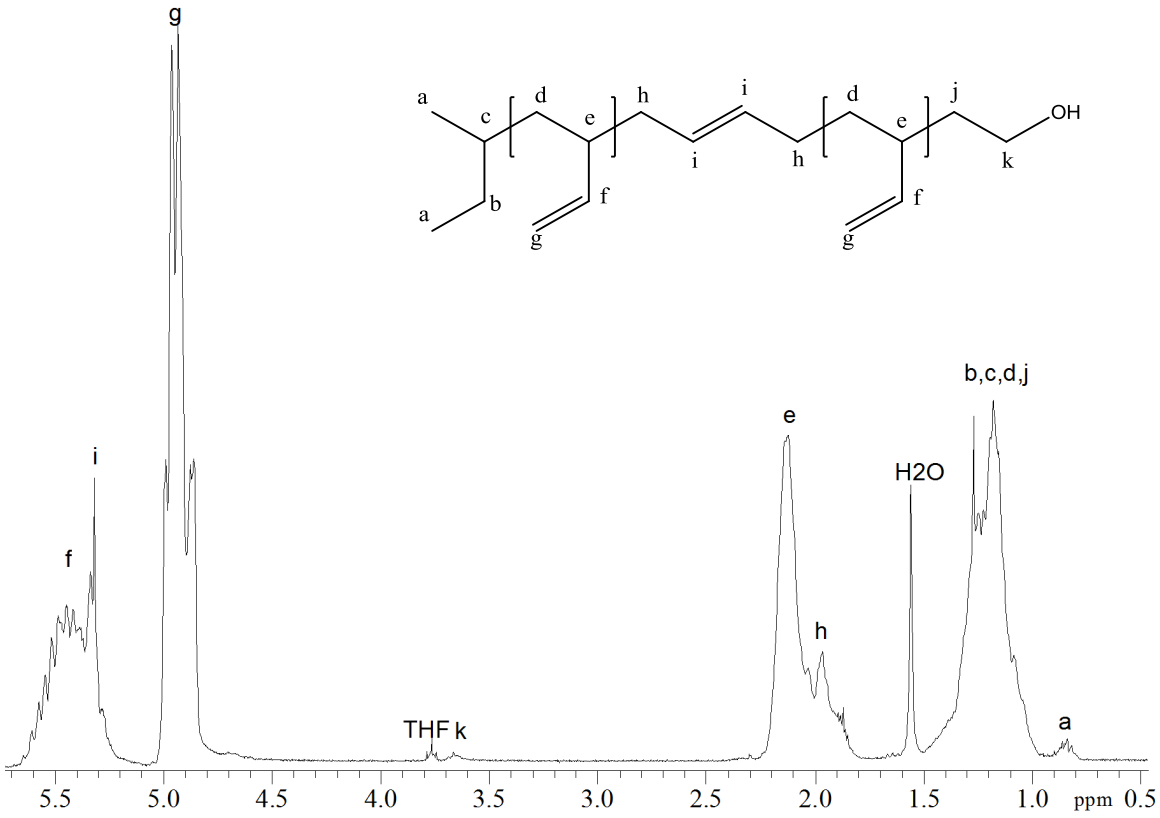

Figure 4.3 ^{1}H NMR peak assignments for α-hydroxyl PB in $CDCl_3$.

4.1.2 Poly(ethylene oxide) Block Synthesis

While many block copolymer syntheses can be accomplished by sequential addition of different monomers, the synthesis of OB block copolymers in this manner is not convenient. This is because the activated EO chain end rapidly and strongly associates with the lithium counterion in the PB synthesis, and the activated anionic chain end of EO is not nucleophilic enough to initiate polymerization of dienes.[220,221] There has been some limited success in the sequential polymerization of dienes and ethylene oxide using either crown ethers or phosphazene base to sequester the free lithium ions in the reaction medium, but these techniques have not been extensively developed.[225–227] Thus, OB block copolymers were synthesized in two sequential synthetic steps.

First a mono-hydroxyl substituted poly(butadiene) homopolymer was synthesized as discussed above, then this PB homopolymer was converted in-situ to a macroinitiator from which ethylene oxide was polymerized, as shown in Figure 4.4.

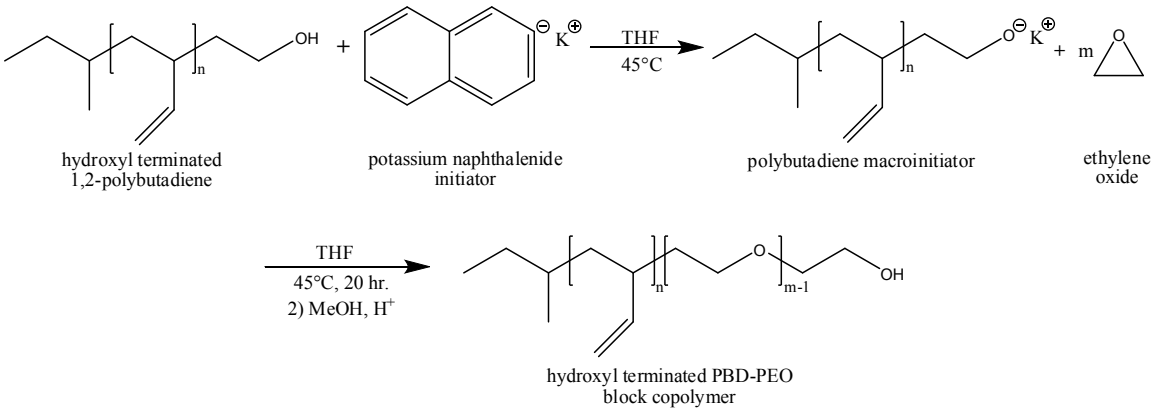

Figure 4.4 Reaction scheme for the polymerization of the poly(ethylene oxide) block in OB diblock copolymer.

Hydroxyl terminated PB was dissolved in benzene and then freeze dried in the reactor that will be used for poly(ethylene oxide), PEO, synthesis. This rigorously removed moisture from the reactor and the PB homopolymer. THF was obtained dry and degassed after passing through a home built solvent purification system consisting of activated alumina columns.[219] Approximately 20 ml of THF for every gram of final polymer was added to the reactor and the PB was allowed to dissolve completely. The ethylene oxide (EO) monomer was freeze pump thawed to remove oxygen and purified twice using Butyl-MgCl, then stored in a dry-ice bath. Potassium naphthalenide initiator was titrated into the reactor until a light green color persisted, indicating that all the PB hydroxyl groups had been converted to the corresponding potassium alkoxide salts. The purified EO monomer was added to the reactor and proceeded to polymerize from the anionic PB macroinitiators. The reaction was allowed to proceed for 20 h at 45 °C, after which acidic methanol was added to terminate the polymerization.

The resulting diblock copolymer was further processed and purified before storage. The THF solvent was completely removed, first by rotovapping and then by drying under high vacuum. The dry polymer was then dissolved in dichloromethane and extracted 4-5 times, first against saturated sodium bicarbonate solution, then against brine, and finally against distilled water to remove salts. The final recovery of polymer rich dichloromethane was rotovapped and then dissolved in benzene for freeze drying. Finally the purified dry polymer was stored under Argon at -25 °C. The final OB block copolymer was characterized by NMR and SEC, in similar fashion to the PB homopolymer. To separate peaks and clarify the NMR spectra of OB α-hydroxyl groups

were reacted with trifluoroacetic anhydride directly before NMR analysis and within the NMR tube. Trifluoroacetic anhydride reacts quantitatively at room temperature in chloroform with primary alcohols, as shown in Figure 4.5. This pushes the chemical shifts of the 2 methyl protons closest to the hydroxyl group up from ~3.65 to ~4.4 ppm. The NMR peak assignments used for hydroxyl terminated OB are shown in Figure 4.9A.

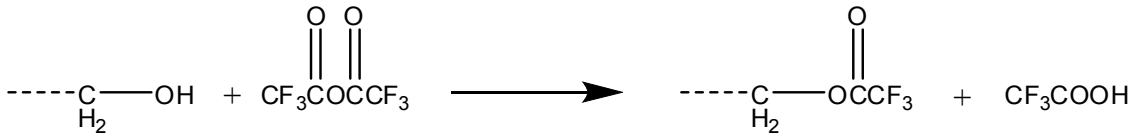

Figure 4.5 Reaction of α-hydroxyl groups with trifluoroacetic anhydride shifts the corresponding methyl protons up to approximately 4.4 ppm.

4.1.3 End-Group Functionalization

The termination step shown in Figure 4.4 results in a hydroxyl group at the end of the PEO chain. The PEO block can be easily functionalized with a variety of different functional groups. A number of different end-group functionalization reactions were attempted on OB block copolymers as we sought for a convenient chemistry for peptide conjugation onto OB block copolymers, including carboxyl end-capping followed by n-hydroxysuccinimide conjugation and thiophenol end-capping followed by native chemical ligation. End-capping with a carboxyl group was easily achieved by reaction with succinic anhydride, as shown in Figure 4.6.[226] A five times excess of purified succinic anhydride was dissolved in a small amount of dry THF and then added to the reactor. As shown in Figure 4.6 only one succinic anhydride was added per chain end. To remove the excess succinic anhydride two extractions against 10% hydrochloric acid solution were rapidly performed before other extractions. The acidic solution hydrolyzes the succinic anhydride making it more water soluble. Carboxyl end-capped OB polymer

was conjugated with peptide ligands by reaction with N-hydroxysuccinimide, followed by conjugation onto a peptide ligand bound to a solid support using standard solid phase peptide synthesis techniques, as described previously.[118,228,229] However, this conjugation procedure gave extremely low yields, was kinetically very slow (requiring many days of reaction with the peptide on the solid support), and did not allow for conjugation of peptides after polymer vesicle formation. So it was forgone for a more novel peptide conjugation scheme utilizing azide-alkyne "click" chemistry.

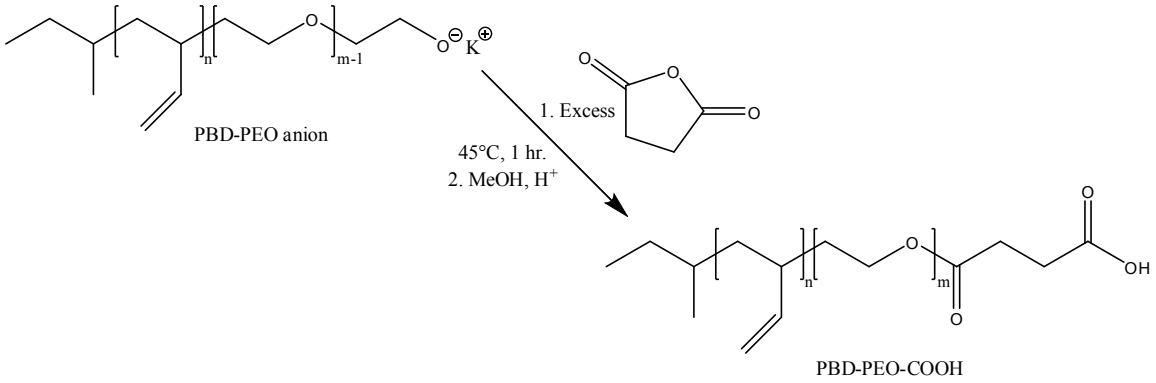

Figure 4.6 Carboxyl end functionalization of OB using succinic anhydride

It was found that an alkyne functional group can also easily be end-capped onto a living OB block copolymer, as shown in Figure 4.7. In similar fashion to carboxyl end functionalization with succinic anhydride, propargyl bromide was added, as purchased, in excess to the living OB chain to terminate the polymerization and end-cap the polymer with an alkyne group. Propargyl bromide was added at 45 °C and allowed to react for 1 h before the OB polymer was recovered and purified as described previously. Alkyne end-group functionalization proceeded quantitatively, as determined by NMR, but for reasons that will be discussed later was not extensively investigated. Instead, azide end-group

functionalized OB was chosen for the "click" chemistry conjugation of peptides onto polymer vesicles.

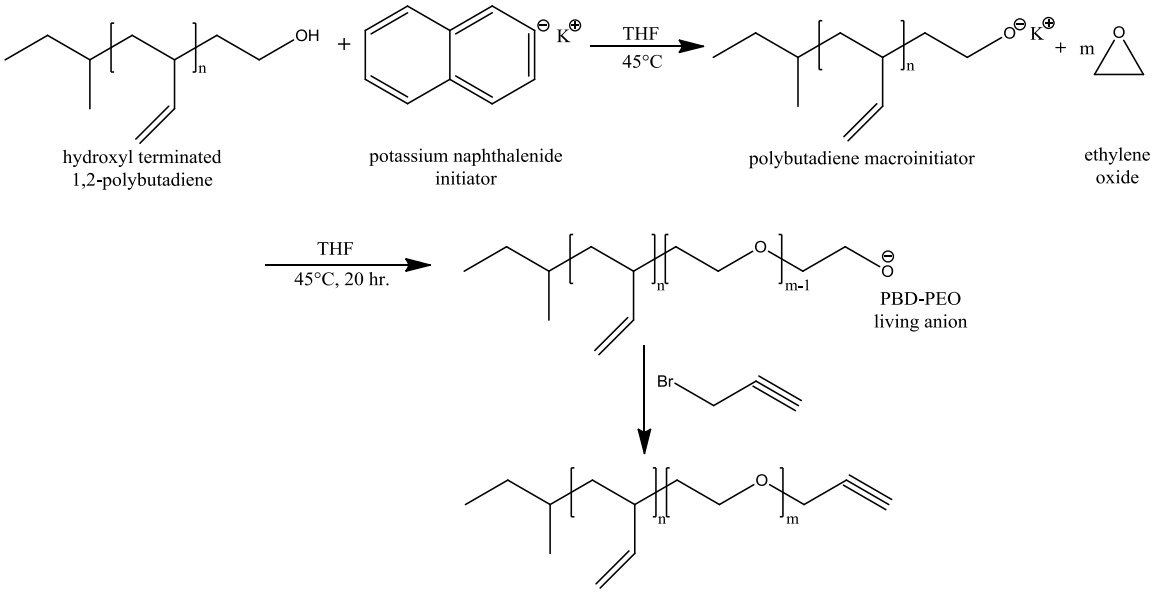

Figure 4.7 Alkyne end functionalization of OB using propargyl bromide

Functionalization of OB with an azide group was achieved through a two step sequential synthesis performed on hydroxyl terminated OB block copolymer. The hydroxyl end group of the OB polymer was replaced with an azide group via mesylation followed by reaction with sodium azide, as shown in Figure 4.8. OB diblock was dissolved in dichloromethane (DCM) at a concentration of 10 mM to which a 5 times excess of triethylamine was added. The solution was cooled to 0 °C, a 2.5 fold excess of methanesulfonyl chloride (mesyl chloride) was added dropwise, and the mixture was stirred overnight at room temperature (RT).[128,129] The resulting mesylated OB polymer, OB polymer with a methanesulfonyl end-group in the place of the hydroxyl end-group, was recovered by rapid washes with cold distilled water, slightly acidic water (10% (v/v)

HCl in distilled water), saturated sodium bicarbonate solution, and finally brine (saturated NaCl solution). Dry polymer was recovered by rotary evaporation, followed by vacuum distillation from a benzene solution.

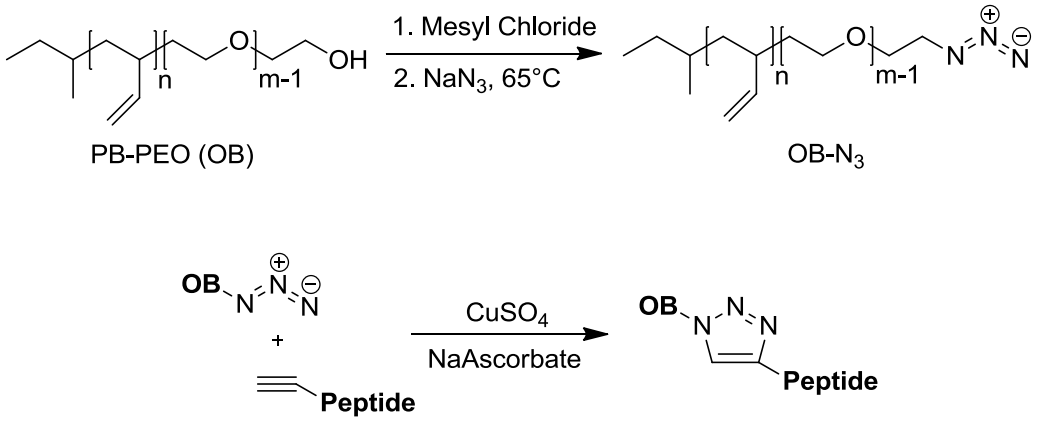

Figure 4.8 Azide end functionalization of OB by mesylation followed by reaction with sodium azide, and the "click" chemistry conjugation of a peptide to azide functionalized OB block copolymer.

In the second step of the synthesis, this mesylated OB polymer was reacted with sodium azide to give azide end-capped OB diblock. All dichloromethane must be rigourously removed from the polymer, as it will readily react with sodium azide to form a potentially explosive compound. Dry mesylated OB was dissolved in N,N-dimethylformamide (DMF) at a concentration of 8 mM and a 3 times excess of sodium azide was added. The reactor was charged with Argon, heated to 65 °C, and stirred overnight. To sequester any unreacted sodium azide before adding DCM a 5 fold excess of 3-bromopropionic acid was added and the reactor stirred overnight. DMF was removed by vacuum distillation at 65 °C, and the resulting polymer was washed and recovered as before. Quantitative addition of the azide end group to form OB-N_3 was confirmed by ^{1}H NMR, as shown in Figure 4.9.

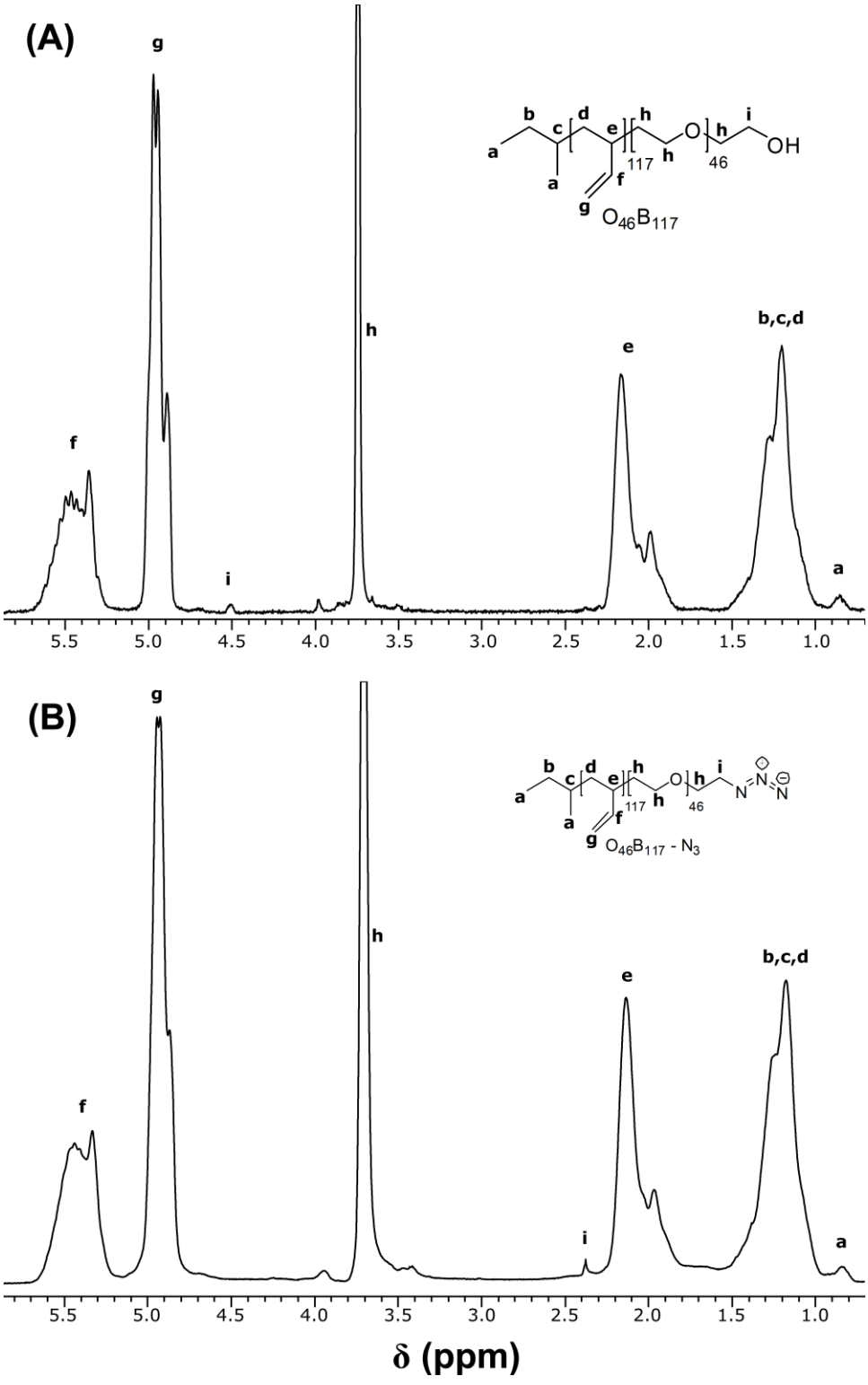

Figure 4.9 ^{1}H NMR spectra of OB (A), and OB-N_3 (B) diblock copolymers in $CDCl_3$ + 1% (v/v) trifluoroacetic anhydride.

4.2 Poly(ethylene oxide)-*b*-poly(γ-methyl-ε-caprolactone) Synthesis

Although further research with poly(ethylene oxide)-b-poly(γ-methyl-ε-caprolactone) (PEO-PMCL or OMCL for short) was not pursued, some preliminary synthetic work was conducted with this polymer. This section records the results of that synthetic work.

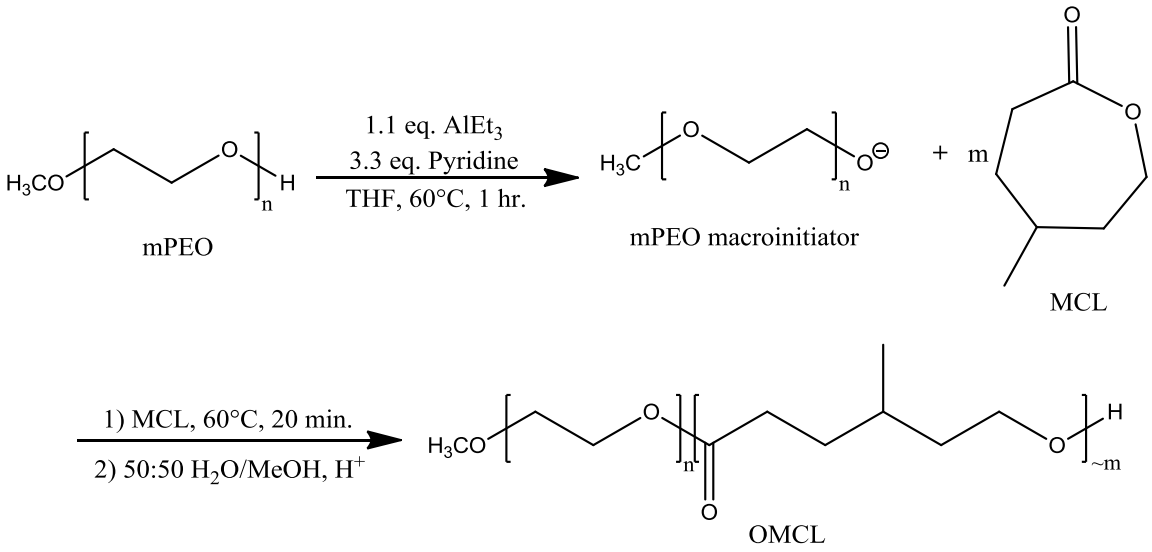

Figure 4.10 Synthetic scheme for the anionic polymerization of OMCL from an α-methyl-poly(ethylene oxide) (mPEO) macroinitiator in tetrahydrofuran (THF) at 60 °C.

OMCL, like the OB block copolymer, is synthesized in a two step process, this time growing the PMCL block off of a PEO macroinitiator, as shown in Figure 4.10. The initial synthesis of this block copolymer was performed primarily following the work of Zupancich et al.[227,230] Alpha-methyl-poly(ethylene oxide), in this case purchased from Sigma Aldrich, was dissolved in benzene and then freeze dried in a high pressure thick walled glass reactor. Tri-ethyl aluminum at a 1.1 fold molar excess along with pyridine at 3.3 fold molar excess was added to deprotonate the hydroxyl PEO chain end, and the reactor was heated to 60 °C. The initiating system was maintained at 60 °C for 1 h to

give all the PEO chains adequate time to initiate, then γ-methyl-ε-caprolactone (MCL) monomer was added and the reaction stirred for 20 minutes at 60 °C. At exactly 20 minutes the reaction was terminated by adding acidic methanol. The reaction must be terminated before reaching 100% conversion to avoid the transesterification reaction which acts to increase PDI. The 20 minute time point was reported to give ~60% conversion at 60 °C in THF, and this was found to hold true experimentally. A polymer close to the desired OMCL polymer was synthesized.

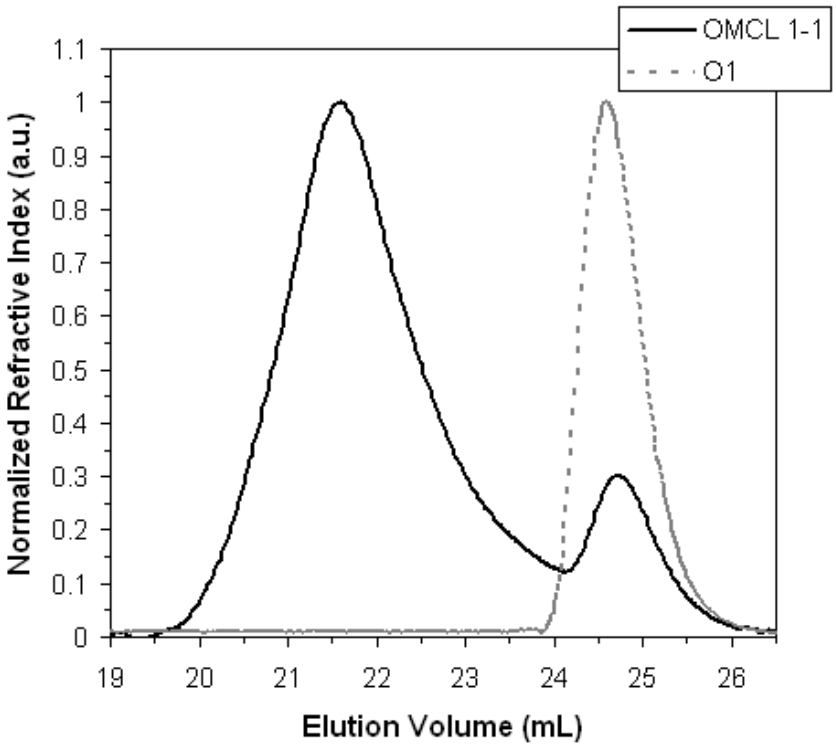

Figure 4.11 Size exclusion chromatography (SEC) elution curves for the precursor PEO polymer (O1) and the OMCL diblock copolymer (OMCL 1-1) synthesized in THF at 60 °C.

However, in our experience these reaction conditions left a significant fraction of the PEO unreacted, as shown by the SEC elution curves in Figure 4.11. Additionally it

was observed, that even upon heating to 60 °C, the PEO homopolymer was not easily dissolved in THF. We suspected that solvation issues, and potentially the formation of small PEO aggregates in THF could be the cause of the unreacted PEO. A literature search revealed similar solvation concerns for this synthesis by the Jérôme research group in Belgium, and corroborated our expectations that dichloromethane (DCM) could be a more suitable solvent for this polymerization.[231–236] The use of DCM, a very good solvent for PEO, also allowed the temperature of the reaction to be lowered and therefore the reaction to be carried out in a more controlled manner, as shown in Figure 4.12.

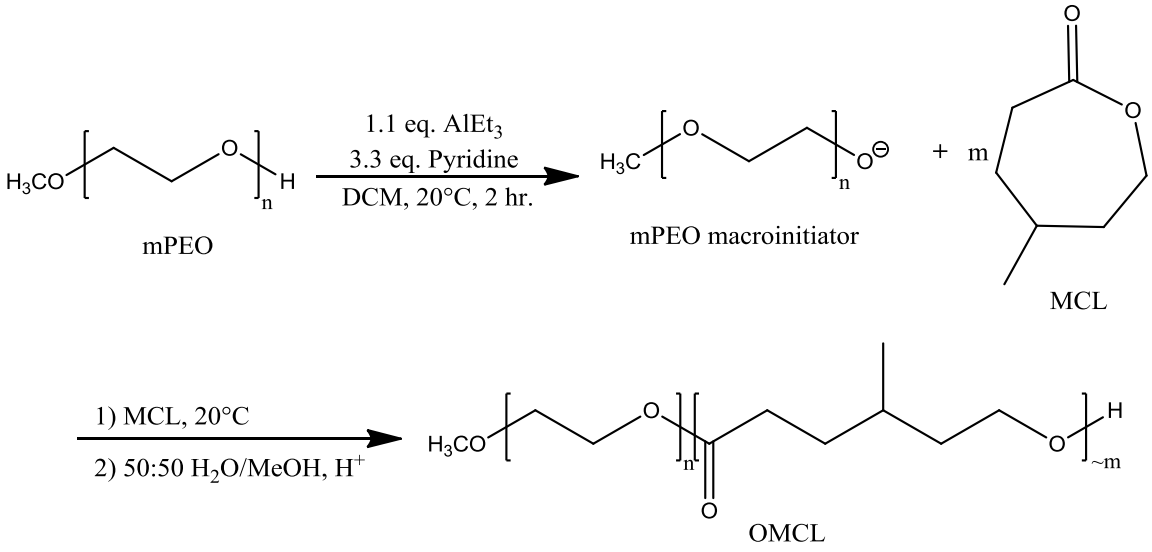

Figure 4.12 Synthetic scheme for the anionic polymerization of OMCL diblock copolymer in dichloromethane (DCM) at 20 °C.

In fact the reaction was slowed down enough that real time tracking of the progress of the reaction could be carried out using NMR. At regular intervals a small aliquot was taken from the reactor and directly analyzed by NMR. Comparing the peak integrals deriving from the monomer (δ 2.56-2.71) to that deriving from the PMCL backbone (δ

2.3) allowed for a simple calculation of percent conversion of the polymerization. Reaction termination at 22-24 h was found to give ~70% conversion of monomer to polymer under these conditions, and more importantly polymerization in a DCM solvent gave essentially uniform polymerization from all PEO macroinitiators, as evidenced by the resulting SEC elution curves shown in Figure 4.13.

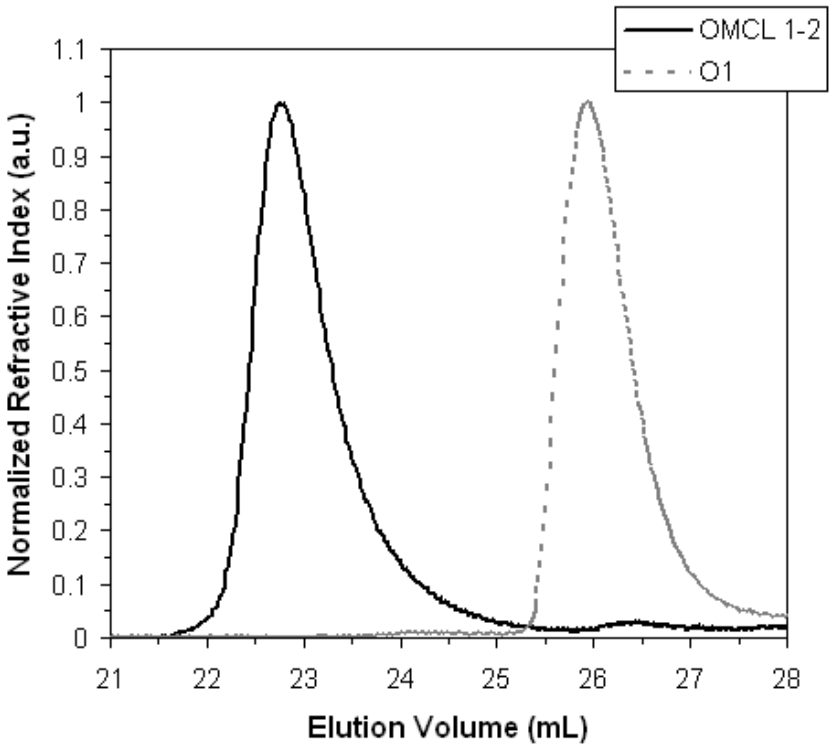

Figure 4.13 Size exclusion chromatography (SEC) elution curves for the precursor PEO polymer (O1) and the OMCL diblock copolymer (OMCL 1-2) synthesized in DCM at 20 °C.

4.3 Peptide Functionalization of Polymer Vesicles

Peptide functionalization of polymer vesicles was achieved by azide-alkyne "click" conjugation of peptides onto pre-formed polymer vesicles. It is thought that conjugation of peptides onto pre-formed polymer vesicles is advantageous to conjugating peptides

onto block copolymers and then attempting to form polymer vesicles in solution. Past evidence indicates that the non-ergodic nature of OB morphology evolution in aqueous solutions allows for polymer vesicles to be predictably formed by a single block copolymer to which multiple different peptide ligands can be conjugated.[48,53] Thus, unexpected morphological shifts deriving from the conjugation of a large peptide, such as PR_b, onto the OB block copolymers can be averted.

The "click" conjugation reaction was carried out as stated in Chapter 3, between azide end-capped OB polymer chains and alkyne end-capped peptides. Azide end-capped OB polymer was synthesized and the click reaction was carried out as shown in Figure 4.8. Alkyne end-capped peptides were synthesized by reaction of the peptide chain, still attached to its solid support with side groups protected, with 4-pentynoic acid using standard FMOC solid phase peptide synthesis chemistry, as detailed in Chapter 2.

The alternate strategy involving conjugation of azide functionalized peptides onto alkyne functionalized OB polymer chains was also attempted. Alkyne end-capped OB polymer was synthesized as shown in Figure 4.7. Azide end-capped peptide was synthesized by addition of 3-bromoproprionic acid to the growing peptide chain on its solid support using standard solid phase peptide synthesis chemistry, followed by cleavage, deprotection, purification, and reaction of the peptide with a slight excess of sodium azide in DMF at 65 °C overnight. Ultimately this route to peptide functionalized polymer vesicles was dropped for a combination of reasons.

Firstly, some evidence of polymer vesicle aggregation was observed when the "click" copper catalyst system was added to aqueous polymer vesicle dispersions of

100% alkyne functionalized OB polymer (lower alkyne functionalization levels were not assessed). A TEM image of alkyne end-capped OB polymer vesicles exposed to the copper catalyst system for over a week is shown in Figure 4.14. One can see how polymer vesicle surfaces seem to be favorably adhering to one another in this image. However, it is unclear how much the concentrating and confinement of these polymer vesicles by TEM sample preparation including blotting is responsible for the close packing of vesicles that is observed.

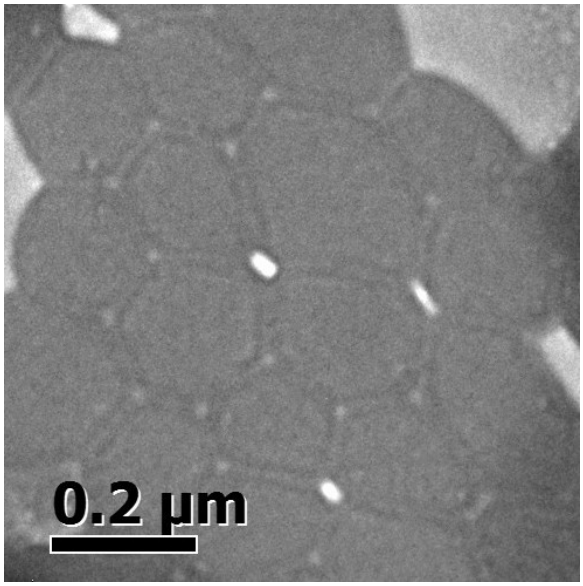

Figure 4.14 Transmission electron microscopy (TEM) image of alkyne end-capped OB polymer vesicles after exposure to the copper catalyst conditions used in "click" chemistry conjugation of peptides.

Alkyne-alkyne homocoupling was one possible explanation for this aggregation behavior, however this was found to be unlikely, given that aggregates could be readily broken up by gentle sonication. Also, more authoritatively OB polymer was recovered from vesicle dispersions before and after addition of the copper catalyst system and run

trough SEC. In this experiment no discernable change in OB block copolymer size was observed.

Secondly, only low peptide conjugation yields were achieved with this conjugation scheme. It is thought that aggregation as well as the hydrophobic alkyne OB end-group not being readily available for reaction at the periphery of the PEO brush layer were the causes for this low yield. Non-optimal "click" chemistry reaction conditions could have also contributed to the low yield, as the reaction conditions were further refined after dropping this peptide conjugation scheme. In particular, the switch from using calcein as the fluorescent vesicle encapsulate to using carboxyfluorescein was later found to be highly advantageous. Calcein is a good ligand for most divalent cations including Cu^{2+}, and readily sequesters copper, thus preventing the copper catalyzed "click" conjugation reaction from proceeding.[237,238]

Because of these difficulties, the conjugation of alkyne end-capped peptides to azide functionalized polymer vesicles was selected. The level of peptide conjugation was quantified by determining both the peptide concentration and the polymer concentration of each polymer vesicle sample.

The concentration of peptide in a polymer vesicle dispersion was assessed fluorescently by way of a fluorescamine assay. Fluorescamine reacts rapidly with any free primary amines in solution to give a fluorescent conjugate (ex/em 390/475 nm). This reaction occurs very rapidly, with a half-life at room temperature of 100-500 ms.[135,136,239] Additionally, fluorescamine decomposes in the presence of water to form non-fluorescent degradation products. The degradation of fluorescamine occurs

somewhat less rapidly than its reaction with free amines, with a half-life of 5-10 s. Thus, upon addition of a large excess of fluorescamine to an aqueous sample fluorescence is generated in proportion to the number of amines in solution.

Because fluorescamine degrades rapidly in the presence of water it was stored in dry acetone. To react with any free primary amines in polymer vesicle samples, this concentrated fluorescamine solution was added rapidly to a small volume of polymer vesicle sample. The exact procedure used is listed in Chapter 2. A total volume of only 100 μl was used to facilitate the rapid mixing that is needed to achieve accuracy with this assay.[134] In addition, because fluorescamine reacts indiscriminately with any free amines, care was taken to not allow outside sources of primary amines other than from the peptide into the sample.

Some small changes to the fluorescamine assay were found to improve its accuracy when analyzing polymer vesicle samples. The inclusion of the surfactant Trition X-100 at a level of at least 5% (v/v) breaks up the polymer vesicles and clarifies the solution. It is not necessary, however when applicable it was found convenient because issues of polymer vesicle buoyancy were not a concern and achieving a homogeneous distribution of fluorescence in the cuvette was simple. Additionally, when a fluorophore was encapsulated within polymer vesicles (e.g. carboxyfluorescein), photobleaching of this fluorophore by exposing the polymer vesicle sample to light for 1 week before reacting with fluorescamine was found to slightly decrease noise in the fluorescamine assay results. Finally, the fluorescence observed from conjugated fluorescamine is somewhat dynamic, increasing in the first ~1 h then decreasing after ~3h. This means that the

fluorescence of fluorescamine should always be measured at the exact same time interval after addition of fluorescamine to the sample (ideally 2 or 2.5 h after addition of the fluorescamine reagent).

The concentration of polymer in each polymer vesicle sample was determined by a simple absorbance assay, as discussed in Chapter 2. Polymer vesicle dispersions are opaque, even after extrusion, and the visible light absorbance of polymer vesicle samples was found to be essentially featureless, decreasing steadily with increasing wavelength. The wavelength of 575 nm was chosen because there was negligible interference from other common constituents in polymer vesicle samples (e.g. carboxyfluorescein, peptides, etc.). The absorbance of polymer vesicles was observed to be essentially independent of size over the admittedly narrow size regime produced by separate extrusions through 200 nm extrusion membranes. The origin of this absorbance is speculated to derive from the condensed region of PEO that forms at the PB interface. It has been shown that while the PEO chains of OB diblock copolymers do form hydrated brushes around polymer vesicles, in a region very near the PEO-PB interface PEO is actually in a condensed state where water is essentially excluded.[113,240] Indeed, even dispersions of polymer micelles formed from OB diblock copolymers, which are only ~10-20 nm in diameter, are seen to be opaque, lending credence to this assertion. A final point concerning the details of conducting this absorbance assay, the dilute polymer vesicle sample was always well mixed and then absorbance measured within 5 minutes of mixing, to ensure a homogeneous sample was measured.

4.4 siRNA Encapsulation within Polymer Vesicles

Relatively high levels of siRNA encapsulation were achieved by forming concentrated dispersions of polymer vesicle and by rigorously protecting siRNA samples from ribonucleases (RNase). siRNA was encapsulated in polymer vesicles by simple film hydration at a relatively high polymer concentration of 5% (w/w). Based on the lyotrophic phase behavior studies of OB diblock copolymer systems it may be possible to go to higher weight percentages of polymer, however at 5% (w/w) the dispersion was already beginning to become noticeably more viscous and extrusion of samples by hand was increasingly difficult.[203,241,242] One potential alternative in this regard may be an alternative method of extrusion, involving passage through hollow fibers.[243]

RNase is ubiquitous; it is on our skin, on surfaces, in our breath, and in dust.[244] In addition, RNase will rapidly degrade any RNA it comes in contact with including siRNA molecules. So that siRNA must be rigorously protected from exposure to RNase. All solutions were either purchased RNase free or treated with diethylpyrocarbonate (DEPC), which degrades active RNase molecules. Treatment with DEPC involved adding 0.1% (v/v) DEPC to an aqueous solution followed by overnight incubation at 37 °C, and then autoclaving. Tubes and pipet tips were purchased RNase free from a reliable source, and pipet tips were filtered. Whenever RNA was being worked with, surfaces were wiped down with a 10% (v/v) bleach solution in milli-Q water, and gloves were regularly changed.

Once siRNA is encapsulated within polymer vesicles we found it to be quite stable, however care must be taken to protect siRNA from RNase when forming the polymer vesicles. The glass vials in which polymer vesicles were formed were tightly capped

with aluminum foil and heated in a kiln to 570 °C. The stir-bars used were washed 3 times each with chloroform, tetrahydrofuran, and RNase free water, then enclosed in a RNase free beaker (kiln heated) with aluminum foil and dried overnight at 250 °C. Any metal instruments (e.g. weighing spatulas and tweezers) used to handle polymer or stir bars were first heated over a flame for ~15 s and allowed to cool before use. siRNA in RNase free water with 5 μM RNAsecure (Ambion) was added to polymer films at a temperature of 60 °C, then immediately stirred for 15 minutes at 60 °C. After this first 15 minutes the temperature was lowered to 45 °C and the polymer vesicle samples were stirred for 2 days at this temperature, before being allowed to cool to room temperature. The RNAsecure enzyme degrades all different types of RNase and begins to be active at ~45 °C, but is optimally active at ~60 °C. These polymer vesicles were again heated to 60 °C for extrusion.

4.5 Cell Viability (MTT) Assay

The optimized experimental procedure for the MTT cell viability assay is recorded in Chapter 3. Here however are some more in depth experimental details concerning the MTT assay.

The MTT assay was conducted on 96-well plates for incubation periods of 24-72 h. These long incubation periods present problems with un-even evaporation from the wells of the plate. Even in the humidified environment of a cell incubator, using plates with lids, evaporation from exterior wells was found to be a significant source of error. This is really a general concern for any plate experiment requiring a long incubation time. To assess the effects of edge evaporation on the MTT assay a simple experiment was run. A

96-well plate was uniformly seeded and treated so that edge effects could be clearly distinguished. Each well was seeded with 5000 MCF10A cells per well in 150 µl DMEM/F12 media with only 2% (v/v) FBS. Cells were incubated at 37 °C, 5% CO_2 for 72 h, then 15 µl of MTT reagent (4.75 mg/ml thiazolyl blue tetrazolium bromide in PBS) was added to each well, and the plate was incubated for 4 h more at 37 °C, 5% CO_2. A solubilizing solution of 75% DMSO:25% H_2O (v/v) plus 5% SDS (w/v) was added to the plate (150 µl per well), and the plate was further incubated, protected from light, for 24 h at R.T. Finally, the plate was shaken gently and the absorbance and background absorbance were measured at 570 nm and 690 nm respectively using a SpectraMax Plus spectrophotometer (Molecular Devices). The results of this simple experiment can be seen in Figure 4.15. From this analysis it was determined that plate edge effects could be significant and the inner 32 wells (C3:F10) were selected and used for all further MTT assays. Exterior wells were filled with sterile PBS, to act as a stopgap for evaporation. For shorter incubation times and depending on the particular assay it is likely that experiments could be conducted utilizing all but the outer most wells, however from this analysis it seems likely that only experiments utilizing very short incubation times (around a few hours) should use the entire plate.

(A)

	1	2	3	4	5	6	7	8	9	10	11	12
A	0.97	1.21	1.15	1.24	1.19	1.06	1.03	1.20	1.19	1.15	1.20	0.91
B	1.15	1.25	1.33	1.20	1.36	1.25	1.34	1.42	1.26	1.21	1.28	1.15
C	1.13	1.21	1.40	1.36	1.33	1.42	1.38	1.35	1.33	1.31	1.19	0.96
D	1.16	1.29	1.47	1.35	1.35	1.37	1.37	1.44	1.33	1.37	1.22	1.11
E	1.22	1.31	1.38	1.36	1.46	1.30	1.39	1.34	1.29	1.29	1.31	1.07
F	1.08	1.24	1.34	1.38	1.34	1.31	1.25	1.34	1.28	1.34	1.21	0.93
G	1.09	1.13	1.25	1.25	1.34	1.23	1.24	1.31	1.36	1.24	1.07	0.97
H	1.01	1.06	1.15	1.14	1.27	1.20	1.14	1.17	1.13	1.07	1.14	0.92

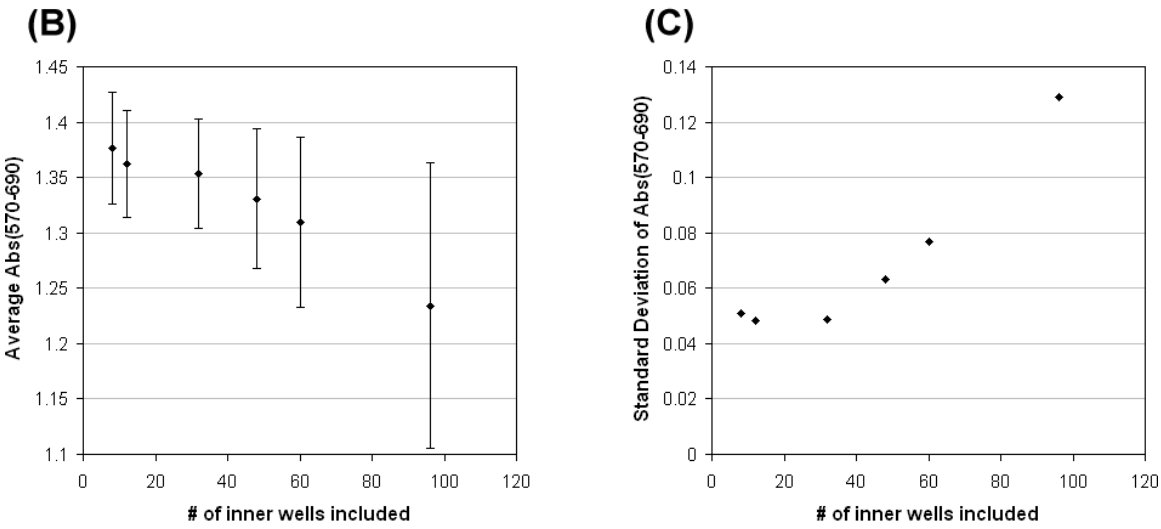

Figure 4.15 Raw MTT data for absorbance (570 – 690) nm from a uniformly treated 96-well plate, with coloration added to illustrate the effects of edge evaporation (green indicating high absorbance and yellow representing low absorbance) (A). The average (B) and standard deviation of (C) absorbance (570 – 690) nm for varying numbers of inner wells included in the analysis. The inner wells averaged over were as follows: 8 wells (D5:E8), 12 wells (D4:E9), 32 wells (C3:F10), 48 wells (B3:G10), 60 wells (B2:G11), 96 wells (A1:H12). Figure (C) simply plots the standard deviations shown as error bars in Figure (B).

The other critical aspect of the MTT assay is the selection of the solubilization solution. A range of different solubilization solutions have been reported in the literature, and we tested a number of these ourselves.[245–249] MCF10A cells were seeded at a range

of different initial cells per well and incubated for 24 h at 37 °C, 5% CO_2. The MTT reagent was added as before and cells were further incubated for 4 h at 37 °C, 5% CO_2, after which varying solubilization solutions were added to the wells (150 µl per well). MTT absorbance was measured at a range of time points and wavelengths and the performance of each solubilization solution was compared. The optimal wavelength was found to be 570 nm with a background subtraction at 690 nm. For all time points two solubilization solutions preformed best, 75% DMSO (dimethyl sulfoxide) + 25% milli-Q water (v/v) + 5% SDS (w/v), and 50% DMF (n,n-dimethylformamide) + 50% milli-Q water (v/v) + 20% SDS (w/v), 0.1 M HCl. The best results were obtained at a 24 h time point after adding the solubilization solution, and this data is shown in Figure 4.16. Because the DMSO based solubilization solution gave slightly more linear results with slightly less variability, and because it was more convenient to prepare, it was chosen for use in future MTT assays. An experimental detail that was learned is that because these solutions contain surfactants they tend to form bubbles when pipetted and these bubbles can be long lasting. Therefore it was found to be advantageous to not "push out" the tiny volume that remained at the very tip of the pipets when adding these solubilization solutions to the wells. Finally, it should be noted that the MTT assay can be oversaturated by including too many cells per well. For the optimized procedure discussed here saturation was found to be reached at ~50,000 cells per well, however whenever possible it is best to operate far below this limit.

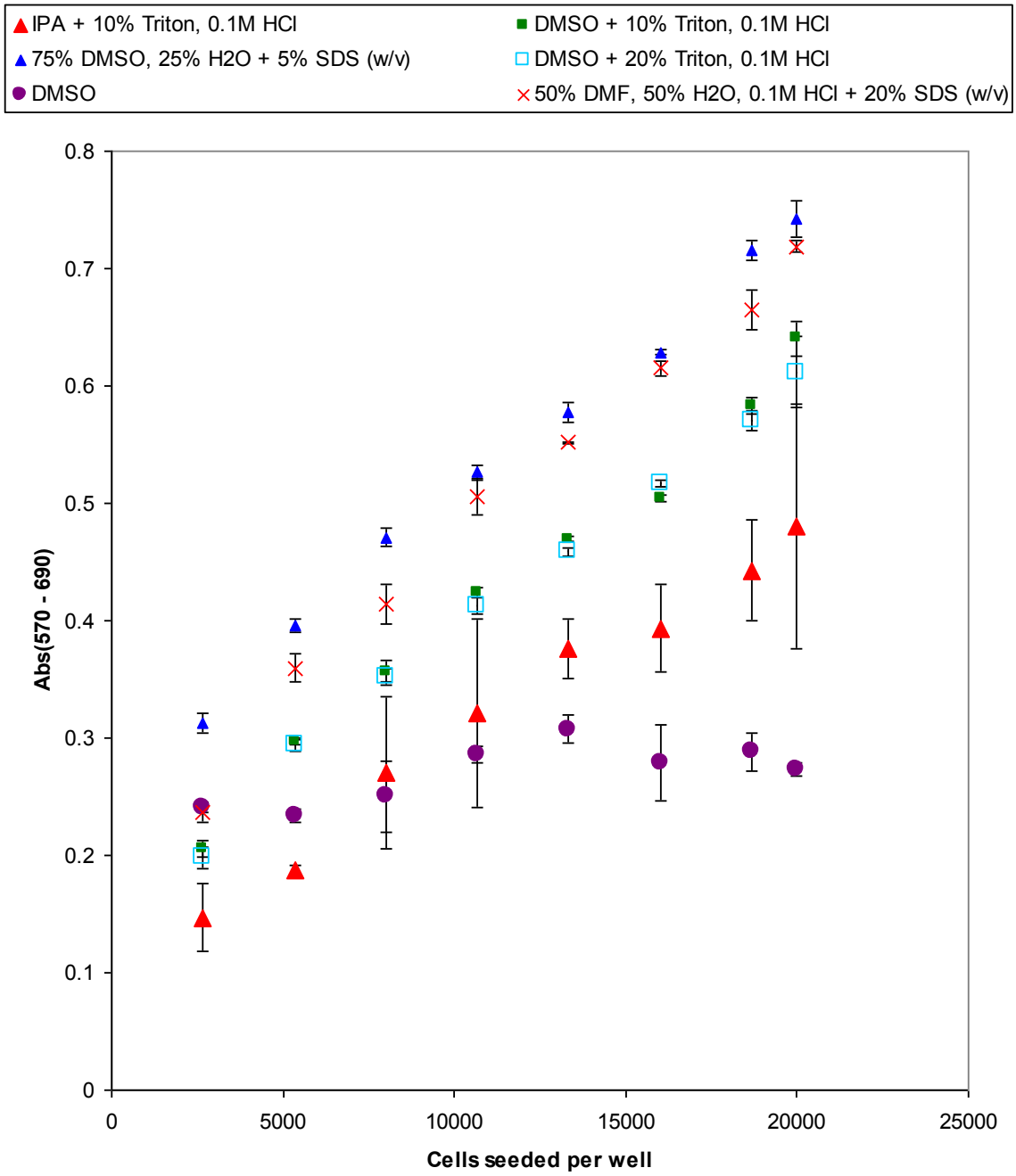

Figure 4.16 Comparison of the performance of different solubilization solutions in the MTT assay.

It was found that a small amount of background absorbance, not accounted for by subtracting the absorbance at 690 nm, deriving from the OB polymer in each well. This was accounted for by running a comparable assay (same incubation times, same solubilization solution) without cells but with polymer vesicles at varying concentrations. From this control experiment the background absorbance deriving from the OB block copolymer itself could be subtracted out of the MTT assay results before cell viability was calculated. This was observed to be a small, but noticeable effect.

Many other cell viability and cytotoxicity assays exist in addition to the MTT assay. The sulforhodamine B (SRB) assay was also tried, and the MTT assay was found to be far superior, mainly due to the fact that washing is not required in the MTT assay.[250,251] There are also a host of other "second generation" MTT-like assays (e.g. WST, XTT, MTS) that do not require the use of a solubilization solution because the formazan dye that is formed is water soluble. These would likely be more convenient and perform as well as, if not better, than the MTT assay, however they are significantly more expensive.

5 Conclusion

Polymer vesicles functionalized with PR_b targeting peptides via "click" chemistry are effective targeted drug delivery vectors. The azide-alkyne "click" Huisgen cycloaddition reaction was demonstrated to be a robust and versatile conjugation reaction for the functionalization of polymer vesicles with targeting ligands. Polymersomes functionalized with the PR_b targeting peptide were shown to bind and internalize effectively into colon and breast cancer cells. In all cases tested PR_b functionalized polymer vesicles were found to outperform GRGDSP functionalized and non-functionalized polymer vesicles, both in terms of delivery efficacy and specificity, as shown by anti-$\alpha_5\beta_1$ blocking studies and delivery to minimally $\alpha_5\beta_1$ expressing cells. Additionally, peptide funcitionalized polymer vesicles were demonstrated to release the chemotherapeutic drug doxorubicin effectively and allow for at least limited release of more hydrophilic encapsulants such as siRNA.

Future improvement to polymer vesicle drug delivery systems might include polymer vesicles that can more rapidly release upon internalization within an endosome or lysosome. An attractive route to this release is disulfide bond breakage, because as opposed to polymer degradation as a release mechanism it should be orders of magnitude more rapid since it involves the catalyzed breakage of only a single bond rather than the breakage of many bonds.[217,252–254] To allow for surface availiability of the disulfide bonds and avoid steric hinderance to their intracellular cleavage it may be advantageous to install them within the length of the PEO block of the polymer vesicle forming

diblock. Then when the disulfide bond is broken the bilayer morphology would likely become unstable and collapse, realeasing the vesicle encapsulates.

6 References

(1) Winau, F.; Westphal, O.; Winau, R. *Microbes Infect.* **2004**, *6*, 786-789.

(2) Ehrlich, P. *Münch. Med. Wschr.* **1901**, *18*, 2123-2124.

(3) Matsumura, Y.; Maeda, H. *Cancer Res.* **1986**, *46*, 6387-6392.

(4) Folkman, J. *Nat. Med.* **1995**, *1*, 27-30.

(5) Skinner, S. A.; Tutton, P. J. M.; O'Brien, P. E. *Cancer Res.* **1990**, *50*, 2411-2417.

(6) Maeda, H.; Wu, J.; Sawa, T.; Matsumura, Y.; Hori, K. *J. Control. Release* **2000**, *65*, 271-284.

(7) Maeda, H.; Sawa, T.; Konno, T. *J. Control. Release* **2001**, *74*, 47-61.

(8) Iyer, A. K.; Khaled, G.; Fang, J.; Maeda, H. *Drug Discov. Today* **2006**, *11*, 812-818.

(9) Noguchi, Y.; Wu, J.; Duncan, R.; Strohalm, J.; Ulbrich, K.; Akaike, T.; Maeda, H. *Cancer Sci.* **1998**, *89*, 307-314.

(10) Stroh, M.; Zimmer, J. P.; Duda, D. G.; Levchenko, T. S.; Cohen, K. S.; Brown, E. B.; Scadden, D. T.; Torchilin, V. P.; Bawendi, M. G.; Fukumura, D.; Jain, R. K. *Nat. Med.* **2005**, *11*, 678-682.

(11) Maeda, H. *Adv. Drug Delivery Rev.* **2001**, *46*, 169-185.

(12) Yuan, F.; Dellian, M.; Fukumura, D.; Leunig, M.; Berk, D. A.; Torchilin, V. P.; Jain, R. K. *Cancer Res.* **1995**, *55*, 3752-3756.

(13) Brigger, I.; Dubernet, C.; Couvreur, P. *Adv. Drug Delivery Rev.* **2002**, *54*, 631-651.

(14) Lasic, D. D.; Needham, D. *Chem. Rev.* **1995**, *95*, 2601-2628.

(15) Oku, N. *Adv. Drug Delivery Rev.* **1999**, *40*, 63-73.

(16) Woodle, M. C.; Matthay, K. K.; Newman, M. S.; Hidayat, J. E.; Collins, L. R.; Redemann, C.; Martin, F. J.; Papahadjopoulos, D. *Biochim. Biophys. Acta, Biomembr.* **1992**, *1105*, 193-200.

(17) Woodle, M. C. *Chem. Phys. Lipids* **1993**, *64*, 249-262.

(18) Photos, P. J.; Bacakova, L.; Discher, B.; Bates, F. S.; Discher, D. E. *J. Control. Release* **2003**, *90*, 323-334.

(19) Huang, S. K.; Mayhew, E.; Gilani, S.; Lasic, D. D.; Martin, F. J.; Papahadjopoulos, D. *Cancer Res.* **1992**, *52*, 6774-81.

(20) Unezaki, S. *Int. J. Pharm.* **1995**, *126*, 41-48.

(21) Gabizon, A.; Catane, R.; Uziely, B.; Kaufman, B.; Safra, T.; Cohen, R.; Martin, F.; Huang, A.; Barenholz, Y. *Cancer Res.* **1994**, *54*, 987-992.

(22) Chang, C. W.; Barber, L.; Ouyang, C.; Masin, D.; Bally, M. B.; Madden, T. D. *British J. Cancer* **1997**, *75*, 169-77.

(23) Sadzuka, Y.; Hirotsu, S.; Hirota, S. *Cancer Lett.* **1998**, *127*, 99-106.

(24) Lu, W.-L.; Qi, X.-R.; Zhang, Q.; Li, R.-Y.; Wang, G.-L.; Zhang, R.-J.; Wei, S.-L. *J. Pharm. Sci.* **2004**, *95*, 381-9.

(25) Gabizon, A.; Chemla, M.; Tzemach, D.; Horowitz, A. T.; Goren, D. *J. Drug Targeting* **1996**, *3*, 391-8.

(26) Mayer, L. D.; Dougherty, G.; Harasym, T. O.; Bally, M. B. *J. Pharm. Exp. Ther.* **1997**, *280*, 1406-14.

(27) Parr, M. J.; Masin, D.; Cullis, P. R.; Bally, M. B. *J. Pharm. Exp. Ther.* **1997**, *280*, 1319-27.

(28) Hong, R. L.; Huang, C. J.; Tseng, Y. L.; Pang, V. F.; Chen, S. T.; Liu, J. J.; Chang, F. H. *Clin. Cancer Res.* **1999**, *5*, 3645-52.

(29) Drummond, D. C.; Meyer, O.; Hong, K.; Kirpotin, D. B.; Papahadjopoulos, D. *Pharmacol. Rev.* **1999**, *51*, 691-744.

(30) Cheng, Z.; Tsourkas, A. *Langmuir* **2008**, *24*, 8169-8173.

(31) Liu, G.; Ma, S.; Li, S.; Cheng, R.; Meng, F.; Liu, H.; Zhong, Z. *Biomaterials* **2010**, *31*, 7575-85.

(32) Binder, W. H.; Sachsenhofer, R. *Macromol. Rapid Comm.* **2008**, *29*, 1097-1103.

(33) Marsden, H. R.; Quer, C. B.; Sanchez, E. Y.; Gabrielli, L.; Jiskoot, W.; Kros, A. *Biomacromolecules* **2010**, *11*, 833-838.

(34) Ahmed, F.; Pakunlu, R. I.; Brannan, A.; Bates, F.; Minko, T.; Discher, D. E. *J. Control. Release* **2006**, *116*, 150-158.

(35) Parnell, A. J.; Tzokova, N.; Topham, P. D.; Adams, D. J.; Adams, S.; Fernyhough, C. M.; Ryan, A. J.; Jones, R. A. L. *Faraday Disc.* **2009**, *143*, 29-46.

(36) Binder, W. H.; Sachsenhofer, R.; Farnik, D.; Blaas, D. *Phys. Chem. Chem. Phys.* **2007**, *9*, 6435-6441.

(37) Krack, M.; Hohenberg, H.; Kornowski, A.; Lindner, P.; Weller, H.; Förster, S. *J. Am. Chem. Soc.* **2008**, *130*, 7315-7320.

(38) Ghoroghchian, P. P.; Lin, J. J.; Brannan, A. K.; Frail, P. R.; Bates, F. S.; Therien, M. J.; Hammer, D. A. *Soft Matter* **2006**, *2*, 973-980.

(39) Mueller, W.; Koynov, K.; Fischer, K.; Hartmann, S.; Pierrat, S.; Basché, T.; Maskos, M. *Macromolecules* **2008**, *42*, 357-361.

(40) Mai, Y.; Eisenberg, A. *J. Am. Chem. Soc.* **2010**, *132*, 10078-10084.

(41) Battaglia, G.; Ryan, A. J.; Tomas, S. *Langmuir* **2006**, *22*, 4910-4913.

(42) Mecke, A.; Dittrich, C.; Meier, W. *Soft Matter* **2006**, *2*, 751-759.

(43) Carlsen, A.; Glaser, N.; Le Meins, J.-F.; Lecommandoux, S. *Langmuir* **2011**, *27*, 4884-4890.

(44) Discher, B. M.; Won, Y. Y.; Ege, D. S.; Lee, J. C. M.; Bates, F. S.; Discher, D. E.; Hammer, D. A. *Science* **1999**, *284*, 1143-1146.

(45) Jain, S.; Bates, F. S. *Science* **2003**, *300*, 460-464.

(46) Jain, S. Aqueous Mixtures of Block Copolymer Surfactants. *Department of Chemical Engineering and Material Science* **2005**, 334.

(47) Halperin, A. *Macromolecules* **1987**, *20*, 2943-2946.

(48) Zupancich, J. A.; Bates, F. S.; Hillmyer, M. A. *Biomacromolecules* **2009**, *10*, 1554-1563.

(49) Petersen, M. A.; Yin, L.; Kokkoli, E.; Hillmyer, M. A. *Polymer Chem.* **2010**, *1*, 1281-1290.

(50) Christian, N. A.; Milone, M. C.; Ranka, S. S.; Li, G.; Frail, P. R.; Davis, K. P.; Bates, F. S.; Therien, M. J.; Ghoroghchian, P. P.; June, C. H.; Hammer, D. A. *Bioconjugate Chem.* **2007**, *18*, 31-40.

(51) Pang, Z.; Lu, W.; Gao, H.; Hu, K.; Chen, J.; Zhang, C.; Gao, X.; Jiang, X.; Zhu, C. *J. Control. Release* **2008**, *128*, 120-7.

(52) Pangburn, T. O.; Bates, F. S.; Kokkoli, E. *Soft Matter* **2012**, *8*, 4449-4461.

(53) Jain, S.; Bates, F. S. *Macromolecules* **2004**, *37*, 1511-1523.

(54) Won, Y. Y.; Davis, H. T.; Bates, F. S. *Macromolecules* **2003**, *36*, 953-955.

(55) Discher, D. E.; Ahmed, F. *Annu. Rev. Biomed. Eng.* **2006**, *8*, 323-341.

(56) Pata, V.; Ahmed, F.; Discher, D. E.; Dan, N. *Langmuir* **2004**, *20*, 3888-3893.

(57) Hamersky, M. W.; Tirrell, M.; Lodge, T. P. *J. Polymer Sci. B: Polymer Phys.* **1996**, *34*, 2899-2909.

(58) Hamersky, M. W.; Tirrell, M.; Lodge, T. P. *Langmuir* **1998**, *14*, 6974-6979.

(59) Pankov, R. *J. Cell Sci.* **2002**, *115*, 3861-3863.

(60) Hynes, R. O. *Science* **2009**, *326*, 1216-9.

(61) Singh, P.; Carraher, C.; Schwarzbauer, J. E. *Ann. Rev. Cell Devel. Bio.* **2010**, *26*, 397-419.

(62) Aota, S.; Nomizu, M.; Yamada, K. M. *J. Biol. Chem.* **1994**, *269*, 24756-24761.

(63) Redick, S. D.; Settles, D. L.; Briscoe, G.; Erickson, H. P. *J. Cell Biol.* **2000**, *149*, 521-527.

(64) Engel, J.; Odermatt, E.; Engel, A.; Madri, J. A.; Furthmayr, H.; Rohde, H.; Timpl, R. *J. Mol. Bio.* **1981**, *150*, 97-120.

(65) Altroff, H.; Choulier, L.; Mardon, H. J. *J. Biol. Chem.* **2003**, *278*, 491-497.

(66) Leahy, D. J.; Aukhil, I.; Erickson, H. P. *Cell* **1996**, *84*, 155-164.

(67) Main, A. L.; Harvey, T. S.; Baron, M.; Boyd, J.; Campbell, I. D. *Cell* **1992**, *71*, 671-678.

(68) Sechler, J. L.; Takada, Y.; Schwarzbauer, J. E. *J. Cell Biol.* **1996**, *134*, 573-583.

(69) Sottile, J.; Hocking, D.; Langenbach, K. *J. Cell Sci.* **2000**, *113*, 4287-4299.

(70) Danen, E. H. J.; Sonneveld, P.; Brakebusch, C.; Fassler, R.; Sonnenberg, A. *J. Cell Biol.* **2002**, *159*, 1071-86.

(71) Huveneers, S.; Truong, H.; Fässler, R.; Sonnenberg, A.; Danen, E. H. J. *J. Cell Sci.* **2008**, *121*, 2452-2462.

(72) Geiger, B.; Bershadsky, A.; Pankov, R.; Yamada, K. M. *Nature Rev. Mol. Cell Biol.* **2001**, *2*, 793-805.

(73) Li, Z.; Kreiner, M.; van der Walle, C. F.; Mardon, H. J. *Biochem. Biophys. Res. Comm.* **2011**, *407*, 777-82.

(74) Kreiner, M.; Li, Z.; Beattie, J.; Kelly, S. M.; Mardon, H. J.; van der Walle, C. F. *Protein Eng. Design Selection* **2008**, *21*, 553-60.

(75) Ruoslahti, E. *Annu. Rev. Cell Dev. Biol.* **1996**, *12*, 697-715.

(76) Hersel, U.; Dahmen, C.; Kessler, H. *Biomaterials* **2003**, *24*, 4385-4415.

(77) Pasqualini, R.; Koivunen, E.; Ruoslahti, E. *Nature Biotech.* **1997**, *15*, 542-6.

(78) Petrie, T. A.; Capadona, J. R.; Reyes, C. D.; Garcia, A. J. *Biomaterials* **2006**, *27*, 5459-5470.

(79) Dillow, A. K.; Ochsenhirt, S. E.; McCarthy, J. B.; Fields, G. B.; Tirrell, M. *Biomaterials* **2001**, *22*, 1493-1505.

(80) Kokkoli, E.; Ochsenhirt, S. E.; Tirrell, M. *Langmuir* **2004**, *20*, 2397-2404.

(81) Kao, W. J.; Lee, D.; Schense, J. C.; Hubbell, J. A. *J. Biomed. Mat. Res.* **2001**, *55*, 79-88.

(82) Hojo, K.; Susuki, Y.; Maeda, M.; Okazaki, I.; Nomizu, M.; Kamada, H.; Yamamoto, Y.; Nakagawa, S.; Mayumi, T.; Kawasaki, K. *Bioorg. Med. Chem. Lett.* **2001**, *11*, 1429-1432.

(83) Aucoin, L.; Griffith, C. M.; Pleizier, G.; Deslandes, Y.; Sheardown, H. *J. Biomat. Sci.-Poly. Ed.* **2002**, *13*, 447-462.

(84) Kao, W. J. *Biomaterials* **1999**, *20*, 2213-2221.

(85) Kim, T. I.; Jang, J. H.; Lee, Y. M.; Ryu, I. C.; Chung, C. P.; Han, S. B.; Choi, S. M.; Ku, Y. *Biotechnol. Lett.* **2002**, *24*, 2029-2033.

(86) Benoit, D. S. W.; Anseth, K. S. *Biomaterials* **2005**, *26*, 5209-5220.

(87) Ochsenhirt, S. E.; Kokkoli, E.; McCarthy, J. B.; Tirrell, M. *Biomaterials* **2006**, *27*, 3863-3874.

(88) Mardilovich, A.; Kokkoli, E. *Biomacromolecules* **2004**, *5*, 950-957.

(89) Mardilovich, A.; Craig, J. A.; McCammon, M. Q.; Garg, A.; Kokkoli, E. *Langmuir* **2006**, *22*, 3259-3264.

(90) Craig, J. A.; Rexeisen, E. L.; Mardilovich, A.; Shroff, K.; Kokkoli, E. *Langmuir* **2008**, *24*, 10282-10292.

(91) Garg, A.; Tisdale, A. W.; Haidari, E.; Kokkoli, E. *Int. J. Pharm.* **2009**, *366*, 201-210.

(92) Demirgöz, D.; Garg, A.; Kokkoli, E. *Langmuir* **2008**, *24*, 13518-13524.

(93) Garg, A.; Kokkoli, E. *Curr. Pharm. Biotechnol.* **2011**, *12*, 1135-1143.

(94) Atchison, N. A.; Fan, W.; Papas, K. K.; Hering, B. J.; Tsapatsis, M.; Kokkoli, E. *Langmuir* **2010**, *26*, 14081-14088.

(95) Varner, J. A.; Cheresh, D. A. *Curr. Opin. Cell Biol.* **1996**, *8*, 724-730.

(96) van Golen, K. L.; Bao, L. W.; Brewer, G. J.; Pienta, K. J.; Kamradt, J. M.; Livant, D. L.; Merajver, S. D. *Neoplasia* **2002**, *4*, 373-379.

(97) Kim, S.; Bell, K.; Mousa, S. A.; Varner, J. A. *Am. J. Pathol.* **2000**, *156*, 1345-1362.

(98) Gong, J.; Wang, D.; Sun, L.; Zborowska, E.; Willson, J. K.; Brattain, M. G. *Cell Growth Differ.* **1997**, *8*, 83-90.

(99) Jayne, D. G.; Heath, R. M.; Dewhurst, O.; Scott, N.; Guillou, P. J. *Eur. J. Surg. Oncol.* **2002**, *28*, 30-36.

(100) Ellis, L. M. *Am. Surgeon* **2003**, *69*, 3-10.

(101) Jia, Y.; Zeng, Z.-Z.; Markwart, S. M.; Rockwood, K. F.; Ignatoski, K. M. W.; Ethier, S. P.; Livant, D. L. *Cancer Res.* **2004**, *64*, 8674-8681.

(102) Juhua, C.; De, S.; Brarnard, J.; Byzova, T. V. *Cell Commun. Adhes.* **2004**, *11*, 1-11.

(103) Muschler, J.; Horwitz, A. *Development* **1991**, *113*, 327-337.

(104) Maglott, A.; Bartik, P.; Cosgun, S.; Klotz, P.; Ronde, P.; Fuhrmann, G.; Takeda, K.; Martin, S.; Dontenwill, M. *Cancer Res.* **2006**, *66*, 6002-6007.

(105) Takenaka, K.; Shibuya, M.; Takeda, Y.; Hibino, S.; Gemma, A.; Ono, Y.; Kudoh, S. *Int. J. Oncol.* **2000**, *17*, 1187.

(106) Dingemans, A.-M. C.; van den Boogaart, V.; Vosse, B. A.; van Suylen, R.-J.; Griffioen, A. W.; Thijssen, V. L. *Mol. Cancer* **2010**, *9*, 152.

(107) Muller, P. A. J.; Caswell, P. T.; Doyle, B.; Iwanicki, M. P.; Tan, E. H.; Karim, S.; Lukashchuk, N.; Gillespie, D. A.; Ludwig, R. L.; Gosselin, P.; Cromer, A.; Brugge, J. S.; Sansom, O. J.; Norman, J. C.; Vousden, K. H. *Cell* **2009**, *139*, 1327-1341.

(108) Pangburn, T. O.; Petersen, M. A.; Waybrant, B.; Adil, M. M.; Kokkoli, E. *J. Biomech. Eng.* **2009**, *131*, 74005.

(109) Discher, D. E.; Ortiz, V.; Srinivas, G.; Klein, M. L.; Kim, Y.; Christian, D.; Cai, S.; Photos, P.; Ahmed, F. *Prog. Polym. Sci.* **2007**, *32*, 838-857.

(110) Meng, F.; Zhong, Z.; Feijen, J. *Biomacromolecules* **2009**, *10*, 197-209.

(111) Kita-Tokarczyk, K.; Grumelard, J.; Haefele, T.; Meier, W. *Polymer* **2005**, *46*, 3540-3563.

(112) Battaglia, G.; Ryan, A. J. *J. Am. Chem. Soc.* **2005**, *127*, 8757-8764.

(113) Won, Y. Y.; Davis, H. T.; Bates, F. S.; Agamalian, M.; Wignall, G. D. *J. Phys. Chem. B* **2000**, *104*, 7134-7143.

(114) Lee, J. C.-M.; Bermudez, H.; Discher, B. M.; Sheehan, M. A.; Won, Y.-Y.; Bates, F. S.; Discher, D. E. *Biotechnol. Bioeng.* **2001**, *73*, 135-145.

(115) Lomas, H.; Canton, I.; MacNeil, S.; Du, J.; Armes, S. P.; Ryan, A. J.; Lewis, A. L.; Battaglia, G. *Adv. Mater.* **2007**, *19*, 4238-4243.

(116) Jain, J. P.; Kumar, N. *Biomacromolecules* **2010**, *11*, 1027-1035.

(117) Won, Y.-Y.; Brannan, A. K.; Davis, H. T.; Bates, F. S. *J. Phys. Chem. B* **2002**, *106*, 3354-3364.

(118) Demirgöz, D.; Pangburn, T. O.; Davis, K. P.; Lee, S.; Bates, F. S.; Kokkoli, E. *Soft Matter* **2009**, *5*, 2011-2019.

(119) Upadhyay, K. K.; Bhatt, A. N.; Mishra, A. K.; Dwarakanath, B. S.; Jain, S.; Schatz, C.; Le Meins, J.-F.; Farooque, A.; Chandraiah, G.; Jain, A. K.; Misra, A.; Lecommandoux, S. *Biomaterials* **2010**, *31*, 2882-2892.

(120) Ahmed, F.; Pakunlu, R. I.; Srinivas, G.; Brannan, A.; Bates, F.; Klein, M. L.; Minko, T.; Discher, D. E. *Mol. Pharmaceutics* **2006**, *3*, 340-350.

(121) Ben-Haim, N.; Broz, P.; Marsch, S.; Meier, W.; Hunziker, P. *Nano Lett.* **2008**, *8*, 1368-1373.

(122) Broz, P.; Benito, S. M.; Saw, C.; Burger, P.; Heider, H.; Pfisterer, M.; Marsch, S.; Meier, W.; Hunziker, P. *J. Control. Release* **2005**, *102*, 475-488.

(123) Broz, P.; Ben-Haim, N.; Grzelakowski, M.; Marsch, S.; Meier, W.; Hunziker, P. *J. Cardiovasc. Pharmacol.* **2008**, *51*, 246-252.

(124) Kokkoli, E.; Mardilovich, A.; Wedekind, A.; Rexeisen, E. L.; Garg, A.; Craig, J. A. *Soft Matter* **2006**, *2*, 1015-1024.

(125) Garcia, A. J.; Schwarzbauer, J. E.; Boettiger, D. *Biochemistry* **2002**, *41*, 9063-9069.

(126) Kim, S.; Harris, M.; Varner, J. A. *J. Biol. Chem.* **2000**, *275*, 33920-33928.

(127) Hillmyer, M. A.; Bates, F. S. *Macromolecules* **1996**, *29*, 6994-7002.

(128) Crossland, R. K.; Servis, K. L. *J. Org. Chem.* **1970**, *35*, 3195-3196.

(129) Chen, G.; Tao, L.; Mantovani, G.; Ladmiral, V.; Burt, D. P.; Macpherson, J. V.; Haddleton, D. M. *Soft Matter* **2007**, *3*, 732-739.

(130) Rostovtsev, V. V.; Green, L. G.; Fokin, V. V.; Sharpless, K. B. *Angew. Chem., Int. Edit.* **2002**, *41*, 2596-2599.

(131) Lewis, W. G.; Magallon, F. G.; Fokin, V. V.; Finn, M. G. *J. Am. Chem. Soc.* **2004**, *126*, 9152-9153.

(132) Gupta, S. S.; Kuzelka, J.; Singh, P.; Lewis, W. G.; Manchester, M.; Finn, M. G. *Bioconjugate Chem.* **2005**, *16*, 1572-1579.

(133) Rodionov, V. O.; Presolski, S. I.; Díaz Díaz, D.; Fokin, V. V.; Finn, M. G. *J. Am. Chem. Soc.* **2007**, *129*, 12705-12712.

(134) Castell, J. V.; Cervera, M.; Marco, R. *Analytical Biochem.* **1979**, *99*, 379-391.

(135) Udenfriend, S.; Stein, S.; Bohlen, P.; Dairman, W.; Leimgruber, W.; Weigele, M. *Science* **1972**, *178*, 871-872.

(136) Viets, J. W.; Deen, W. M.; Troy, J. L.; Brenner, B. M. *Analytical Biochem.* **1978**, *88*, 513-521.

(137) Garg, A.; Kokkoli, E. Targeted drug delivery and enhanced intracellular release using functionalized liposomes. *Material Science and Engineering* **2009**.

(138) Haran, G.; Cohen, R.; Bar, L. K.; Barenholz, Y. *Biochim. Biophys. Acta, Biomembr.* **1993**, *1151*, 201-215.

(139) Bolotin, E. M.; Cohen, R.; Bar, L. K.; Emanuel, N.; Ninio, S.; Barenholz, Y.; Lasic, D. D. *J. Liposome Res.* **1994**, *4*, 455-479.

(140) Lambert, J. B.; Sherwell, H. F.; Lightner, D. A.; Cooks, R. G. *Organic Structural Spectroscopy*; Simon & Schuster: New Jersey, 1998.

(141) Woodle, M. C.; Lasic, D. D. *Biochim. Biophys. Acta, Rev. Biomembr.* **1992**, *1113*, 171-199.

(142) Napper, D. H. *J. Colloid Interface Sci.* **1977**, *58*, 390-407.

(143) Alcantar, N. A.; Aydil, E. S.; Israelachvili, J. N. *J. Biomed. Mat. Res.* **2000**, *51*, 343-351.

(144) Veronese, F. M.; Pasut, G. *Drug Discov. Today* **2005**, *10*, 1451-1458.

(145) Meldal, M.; Torn; xf; e, C. W. *Chem. Rev.* **2008**, *108*, 2952-3015.

(146) Li, B.; Martin, A. L.; Gillies, E. R. *Chem. Commun.* **2007**, 5217-5219.

(147) Martin, A. L.; Li, B.; Gillies, E. R. *J. Am. Chem. Soc.* **2008**, *131*, 734-741.

(148) van Dongen, S. F. M.; Teeuwen, R. L. M.; Nallani, M.; van Berkel, S. S.; Cornelissen, J. J. L. M.; Nolte, R. J. M.; van Hest, J. C. M. *Bioconjugate Chem.* **2008**, *20*, 20-23.

(149) van Dongen, S. F. M.; Nallani, M.; Schoffelen, S.; Cornelissen, J. J. L. M.; Nolte, R. J. M.; van Hest, J. C. M. *Macromol. Rapid Commun.* **2008**, *29*, 321-325.

(150) van Dongen, S. F. M.; de Hoog, H.-P. M.; Peters, R. J. R. W.; Nallani, M.; Nolte, R. J. M.; van Hest, J. C. M. *Chem. Rev.* **2009**, *109*, 6212-6274.

(151) Opsteen, J. A.; Brinkhuis, R. P.; Teeuwen, R. L. M.; Lowik, D. W. P. M.; van Hest, J. C. M. *Chem. Commun.* **2007**, 3136-3138.

(152) Pakalns, T.; L. Haverstick, K.; Fields, G. B.; McCarthy, J. B.; L. Mooradian, D.; Tirrell, M. *Biomaterials* **1999**, *20*, 2265-2279.

(153) Woodle, M. C.; Scaria, P.; Ganesh, S.; Subramanian, K.; Titmas, R.; Cheng, C.; Yang, J.; Pan, Y.; Weng, K.; Gu, C.; Torkelson, S. *J. Control. Release* **2001**, *74*, 309-311.

(154) Nasongkla, N.; Shuai, X.; Ai, H.; Weinberg, B. D.; Pink, J.; Boothman, D. A.; Gao, J. *Angew. Chem., Int. Ed.* **2004**, *43*, 6323-6327.

(155) Xiong, X. B.; Mahmud, A.; Uludag, H.; Lavasanifar, A. *Biomacromolecules* **2007**.

(156) Ishikawa, A.; Zhou, Y.-M.; Kambe, N.; Nakayama, Y. *Bioconjugate Chem.* **2008**, *19*, 558-561.

(157) Pasqualini, R.; Bourdoulous, S.; Koivunen, E.; Woods, V. L.; Ruoslahti, E. *Nature Med.* **1996**, *2*, 1197-1203.

(158) Schiffelers, R. M.; Koning, G. A.; ten Hagen, T. L. M.; Fens, M.; Schraa, A. J.; Janssen, A.; Kok, R. J.; Molema, G.; Storm, G. *J. Control. Release* **2003**, *91*, 115-122.

(159) Dubey, P. K.; Mishra, V.; Jain, S.; Mahor, S.; Vyas, S. P. *J. Drug Targeting* **2004**, *12*, 257-264.

(160) Temming, K.; Schiffelers, R. M.; Molema, G.; Kok, R. J. *Drug Resist. Updates* **2005**, *8*, 381-402.

(161) Huang, G. F.; Zhou, Z. M.; Srinivasan, R.; Penn, M. S.; Kottke-Marchant, K.; Marchant, R. E.; Gupta, A. S. *Biomaterials* **2008**, *29*, 1676-1685.

(162) Wheatley, M. A.; Lathia, J. D.; Oum, K. L. *Biomacromolecules* **2007**, *8*, 516-522.

(163) Akiyama, S. K.; Aota, S.; Yamada, K. M. *Cell Adhes. Commun.* **1995**, *3*, 13-25.

(164) Yang, X. B.; Roach, H. I.; Clarke, N. M. P.; Howdle, S. M.; Quirk, R.; Shakesheff, K. M.; Oreffo, R. O. C. *Bone* **2001**, *29*, 523-531.

(165) Hashim, A. I.; Zhang, X.; Wojtkowiak, J. W.; Martinez, G. V.; Gillies, R. J. *NMR Biomed.* **2011**, *24*, 582-91.

(166) Roberts, M. S.; Woods, A. J.; Dale, T. C.; van der Sluijs, P.; Norman, J. C. *Mol. Cell. Biol.* **2004**, *24*, 1505-1515.

(167) Kuwada, S. K.; Li, X. *Mol. Biol. Cell* **2000**, *11*, 2485-2496.

(168) Honoré, S.; Pichard, V.; Penel, C.; Rigot, V.; Prévôt, C.; Marvaldi, J.; Briand, C.; Rognoni, J.-B. *Histochem. Cell Biol.* **2000**, *114*, 323-335.

(169) Croyle, M. A.; Walter, E.; Janich, S.; Roessler, B. J.; Amidon, G. L. *Hum. Gene Ther.* **1998**, *9*, 561-573.

(170) Kozlova, N. I.; Morozevich, G. E.; Chubukina, A. N.; Berman, A. E. *Oncogene* **2001**, *20*, 4710-7.

(171) Peters, W. H. M.; Roelofs, H. M. J. *Cancer Res.* **1992**, *52*, 1886-1890.

(172) Dunehoo, A. L.; Anderson, M.; Majumdar, S.; Kobayashi, N.; Berkland, C.; Siahaan, T. J. *J. Pharm. Sci.* **2006**, *95*, 1856-1872.

(173) Fire, A.; Xu, S.; Montgomery, M. K.; Kostas, S. A.; Driver, S. E.; Mello, C. C. *Nature* **1998**, *391*, 806-11.

(174) Dorsett, Y.; Tuschl, T. *Nat. Rev. Drug Discovery* **2004**, *3*, 318-29.

(175) Hamilton, A. J. *Science* **1999**, *286*, 950-952.

(176) Carthew, R. W.; Sontheimer, E. J. *Cell* **2009**, *136*, 642-55.

(177) Pai, S. I.; Lin, Y.-Y.; Macaes, B.; Meneshian, A.; Hung, C.-F.; Wu, T.-C. *Gene Ther.* **2006**, *13*, 464-77.

(178) Faouzi, M.; Hague, F.; Potier, M.; Ahidouch, A.; Sevestre, H.; Ouadid-Ahidouch, H. *J. Cell. Physiol.* **2010**, *226*, 542-551.

(179) Roberts-Thomson, S. J.; Peters, A. A.; Grice, D. M.; Monteith, G. R. *Pharmacol. Ther.* **2010**, *127*, 121-130.

(180) Gwack, Y.; Srikanth, S.; Feske, S.; Cruz-Guilloty, F.; Oh-hora, M.; Neems, D. S.; Hogan, P. G.; Rao, A. *J. Biol. Chem.* **2007**, *282*, 16232-16243.

(181) Potier, M.; Gonzalez, J. C.; Motiani, R. K.; Abdullaev, I. F.; Bisaillon, J. M.; Singer, H. A.; Trebak, M. *FASEB J.* **2009**, *23*, 2425-2437.

(182) Kahl, C. R.; Means, A. R. *Endocr. Rev.* **2003**, *24*, 719-736.

(183) Taylor, J. T.; Zeng, X.-B.; Pottle, J. E.; Lee, K.; Wang, A. R.; Yi, S. G.; Scruggs, J. A. S.; Sikka, S. S.; Li, M. *World J. Gastroenterol.* **2008**, *14*, 4984-91.

(184) Motiani, R. K.; Abdullaev, I. F.; Trebak, M. *J. Biol. Chem.* **2010**, *285*, 19173-19183.

(185) Strobl, J. S.; Wonderlin, W. F.; Flynn, D. C. *Gen. Pharmacol.* **1995**, *26*, 1643-9.

(186) Yang, S.; Zhang, J. J.; Huang, X.-Y. *Cancer Cell* **2009**, *15*, 124-34.

(187) Mignen, O.; Thompson, J. L.; Shuttleworth, T. J. *J. Physiol.* **2008**, *586*, 185-95.

(188) Masiero, M.; Nardo, G.; Indraccolo, S.; Favaro, E. *Mol. Aspects Med.* **2007**, *28*, 143-66.

(189) Whitehead, K. A.; Langer, R.; Anderson, D. G. *Nat. Rev. Drug Discovery* **2009**, *8*, 129-38.

(190) Lechner, M. C.; Duque Magalhães, M. C. *Experientia* **1973**, *29*, 1479-1480.

(191) Kurreck, J. *Eur. J. Biochem.* **2003**, *270*, 1628-1644.

(192) Mintzer, M. A.; Simanek, E. E. *Chem. Rev.* **2009**, *109*, 259-302.

(193) Christian, D. A.; Cai, S.; Bowen, D. M.; Kim, Y.; Pajerowski, J. D.; Discher, D. E. *Eur. J. Pharm. Biopharm.* **2009**, *71*, 463-474.

(194) Pangburn, T. O.; Georgiou, K.; Bates, F. S.; Kokkoli, E. *Langmuir* **2012**, *in press*.

(195) Fernandez-Cobo, M.; Holland, J. F.; Pogo, B. G. T. *BMC Cancer* **2006**, *6*, 99.

(196) Saad, S.; Bendall, L. J.; James, A.; Gottlieb, D. J.; Bradstock, K. F. *Breast Cancer Res. Treat.* **2000**, *63*, 105-115.

(197) van der Pluijm, G.; Vloedgraven, H.; Papapoulos, S.; Löwick, C.; Grzesik, W.; Kerr, J.; Robey, P. G. *Laboratory Invest.* **1997**, *77*, 665-75.

(198) Rodionov, V. O.; Presolski, S. I.; Gardinier, S.; Lim, Y. H.; Finn, M. G. *J. Am. Chem. Soc.* **2007**, *129*, 12696-12704.

(199) Abramoff, M. D.; Magalhaes, P. J.; Ram, S. J. *Biophotonics Int.* **2004**, *11*, 36-42.

(200) Costes, S. V.; Daelemans, D.; Cho, E. H.; Dobbin, Z.; Pavlakis, G.; Lockett, S. *Biophys. J.* **2004**, *86*, 3993-4003.

(201) Livak, K. J.; Schmittgen, T. D. *Methods* **2001**, *25*, 402-8.

(202) Vandesompele, J.; De Preter, K.; Pattyn, F.; Poppe, B.; Van Roy, N.; De Paepe, A.; Speleman, F. *Genome Biol.* **2002**, *3*, research0034.1-research0034.11.

(203) Jain, S.; Dyrdahl, M. H. E.; Gong, X.; Scriven, L. E.; Bates, F. S. *Macromolecules* **2008**, *41*, 3305-3316.

(204) Wang, X.; Liu, L.; Luo, Y.; Zhao, H. *Langmuir* **2009**, *25*, 744-750.

(205) Flatin, G. E.; Dhanikula, A. B.; Luthman, K.; Brandl, M. *Eur. J. Pharm. Sci.* **2006**, *27*, 80-90.

(206) Kim, Y.; Tewari, M.; Pajerowski, J. D.; Cai, S.; Sen, S.; Williams, J.; Sirsi, S.; Lutz, G.; Discher, D. E. *J. Control. Release* **2009**, *134*, 132-140.

(207) Auguste, D. T.; Furman, K.; Wong, A.; Fuller, J.; Armes, S. P.; Deming, T. J.; Langer, R. *J. Control. Release* **2008**, *130*, 266-274.

(208) Mei, J.; Hu, H.; McEntee, M.; Plummer III, H.; Song, P.; Wang, H.-C. R. *Breast Cancer Res. Treat.* **2003**, *79*, 95-105.

(209) Plopper, G. E.; Domanico, S. Z.; Cirulli, V.; Kiosses, W. B.; Quaranta, V. *Breast Cancer Res. Treat.* **1998**, *51*, 57-69.

(210) Bohley, P.; Seglen, P. *Experientia* **1992**, *48*, 151-157.

(211) Noh, S. M.; Han, S. E.; Shim, G.; Lee, K. E.; Kim, C.-W.; Han, S. S.; Choi, Y.; Kim, Y. K.; Kim, W.-K.; Oh, Y.-K. *Biomaterials* **2011**, *32*, 849-57.

(212) Zhao, M.; Yang, H.; Jiang, X.; Zhou, W.; Zhu, B.; Zeng, Y.; Yao, K.; Ren, C. *Mol. Biotech.* **2008**, *40*, 19-26.

(213) Carralot, J.-P.; Kim, T.-K.; Lenseigne, B.; Boese, A. S.; Sommer, P.; Genovesio, A.; Brodin, P. *J. Biomol. Screening* **2009**, *14*, 151-60.

(214) Pawłowski, K. M.; Popielarz, D.; Szyszko, K.; Gajewska, M.; Motyl, T.; Król, M. *Vet. Comp. Oncol.* **2011**.

(215) Nabzdyk, C. S.; Chun, M.; Pradhan, L.; Logerfo, F. W. *J. Translational Med.* **2011**, *9*, 48.

(216) Brough, R.; Frankum, J. R.; Sims, D.; Mackay, A.; Mendes-Pereira, A. M.; Bajrami, I.; Costa-Cabral, S.; Rafiq, R.; Ahmad, A. S.; Cerone, M. A.; Natrajan, R.; Sharpe, R.; Shiu, K.-K.; Wetterskog, D.; Dedes, K. J.; Lambros, M. B.; Rawjee, T.; Linardopoulos, S.; Reis-Filho, J. S.; Turner, N. C.; Lord, C. J.; Ashworth, A. *Cancer Disc.* **2011**, *1*, 260-273.

(217) Breunig, M.; Hozsa, C.; Lungwitz, U.; Watanabe, K.; Umeda, I.; Kato, H.; Goepferich, A. *J. Control. Release* **2008**, *130*, 57–63.

(218) Suhorutsenko, J.; Oskolkov, N.; Arukuusk, P.; Kurrikoff, K.; Eriste, E.; Copolovici, D.-M.; Langel, U. *Bioconjugate Chem.* **2011**, *22*, 2255-62.

(219) Pangborn, A. B.; Giardello, M. A.; Grubbs, R. H.; Rosen, R. K.; Timmers, F. J. *Organometallics* **1996**, *15*, 1518-1520.

(220) Morton, M.; Fetters, L.; Inomata, J.; Rubio, D.; Young, R. *Rubber Chem. Technol.* **1979**, *49*, 303.

(221) Quirk, R. P.; Ma, J.-J. *J. Polym. Sci. Pol. Chem.* **1988**, *26*, 2031-2037.

(222) E. Santee, J.; Malotky, L.; Morton, M. *Rubber Chem. Technol.* **1973**, *46*, 1156.

(223) Morton, M.; Fetters, L. *Rubber Chem. Technol.* **1975**, *48*, 359–409.

(224) Matsuda, Y.; Nojima, R.; Sato, T.; Watanabe, H. *Macromolecules* **2007**.

(225) Schmalz, H.; Lanzendörfer, M. G.; Abetz, V.; Müller, A. H. E. *Macromol. Chem. Phys.* **2003**, *204*, 1056-1071.

(226) Robson F. Storey, T. P. H. *J. Polymer Sci. A: Polymer Chem.* **1993**, *31*, 1825-1838.

(227) Zupancich, J. A.; Bates, F. S.; Hillmyer, M. A. *Macromolecules* **2006**.

(228) Du, Y. J.; Brash, J. L. *J. Appl. Polym. Sci.* **2003**, *90*, 594-607.

(229) Shuai, X.; Merdan, T.; Unger, F.; Wittmar, M.; Kissel, T. *Macromolecules* **2003**, *36*, 5751-5759.

(230) Trollsas, M.; Kelly, M. A.; Claesson, H.; Siemens, R.; Hedrick, J. L. *Macromolecules* **1999**, *32*, 4917-4924.

(231) Vangeyte, P.; Jérôme, R. *J. Polymer Sci. A: Polymer Chem.* **2004**, *42*, 1132-1142.

(232) Vangeyte, P.; Gautier, S.; Jerome, R. *Colloids Surf., A* **2004**, *242*, 203-211.

(233) Vangeyte, P.; Leyh, B.; Heinrich, M.; Grandjean, J.; Bourgaux, C.; Jerome, R. *Langmuir* **2004**, *20*, 8442-8451.

(234) Dubois, P.; Degee, P.; Jerome, R.; Teyssie, P. *Macromolecules* **1992**, *25*, 2614-2618.

(235) Dubois, P.; Ropson, N.; Jerome, R.; Teyssie, P. *Macromolecules* **1996**, *29*, 1965-1975.

(236) Rieger, J.; Bernaerts, K. V.; DuPrez, F. E.; Jerome, R.; Jerome, C. *Macromolecules* **2004**, *37*, 9738-9745.

(237) Dean, K. E. S.; Klein, G.; Renaudet, O.; Reymond, J.-L. *Bioorg. Med. Chem. Lett.* **2003**, *13*, 1653-1656.

(238) Bandrowski, J. F.; Benson, C. L. *Clin. Chem.* **1972**, *18*, 1411-1414.

(239) Bohlen, P.; Stein, S.; Dairman, W.; Udenfriend, S. *Arch. Biochem. Biophys.* **1973**, *155*, 213-220.

(240) Zheng, Y.; Won, Y. Y.; Bates, F. S.; Davis, H. T.; Scriven, L. E.; Talmon, Y. *J. Phys. Chem. B* **1999**, *103*, 10331-10334.

(241) Hentze, H. P.; Krämer, E.; Berton, B.; Förster, S.; Antonietti, M.; Dreja, M. *Macromolecules* **1999**, *32*, 5803-5809.

(242) Förster, S.; Berton, B.; Hentze, H. P.; Krämer, E.; Antonietti, M.; Lindner, P. *Macromolecules* **2001**, *34*, 4610-4623.

(243) Rameez, S.; Bamba, I.; Palmer, A. F. *Langmuir* **2010**, *26*, 5279-85.

(244) Crooke, S. T. *Ann. Rev. Med.* **1994**, *55*, 61-95.

(245) Kessler, J. H.; Mullauer, F. B.; de Roo, G. M.; Medema, J. P. *Cancer Lett.* **2007**, *251*, 132-45.

(246) Hansen, M.; Nielsen, S.; Berg, K. *J. Immunol. Methods* **1989**, *119*, 203-210.

(247) Rexen, P.; Emborg, C. *Biotech. Techniques* **1992**, *6*, 255-260.

(248) Stowe, R. P.; Koenig, D. W.; Mishra, S. K.; Pierson, D. L. *J. Microbiol. Methods* **1995**, *22*, 283-292.

(249) Alley, M. C.; Scudiero, D. A.; Monks, A.; Assay, M. T.; Scudiere, D. A.; Hursey, M. L.; Czerwinski, M. J.; Fine, D. L.; Abbott, B. J.; Mayo, J. G.; Shoemaker, R. H.; Boyd, M. R. *Cancer Res.* **1988**, *48*, 589-601.

(250) Vichai, V.; Kirtikara, K. *Nat. Protocols* **2006**, *1*, 1112-1116.

(251) Keepers, Y. P.; Pizao, P. E.; Peters, G. J.; van Ark-Otte, J.; Winograd, B.; Pinedo, H. M. *Eur. J. Cancer Clinic. Oncol.* **1991**, *27*, 897-900.

(252) Yang, J.; Chen, H.; Vlahov, I. R.; Cheng, J.-X.; Low, P. S. *PNAS* **2006**, *103*, 13872-13877.

(253) Cerritelli, S.; Velluto, D.; Hubbell, J. A. *Biomacromolecules* **2007**, *8*, 1966-1972.

(254) Meng, F.; Hennink, W. E.; Zhong, Z. *Biomaterials* **2009**, *30*, 2180-2198.